THE BEHAVIOR OF REINFORCED BLOCKWORK MASONRY COLUMNS UNDER AXIAL COMPRESSION

by

Ayşe Elif Özsoy

B.S. in C.E., Boğaziçi University, 1999

Submitted to the Institute for Graduate Studies in Science and Engineering in partial fulfillment of the requirements for the degree of

Master of Science

in

Civil Engineering

Boğaziçi University

2003

ACKNOWLEDGEMENTS

I owe special thanks to Prof. Cengiz Karakoç of Boğaziçi University and Assist. Prof. H. Orhun Köksal and Research Assistant Hakkı Yıldırım of Yıldız Technical University for their helpful guidance and contribution throughout this thesis.

The supply of concrete hollow block units from Yapı Merkezi Prefabrikasyon A.Ş. is also gratefully acknowledged.

Funding provided by Research Fund of Yıldız Technical University for the project under the title of "Experimental and Finite Element Study of Masonry Prisms under Axial Compression" is acknowledged.

I also would like to thank to Research Assistant Onur Ertaş from Boğaziçi University Structures Laboratory, Fahri Karahan, Selçuk Faik Yılmaz and my husband Hakan Özbay for their technical support during the experiments.

Finally, I would like to thank to all members of my family; Cafer Özsoy, Nihal Özsoy, Aslı Özsoy, Ali Özsoy and my friend, Zühal Özbay for their support and endless encouragement.

ABSTRACT

THE BEHAVIOR OF REINFORCED BLOCKWORK MASONRY COLUMNS UNDER AXIAL COMPRESSION

Reinforced masonry columns are common structural elements which are used for supporting compressive vertical loads and providing lateral support to masonry walls. Reinforcement increases the column resistance to axial and flexural loading as long as it is confined by lateral ties. The reinforcing cage also confines the concrete core of the masonry columns and increases the ductility of the member. Reinforced masonry columns have the advantage of eliminating the need for formwork by using hollow block units.

An experimental and analytical study was performed on the ultimate strength and failure mechanism of reinforced masonry columns under axial loading. A total of six columns were constructed as nine course high using 190x190x390 mm two core hollow concrete block units. The effect of using variable compressive strength of infill concrete on the ultimate strength was also investigated. In addition to the experimental study, three-dimensional nonlinear finite element modelling of the columns was developed in order to investigate the nonlinear behavior of reinforced masonry columns under axial loading, analytically.

ÖZET

EKSENEL BASINÇ ALTINDA DONATILI BETON BLOK YIĞMA KOLONLARININ DAVRANIŞI

Donatılı yığma kolonlar, düşey yükleri taşıyan ve yığma duvarlara yanal destek sağlayan yapı elemanlarıdır. Etriyelerle sarılmış olan donatılar, kolonun basınç ve eğilme yüklerine karşı mukavemetini ve sünekliğini artırır. Ayrıca, donatılı yığma kolonlar boşluklu beton blokların kullanılması ile kalıp ihtiyacını ortadan kaldırır.

Bu tez çalışmasının kapsamında, donatılı beton blok yığma kolonlarının eksenel basınç altında taşıma gücü ve kırılma mekanizmaları deneysel ve analitik olarak incelenmiştir. Deney programı için, 190x190x390 mm çift boşluklu beton bloklar kullanılarak dokuz ünite yüksekliğinde altı adet kolon inşa edilmiştir. Ayrıca, dolgu betonu basınç mukavemetinin, taşıma gücü üzerindeki etkisi araştırılmıştır. Deneysel çalışmaya ek olarak, donatılı yığma kolonların eksenel basınç altındaki nonlineer davranışının incelenmesi için, kolonlar üç boyutlu nonlineer sonlu elemanlar modellenmesi ile analiz edilmiştir.

TABLE OF CONTENTS

LIST OF FIGURES

LIST OF TABLES

LIST OF SYMBOLS/ABBREVIATIONS

A_c	Concrete core area
A_g	Column gross area
A_n	Net cross-sectional area of masonry
A_{s1}	Area of lateral ties
A_{s2}	Area of vertical reinforcement
A_{shell}	Area of the masonry shell
[B]	Strain matrix
c_{bl}	Cohesion of concrete block unit
c_c	Cohesion of infill concrete
c_{mr}	Cohesion of mortar
D_{max}	Maximum particle size of aggregates
E_c	Elastic modulus of concrete core
E_g	Elastic modulus of grout
E_m	Elastic modulus of masonry
E_{mr}	Elastic modulus of mortar
E_s	Elastic modulus of reinforcing steel
E_{shell}	Elastic modulus of the masonry shell
f_{bl}'	Compressive strength of concrete block unit
f_c'	150x300 mm concrete cylinder compressive strength
f_g'	Compressive strength of grout
f_k	Characteristic compressive strength of masonry
f_m'	Specified compressive strength of masonry
f_{mr}'	Cube compressive strength of mortar
f_s	Allowable compressive stress of reinforcement
f_y	Minimum yield strength of reinforcement
I_1	First invariant of stress tensor
J_2	Second invariant of stress deviator tensor
J_3	Third invariant of stress deviator tensor
k	Yield stress in pure shear; positive constant in Drucker-Prager criterion
$[K_t]$	Linear tangent stiffness matrix
P_u	Ultimate load capacity

r_{co}	Deviatoric length for compressive meridian
r_{to}	Deviatoric length for tensile meridian
s_1, s_2, s_3	Principal stress deviators
t_b, t_j:	Height of block unit and thickness of mortar joint
α	Positive constant in Drucker-Prager criterion
ε_u	Ultimate strain of column
$\{\Delta R\}_n$	Load change vector at n^{th} increment
$\{\Delta \delta\}_n$	Displacement change vector at n^{th} increment
ϕ_{bl}	Internal friction angle of concrete block unit
ϕ_c	Internal friction angle of infill concrete
ϕ_{mr}	Internal friction angle of mortar
η	Ratio of ungrouted area of masonry to gross area
ν_{bl}	Poisson's ratio of concrete block unit
ν_c	Poisson's ratio of infill concrete
ν_{mr}	Poisson's ratio of mortar
ν_s	Poisson's ratio of steel
θ	Angle of similarity
σ	Normal stress
$\sigma_1, \sigma_2, \sigma_3$	Principal stresses
$\{\sigma\}_n$	Stress vector at n^{th} increment
τ	Limiting shearing stress
ξ	Hydrostatic length
ACI	American Concrete Institute
ASCE	American Society of Civil Engineers
ASTM	American Society for Testing and Materials
B	Width of concrete block units
BS	British Standards
C1,..., C6	Columns specimens in the experiment
CSS	Crushed stone sand
D	Diameter of concrete specimens
H	Height of concrete specimens; height of concrete block units
H1, H2	Mortar mix designs in the experiment

L	Length of concrete block units
LVDT	Linear variable differential transducer
M1, M2, M3	Concrete mix designs in the experiment
M3a, M3b	Column models in the analytical solution
M4a, M4b	Column models in the analytical solution
NO1	No.1 gravel
NO2	No.2 gravel
NSS	Natural sea sand
TMS	The Masonry Standards
TS	Turkish Standards

1. INTRODUCTION

1.1. General Remarks

Reinforced masonry columns are structural elements, which are used as separate assemblages or with other load bearing units such as masonry walls. Main functions of a reinforced masonry column are supporting compressive vertical loads and providing lateral support to masonry walls. In comparison with reinforced concrete columns, masonry columns have the advantage of eliminating the need for formwork through the use of concrete hollow blocks. Similar to the reinforced concrete columns, reinforcement increases the ultimate load carrying capacity and ductility of masonry column under axial or eccentric loading provided that lateral ties are placed around the concrete core to confine vertical reinforcement.

Limited work has been conducted for the purpose of developing strength design procedures of reinforced masonry columns. Detailing of reinforcement, infill concrete strength, block unit strength, mortar strength and interaction of concrete core with block shells are the essential factors determining the strength of a reinforced masonry column. Although a reinforced masonry column is analogous to reinforced concrete column in many aspects, they have different characteristics by the means of ultimate strength equations, detailing of reinforcements and behavior under axial and eccentric loading.

The behavior of the masonry prisms under axial compression has been investigated by developing finite element model and conducting linear elastic analysis, previously. The three dimensional finite element analysis of the masonry prisms was developed adopting eight-noded isoparametric solid elements by Ramamurthy [1]. The eight-noded elements were also used for the linear elastic analysis of the hollow block prisms and wall panels by Hamid and Chukwunenye [2]; Cheema and Klingner [3]; Khalil *et al.*[4]; and Afshari and Kaldjian [5]. Furthermore, Sayed Ahmed and Shrive [6] have developed a nonlinear finite element model of hollow masonry using isoparametric shell elements and the Drucker-Prager failure criteria. Nonlinear finite element modelling of the reinforced masonry

columns under axial loading is a complex problem but further study on the analytical model suggests an idea of the overall behavior in addition to the experimental studies on the reinforced masonry columns.

Research has to be carried out on reinforced masonry columns in order to simulate the nonlinear behavior analytically and to improve present strength equations by the means of analytical and experimental studies. Thus, better predictions on strength and behavior will lead to more economical design of masonry structures.

1.2. Objectives and Scope

The objectives of this study are:

- to examine experimentally the behavior of reinforced masonry columns that are constructed with two core hollow concrete block units with varying infill concrete strength under axial loading;
- to study effects of reinforcement and infill concrete strength on axial load carrying capacity of reinforced masonry columns;
- to describe failure modes of reinforced masonry columns under axial compression;
- to determine ultimate load and elastic modulus of tested columns and to compare the test results with the values obtained from the equations proposed previously;
- to perform an analytical investigation using three dimensional nonlinear finite element model of the columns tested;
- to examine the compression behavior of the reinforced masonry columns by evaluating the analytical and experimental results.

2. LITERATURE REVIEW

2.1. Introduction

A masonry assemblage is a composition of the constituent materials, which are block units, mortar, grout and reinforcement. The characteristic behavior of masonry is mainly dependent on the interactions between the constituent materials and other factors affecting the physical and mechanical properties of the composite.

The design of masonry structures necessitates compressive strength of masonry, f_m' which is essential for determination of design stresses and criteria in load bearing structures. American Society for Testing and Materials (ASTM E447) [7] describe the procedures of the standard prism tests for determination of the compressive strength, f_m'. The strength characteristics of masonry correlated with the compressive strength, f_m' are mainly based on the compression tests made on concrete masonry prisms. The factors affecting the compressive strength of masonry prisms are described with details in Section 2.2.

The reinforced masonry columns are vertical structural members that support compressive vertical loads and provide lateral support to the masonry walls. Reinforcement increases the resistance of the column to flexural load as well as to axial load provided that the longitudinal reinforcements are confined with lateral ties. Lateral ties prevent local buckling of vertical reinforcement and form a reinforcing cage, which confines the grouted core, and increases the ultimate strength of the masonry column. Lateral ties are preferably placed within the grouted core instead of the mortar joints of the masonry units in order to prevent high concentration of the tensile splitting stresses around the lateral ties [8].

The studies carried out about concrete masonry prisms and factors affecting prism compressive strength form a basis for the researches investigating behavior and the ultimate load carrying capacity of the reinforced masonry columns under axial loading. However, previous studies on the concrete masonry prisms are inadequate to express axial

load carrying capacity and interaction between reinforcement, infill concrete, concrete block units and mortar of reinforced masonry columns.

The first study on the reinforced masonry columns was conducted by Feeg [9] in 1978. The author aimed to investigate the effects of reinforcement details on column strength. The columns tested were constructed with 1.63 m height. Thirty-four of the tested columns were fabricated with 200x200x400 mm lightweight two core concrete blocks laid in running bond. The remaining three columns were constructed with 400x400x200 mm single core lightweight pilaster units laid in stack bond. Vertical spacing of the lateral ties was 200 mm due to the restriction of block unit geometry. Types of mortar and grout used for the test were same for all of the columns.

Tie diameter and location (either in mortar joints or confining the vertical reinforcement), percentage (0.7 and 1.3), grade and distribution of the vertical reinforcements were the variables investigated in this study.

The test results showed that the columns behaved elastically up to 75 percent of the ultimate load where the average elastic modulus of masonry was about 800 times the masonry prism strength.

Increasing tie diameter resulted in increasing column strength with decreasing amount of vertical cracks at failure. Placement of ties had no significant effect on the strength, but the columns with vertical bars that were confined with lateral ties provided greater resistance against buckling of the vertical bars.

Increasing vertical bar diameter for a given percentage of vertical reinforcement resulted with decrease in the column strength due to larger differences of the Poisson's ratio between the different materials.

Another essential study on the reinforced masonry columns was conducted by Sturgeon, Longworth and Warwaruk [10] with short concentrically loaded blockwork columns. Column specimens of 1.8 m height were constructed with 400x400x200 mm

single core pilaster units that were in stack bond. All of the columns were nine course high with an h/t ratio of 4.58.

The test variables were the placement and detailing of the lateral ties; the percentage (0.76, 1.30 and 2.60), and grade of the vertical reinforcement and the compressive strength of the grout.

The test results showed that;

- Increasing the percentage of vertical reinforcement caused a reduction in the load contribution of the block masonry shell. However, the load contribution of the vertical reinforcement exceeded this decrease, thus increased the column ultimate load.
- The lateral ties produced an increase of 8-28 percent in the ultimate strength.
- Addition of lateral ties to the grouted columns increased ductility of the column preventing explosive type of column failure.
- Stress-strain curves of the concentrically loaded reinforced or unreinforced columns showed linearity up to 50 percent of the failure stress approximately.

In addition, the authors proposed an empirical formula expressing the ultimate strength for short concentrically loaded reinforced columns, which will be discussed in Section 2.3.

The latest study on reinforced masonry columns forming a basis to this thesis was conducted by Khalaf, Hendry and Fairbairn [11] in 1993. In this study, the columns were constructed six course high with 400x200x200 mm, low strength, two core concrete hollow blocks with full and half cross sections and 1.27 m height. The variables of the column tests were;

- Lateral tie diameter,
- Percentage of vertical reinforcements (0.6 to 4.26).

The test results showed that;

- ϕ8 mm deformed lateral ties gave more consistent results for strain values than other lateral ties.
- The strength of columns reinforced with ϕ6 mm and ϕ8 mm lateral ties was higher compared with the unreinforced filled columns, which was a result of the confining stresses reducing harmful tensile stresses exerted on the block shells by the infill concrete.
- Ultimate load of the columns reinforced with ϕ8 mm lateral ties increased uniformly with increasing percentages of vertical reinforcement similar to reinforced concrete columns.

The authors also proposed an empirical formula for the ultimate load of the reinforced blockwork masonry columns, which will be discussed in Section 2.3.

2.2. Concrete Masonry Prisms and Factors Affecting the Prism Compressive Strength

Masonry prisms are small-scale masonry assemblages, which reflect the behavior of full scale masonry structural assemblages. The behavior of reinforced masonry columns under uniaxial loading resembles the behavior of grouted masonry prisms tested for the determination of compressive strength, f_m' in many aspects. The standard prism tests described in ASTM E447 [7] are generally conducted for the estimation of compressive strength of masonry prisms, f_m'.

Failure mechanisms, compressive strength and ultimate load capacity of reinforced masonry columns are analogous to grouted masonry prism properties with the difference that the effect of reinforcement on the column behavior and capacity should be studied in addition to the other constituent materials of the masonry.

Furthermore, Khalaf, Hendry and Fairbairn [11] have attempted to express the ultimate strength of the concentrically loaded reinforced masonry columns in terms of specified masonry prism compressive strength, f_m'

A summary of the factors effecting the compressive strength of masonry prisms is described briefly in Section 2.2.1 to 2.2.7.

2.2.1. Unit Geometry and Type of Mortar Bedding

Unit geometry of the block directly determines the mortar bedded area, which is subjected to compressive vertical stress and the minimum vertical section resisting lateral tension. Unit geometry has a major effect on the compressive strength of masonry prisms because vertical cracks in prisms are related to development of lateral stresses in the block units.

Prism tests made on hollow blocks having 4 web shells and 3 web shells showed that the strength of prisms with 4 web shells was 13 percent higher than the strength of prisms having 3 web shells [12]. Also, the study of Hamid and Chukwunenye [2] has included comparison of stack bonded hollow prisms with face shell mortar bedding and fully mortar bedding. Tensile stresses develop at the center of the webs by a mechanism analogous to deep beam bending in face shell bedded masonry prisms. Lateral stresses created in the webs for face shell bedded hollow prisms are larger than stress created for fully bedded hollow prisms with highly nonuniform stress distribution compared to fully bedded prisms.

2.2.2. Prism Height and Effective Height to Minimum Thickness Ratio (h/d)

Prisms with h/d around 2 do not exhibit the failure modes of observed structures. Decreasing strength with increasing height is observed which is associated with having sufficient portion of prism away from confining effects of bearing plates to allow the characteristic vertical splitting to take place [13].

Building Code Requirements for Masonry Structures (ACI 530/ASCE 5/TMS 402) [14] limit effective height to minimum thickness (h/d) of a column to 25. Effective height of a column depends on the boundary conditions at top and bottom blocks of the column.

2.2.3. Compressive Strength of Mortar

The study of Hamid and Drysdale [15] and Khalaf, Hendry and Fairbairn [16] show that prism strength increases with increasing mortar strength up to a level, which is not valid for higher strength mortar. Use of the mortar with higher strength is not required due to the fact that workability of the fresh mortar and deformation of mortar to accommodate differential movement under axial compression are much more important for the performance of masonry.

Test results of Hamid and Drysdale [15] indicate that grouting reduces the effect of mortar on masonry strength because of the continuity provided by the grouted cores.

According to the test results of Khalaf, Hendry and Fairbairn [16], mortar joints of low strength contribute greatly to strength of the grouted prisms, whereas above certain strength of mortar (9 megaPascals (MPa)), the effect is negligible verifying the study of Hamid and Drysdale [15] as well.

2.2.4. Block Unit Strength

The compressive strength of block units directly affects masonry prism strength. However; it is not sufficient to explain failure mechanism of the masonry prism. Masonry prisms under axial loading fail in the case of propagating of cracks and weakening of block units which indicates that failure mechanism of masonry prisms or columns is dependent on both compressive and tensile strength of block units and unit geometry.

2.2.5. Bearing Plates

The thickness of steel bearing plates used for axial compression test has a major effect on the behavior and failure mode of masonry prisms and columns. ASTM E447 provisions [7] state the thickness of bearing plates to be equal to at least one half of the distance from edge of bearing plate to the most remote corner of the prism's cross section.

The study of Ganesan and Ramamurthy [17] indicates that insufficient thickness of bearing plates induces large lateral tensile stresses at the top block unit causing premature failure of the prism or the column.

2.2.6. Thickness of Mortar Joints

The experimental studies on grouted and ungrouted masonry prisms investigating the effect of mortar joint thickness on prism strength [15] have shown that mortar joint thickness has a negligible effect on the compressive strength of masonry prisms. This effect is much reduced for grouted prisms or columns due to the continuity of the grout [18].

2.2.7. Infill Concrete Strength

The study of Hamid and Drysdale [15] indicates that the failure loads of grouted prisms are lower than the superposition of the capacity of infill concrete area and the capacity of mortared area.

Also, the grouted prisms show a significant decrease in strength based on gross area compared to unfilled prisms, based on net area according to the study of Khalaf, Hendry and Fairbairn [16]. The strength of the infilled prisms increases uniformly with increasing infill concrete strength.

2.3. Elastic Modulus of Constituent Materials and Concrete Masonry

2.3.1. Reinforcing Steel

Elastic modulus of the reinforcing steel to be used for masonry design is given as;

$E_s = 200\,000$ MPa

by ACI 530/ASCE 5/TMS 402 [14] unless it is determined experimentally. In addition, grades 300 and 400 reinforcing steel (minimum specified yield strength in MPa) are generally used for masonry design where the allowable tensile design stress is 140 or 165 MPa and the allowable axial compressive stress is limited to 40 percent of the yield strength or 165 MPa [19].

2.3.2. Concrete Block Units

Typical stress-strain curves of hollow concrete blocks under axial compression are similar to those of concrete, which reveals a nonlinear behavior up to 25-50 percent of the maximum compressive strength. The elastic modulus for concrete block units can range between 500 to 1000 times the unit compressive strength. Also, the Poisson's ratio used for masonry design is generally taken as 0.2.

2.3.3. Grout

ACI 530/ASCE 5/TMS 402 [14] recommends the elastic modulus of grout as;

$$E_g = 500 \times f_g \tag{2.1}$$

where f_g is the compressive strength of grout.

2.3.4. Mortar

Mortar among the constituent materials of masonry has the main function to bond individual masonry units into a composite assemblage that will withstand the imposed conditions of loads and weather. Mortar types are mainly defined by M, S, N, O and K letters classified according to the volumetric proportions of cement, lime and sand. ASTM C270 [20] identifies mortar types by either proportion or property specification. The most applicable types of mortar for engineered masonry are M, S and N; type M having higher strength and poorer workability, type N having lower strength and good workability and type S having strength and workability properties between M and N.

The ratio of elastic modulus of block unit to mortar, E_{bl}/E_{mr} has an effect on the masonry compressive strength and behavior. An increase in the ratio, E_{bl}/E_{mr} causes an increase of the lateral tensile stresses in the blocks due to the increase of the degree of deformational incompatibility between stronger blocks and weaker mortar, which is not valid for the practical mortar types M, S and N [2]. Thus, it can be concluded that the higher ratio of E_{bl}/E_{mr} has a negative effect on the compressive strength of the masonry.

2.3.5. Concrete Masonry

The stress-strain curve of the concrete masonry under axial compression shows nonlinear behavior beyond the stress level of 50 percent of the maximum compressive strength. ACI 530/ASCE 5/TMS 402 [14] defines the elastic modulus of concrete masonry as the chord modulus estimated from a stress value of 5 to 33 percent of the compressive strength (Figure 2.1). Alternatively, the provision proposes the elastic modulus of concrete masonry to be determined from Table 2.1, which is recreated from the code.

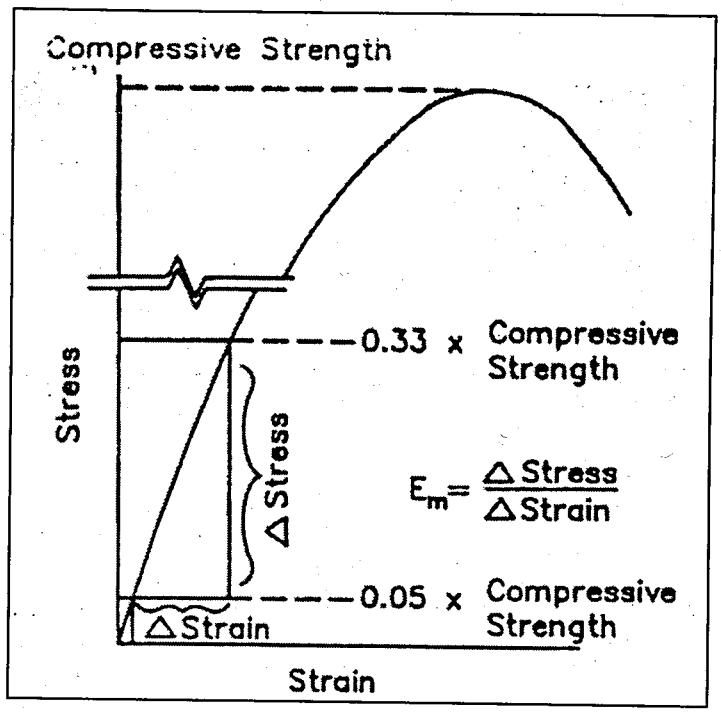

Figure 2.1. Chord modulus of elasticity of masonry [14]

Table 2.1. Elastic modulus for masonry concrete [14]

NET AREA COMPRESSIVE STRENGTH OF UNITS (MPa)	MODULUS OF ELASTICITY E_m* (GPa)	
	TYPE N MORTAR	TYPE M AND S MORTAR
41.5 or greater	-	24.0
34.5	19.5	22.0
27.5	18.0	20.0
20.5	16.0	17.0
17.0	15.0	16.5
14.0	12.5	15.0
10.5	10.5	11.0
*Linear interpolation permitted		

Another formulation [21, 22] expressing the elastic modulus E_m is given as;

$$E_m = \frac{1}{\frac{\delta}{(1-\eta)E_g + \eta E_b} + \frac{1}{(1-\eta)E_g + \eta E_j}} \tag{2.2}$$

where;

η: Ratio of ungrouted area of masonry to gross area

δ: $t_b / (t_b + t_j)$

t_b, t_j: Height of block unit and thickness of mortar joint, respectively

E_g, E_b, E_j: Elastic modulus of grout, block unit and mortar joint, respectively

This expression is derived using the strain compatibility, equilibrium and the linear elastic zone of the constituent materials.

Building Research Station [23] reported an approximate relationship as;

$$E_m = 850 \times f_m' \tag{2.3}$$

In 1978, Hatzinikolas, Longworth and Warwaruk [8] recommended the elastic modulus of concrete masonry as;

$$E_m = 750 \times f_m' \tag{2.4}$$

using the test results on masonry walls. Feeg *et al.* [9] suggested the following expression for the elastic modulus of masonry;

$$E_m = 800 \times f_m' \tag{2.5}$$

which was based on his study of reinforced block columns. Canadian Standards [24] recommended the elastic modulus of concrete masonry as;

$$E_m = 1000 \text{ x } f_m' \leq 20\,690 \text{ MPa} \tag{2.6}$$

Eventually, Sturgeon, Longworth and Warwaruk [10] have proposed the following expression according to the experimental results of their study;

$$E_m = \frac{0.8E_c(A_c - A_s) + E_{shell}A_{shell} + E_sA_s}{A_g} \tag{2.7}$$

where;

E_c: Elastic modulus of the concrete core

A_c: Core area

E_s: Elastic modulus of the vertical reinforcement

A_s: Area of the vertical reinforcement

E_{shell}: Elastic modulus of the masonry shell

A_{shell}: Area of the masonry shell

A_g: Column gross area

2.4. Ultimate Strength Analysis of Concentrically Loaded Reinforced Masonry Columns

The principles of reinforced concrete column ultimate strength design have been applied by the designers to evaluate failure loads for masonry columns. The ultimate strength of the concentrically loaded reinforced concrete columns as determined by Lyse *et al.* [25, 26, 27] and Richart *et al.* [28, 29] is given by;

$$P_u = 0.85f_c'(A_g - A_s) + f_yA_s \tag{2.8}$$

where;

P_u: Ultimate load for a tied column

A_g: Gross cross sectional area of column perpendicular to the applied load

A_s: Cross sectional area of longitudinal reinforcement

f_c': Standard concrete cylinder strength

f_y: Yield strength of longitudinal reinforcement

The formulation above, which is valid for reinforced concrete columns, suggests that the ultimate strength is considered to be made up of:

- Ultimate strength of the concrete core area defined in terms of the standard cylinder strength of the concrete and,
- The load required for stressing the longitudinal reinforcement up to its yield point.

However, for reinforced masonry columns the load contribution of block shell, concrete core and vertical steel is not the same with reinforced concrete columns.

Sturgeon, Longworth and Warwaruk [10] have suggested the following formulation for the ultimate strength of the concentrically loaded short, reinforced concrete blockwork masonry columns. The expression has been proposed depending on the test results of nine course high reinforced masonry columns that were constructed using 400x400x200 mm single core pilaster units and tested under axial loading.

$$P_u = 0.85f_c'(A_c - A_s) + E_sA_s/700 \tag{2.9}$$

where;

A_c: Column core area

E_s: Elastic modulus of longitudinal steel

Moreover, British Standards [30] define the ultimate load as;

$$P_u = (f_kA_g)/1000 \tag{2.10}$$

where;

f_k: Characteristic compressive strength of masonry

A_g: Gross cross sectional area of column

Another expression recommended by ACI 530/ASCE 5/TMS 402 [14] for the evaluation of the ultimate load is given as;

$$P_u = (0.225 f_m' A_g + 0.65 A_s f_s)/1000 \quad (2.11)$$

where;

f_m': Specified compressive strength of blockwork masonry prism

f_s: Allowable compressive stress of the reinforcement [19]

Khalaf, Hendry and Fairbairn [11] claimed that the ultimate load evaluated using the equations given by British Standards [30] and ACI 530/ASCE 5 [14] underestimated ultimate strength of reinforced masonry columns in the light of their experimental study. The authors proposed the following equation for the ultimate strength, which was derived by testing six course high reinforced concrete masonry columns. The tested columns were constructed using 400x200x200 (full and half) concrete hollow blocks.

$$P_u = [f_m'(A_g - A_s) + f_y/2(A_s)]/1000 \quad (2.12)$$

The term $0.85f_c'$ in Equation (2.9) was substituted by prism compressive strength, f_m' derived from testing three course high full and half block prisms. The contribution of the vertical steel to the ultimate strength was assumed to be based on half the yield strength, f_y of the vertical steel according to the test results.

Consequently, examining the proposed equations estimated for the calculation of ultimate strength, it can be deduced that the load contributions of block shell, infill concrete and reinforcing steel are the variables constituting the ultimate strength of the reinforced concrete blockwork masonry columns.

3. EXPERIMENTAL PROGRAM

3.1. Materials

The materials used for the construction of the column specimens are readily available on the commercial market like those used in general-purpose masonry construction. The concrete block units were supplied from a local manufacturing company.

3.1.1. Infill Concrete

Three mix designs of concrete had been prepared for the column specimens. Mix designs coded as M1, M2 and M3 were produced using the same mix proportions of aggregates but with varying water:cement (w/c) ratio in order to provide different compressive strengths (Table 3.1).

Table 3.1. Mix designs for infill concrete

COMPONENTS	SPECIFIC WEIGHT (kg/dm^3)	WEIGHTS PER 1 M3 CONRETE (kg/m^3)		
		M1 (Columns C1, C2)	M2 (Columns C3, C4)	M3 (Columns C5, C6)
NS (Natural Sand)	2.58	509	509	490
CSS (Crushed Stone Sand)	2.60	312	312	300
NO1 (Crushed Stone)	2.60	458	458	441
NO2 (Crushed Stone)	2.60	550	550	529
Cement (PC 42.5)	3.15	300	300	270
Water	1.00	180	225	216
TOTAL		2309	2354	2246

The maximum particle size of aggregates D_{max} to be used for concrete should be less than 1/5 of the minimum dimension of the concrete cross-section and 3/4 of the distance between two reinforcements according to Turkish Standards (TS 500) [31]. D_{max} of the aggregates used for the experiment was 16 mm which satisfied TS 500 [31].

The mix proportions of the aggregates given below were arranged such that the grading curve of the aggregate mixture lied between the limiting curves A_{16} and C_{16} for maximum particle size, D_{max} of 16 mm in TS 706 [32].

Grading curve of the aggregate mixture given in Table 3.2 conformed the requirements of TS 706 for aggregates of maximum particle size 16 mm except for sieve size 0.25 mm. Although the minimum value of percent Passing for sieve size 0.25 mm exceeded the value of the mixture, grading curve mix was satisfactory for the infill concrete which should have higher workability than ordinary structural concrete (Figure 3.1).

Table 3.2. Sieve analysis for concrete aggregates

SIEVE SIZE	% PASSING				
	NS	CSS	NO1	NO2	AGGREGATE MIXTURE*
0.25 mm	2	4	0	0	1.2
0.5 mm	98	9	0	0	29.0
1 mm	99	13	0	0	29.9
2 mm	100	57	0	0	37.7
4 mm	100	98	6	0	46.2
8 mm	100	100	71	1	63.1
16 mm	100	100	100	100	100.0
Fineness Modulus (m)	2.01	4.19	6.23	6.99	5.24

* Aggregate proportions of the mixture by volume is; 28 percent NS, 17 percent CSS, 25 percent NO1 and 30 percent NO2

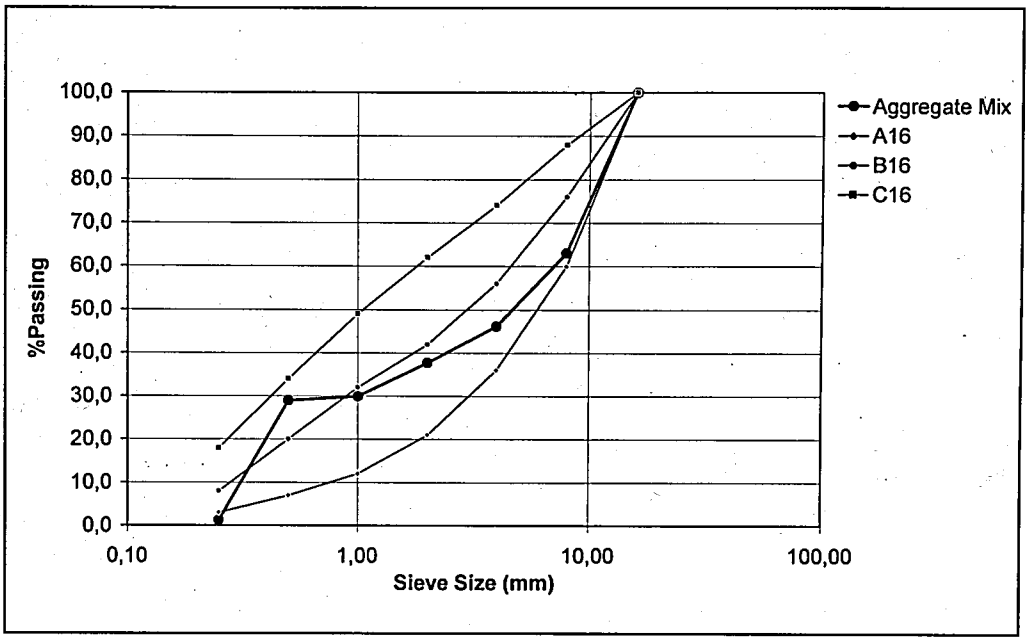

Figure 3.1. Grading curve of aggregate mixture and TS 706 requirements [32]

Volume of each mix design of concrete used for two columns and cylinder specimens, was 125 dm^3. Three cylinder specimens of D = 15 cm and H = 30 cm were cast for each mix design which had been cured under the same conditions with the column specimens for 28 day strength test. Concrete was prepared in a concrete mixer of 250 dm^3 capacity and slump of each mix design was measured by Abrams Cone at the same time (Figure 3.2 and Figure 3.3). Table 3.3 gives w/c ratios, slump values and experimental average cylinder compressive strengths of mix designs M1, M2, M3.

Table 3.3. Mix design characteristics of the infill concrete

MIX DESIGN CHARACTERISTICS	M1	M2	M3
water/cement ratio	0.69	0.77	0.73
Slump	2 cm	15 cm	2 cm
Cylinder compressive strength fc' (28 Days)	31.48 MPa	21.96 MPa	28.23 MPa
Column numbers	C1, C2	C3, C4	C5, C6

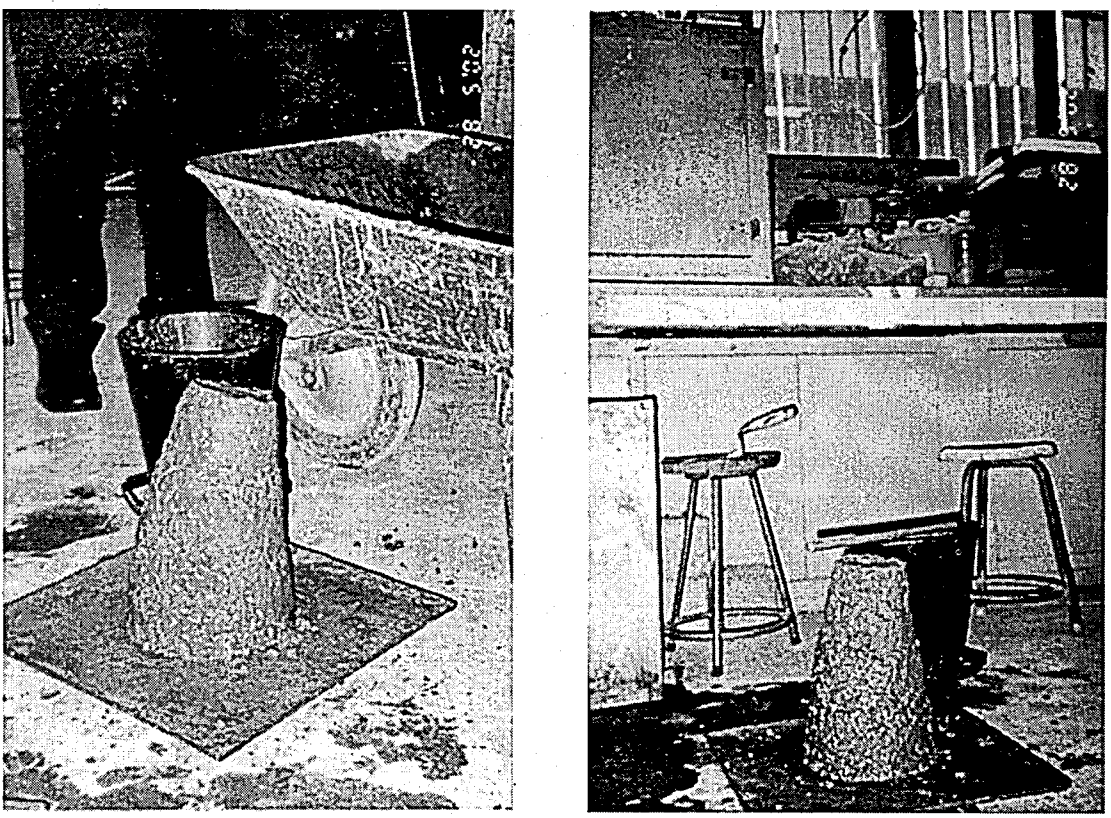

Figure 3.2. Slump tests for the mix designs, M1 and M3

Figure 3.3. Slump tests for the mix design M2

The grout prepared for masonry construction must have high slump values (e.g. 20 cm) in order to ensure the necessary workability and complete filling of the voids of concrete masonry units, in contrast to normal concrete [13]. The mix designs produced for the test had varying slump values, which were dependent on w/c ratios and the aimed strengths. Table 3.4 presents 28 day standard cylinder compressive strength values of the infill concrete specimens.

Table 3.4. Compressive strength of concrete cylinder specimens

SPECIMEN NO.		MAXIMUM LOAD (kN)	COMPRESSIVE STRENGTH (MPa)
M1 (C1, C2)	1	570.10	32.26
	2	544.99	30.95
	3	553.96	31.23
	AVERAGE	**556.35**	**31.48**
M2 (C3, C4)	1	360.80	20.42
	2	419.90	23.76
	3	383.40	21.69
	AVERAGE	**388.03**	**21.96**
M3 (C5, C6)	1	464.60	26.29
	2	562.10	31.81
	3	469.60	26.58
	AVERAGE	**498.77**	**28.23**

3.1.2. Concrete Block Units

The concrete block units are normal weight hollow loadbearing blocks manufactured by the prefabrication factory according to ASTM C90 [33]. The physical and dimensional properties of the two core hollow concrete block units and the bond beam units are given in Table 3.5, Figure 3.4 and Figure 3.5.

Table 3.5. Physical properties of concrete block units

PROPERTIES	STANDARD HOLLOW CONRETE BLOCK UNIT	BOND BEAM UNIT
L (mm)	390	390
B (mm)	190	190
H (mm)	190	190
BLOCK WEIGHT (kg)	17.70	16.95
DENSITY (kg/dm^3)	2.33	2.27
MAXIMUM WATER ABSORPTION	5.81	5.76

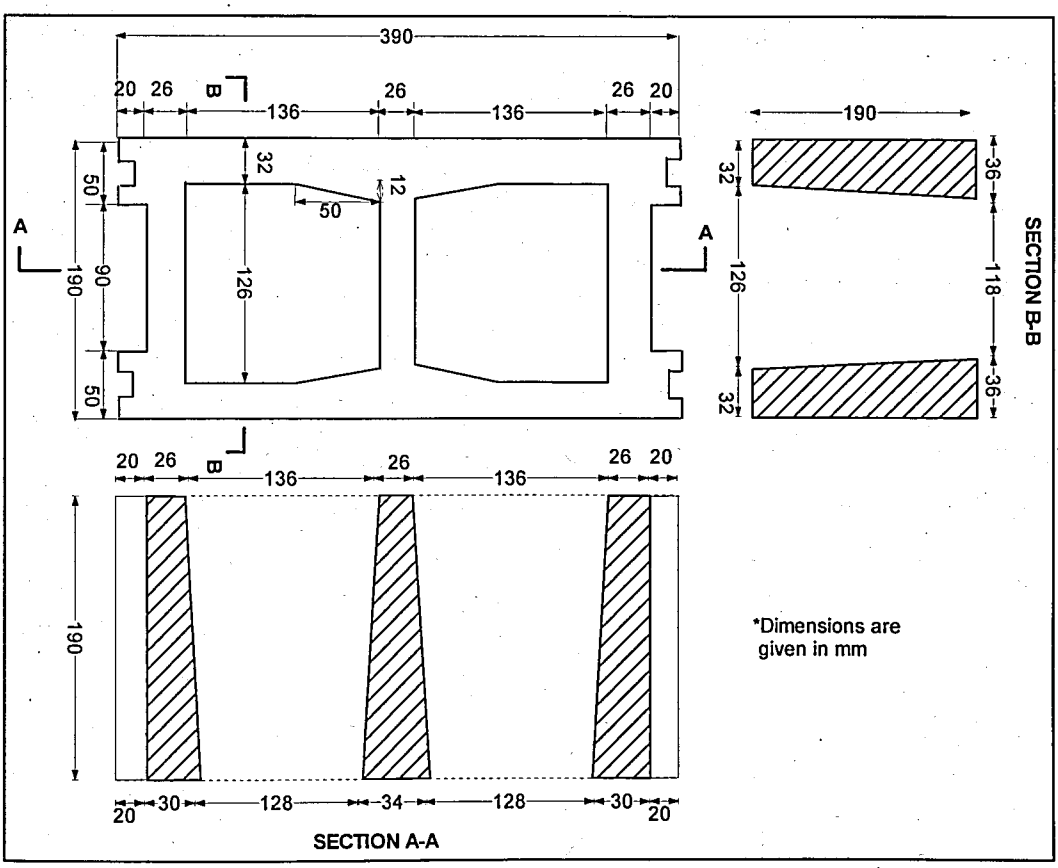

Figure 3.4. Dimensions of hollow concrete block units

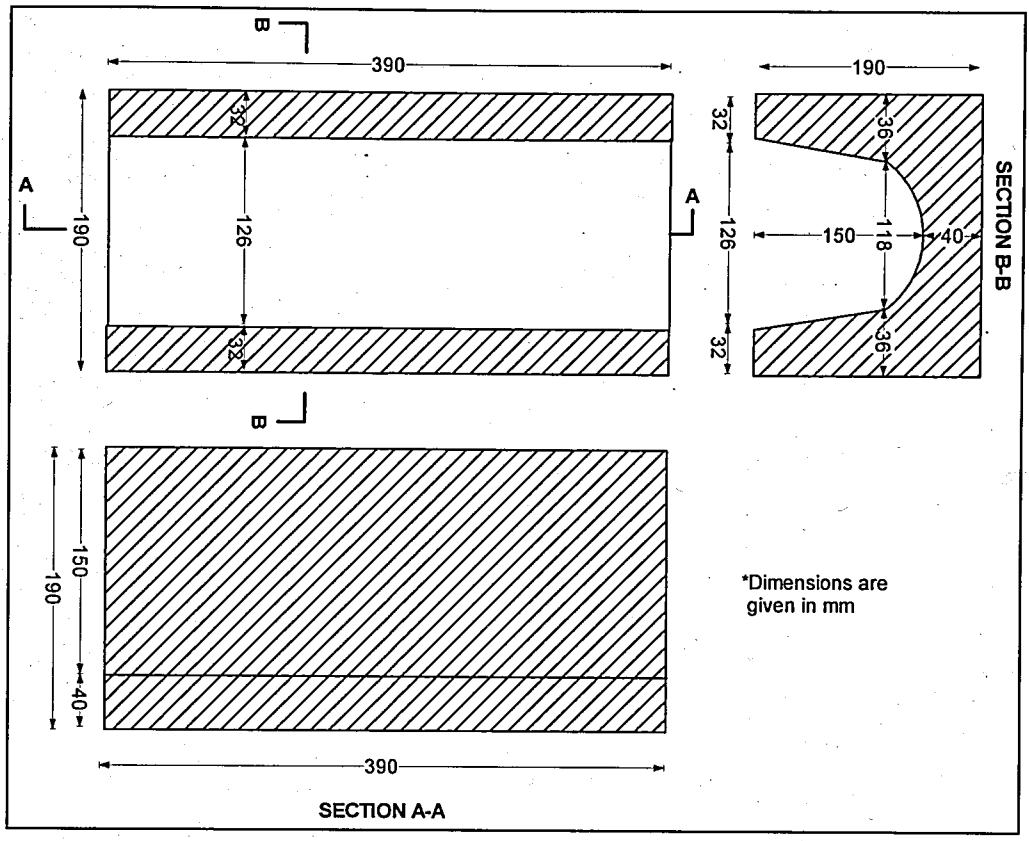

Figure 3.5. Dimensions of bond beam units

Additionally, the compressive strength tests of concrete block units had been carried out by the manufacturer in accordance with ASTM C140 [34]. The results are given in Table 3.6. The compressive strength of the concrete block unit is important because of the following reasons;

- Higher strength gives better durability,
- Unit strength tests together with mortar strength tests can serve as the basis for determining the masonry compressive strength [13].

Concrete masonry products are defined as solid or hollow depending on whether they contain more or less than 75 percent net solid horizontal cross sectional area [13]. The concrete block units used in this experiment were hollow concrete units depending on the classification given by ACI 530/ASCE 5/TMS 402 [14].

Table 3.6. Compressive strength test results of block units

BLOCK TYPE	7 Day ultimate load (kN)	7 Day compressive strength (MPa)	28 Day ultimate load (kN)	28 Day compressive strength (MPa)
Standard hollow concrete block unit	603.70	15.02	687.65	17.11
Bond beam unit	570.83	14.21	650.21	16.19

The bond beam units used in this study are manufactured for the purpose of constructing lintels or beams in general masonry structures. The bond beam concrete units were placed under each column that was composed of totally nine blocks in this study. The function of the bond beams for column construction was to enable to fix the reinforcements and to clear the mortar dropping in the column as the rest of the blocks were laid.

3.1.3. Mortar

Two mortar batches, H1 and H2 were prepared for column construction taking requirements of TS 2848 [35] and TS 2717 [36] into account. TS 2848 [35] classifies the mortar to be used for masonry in five groups according to volumetric proportions of the materials as given in Table 3.7. The mortar prepared for the experiment was Type A which had cement:sand ratio by volume as 3. Also, masonry sand used for mortar production conformed the granulometrical requirements of TS 2717 [36] as given in Table 3.8. The masonry sand falls into coarse sand group as a result of the sieve analysis according to TS 2717 [36] (Table 3.8).

Table 3.7. Mortar types classified with respect to types and proportions of components [35]

MORTAR	TYPE	MORTAR COMPONENT AND NUMBER				
		Sand (1.3)*	Cement (1.2)*	Masonry Cement (1.0)*	Lime Putty (1.3)*	Powdered Lime (0.6)*
		1	2	3	4	5
A	--	3	1	-	-	-
B	1	4	1	-	-	-
	2	4	1	0.5	-	-
	3	4	1	-	-	0.5
	4	4	1	-	-	1
C	1	7 – 9	1	2	-	-
	2	5	1	-	-	-
	3	5	1	-	1	-
D	1	6 – 8	1	-	2	-
	2	6 – 8	1	-	-	3
	3	2 – 3	-	1	-	-
E	--	3	-	-	1	-

*Volume Weights in kg/dm^3
Proportions are given in volumes

Table 3.8. Sieve analysis of masonry sand

SIEVE SIZE	8 mm	4 mm	2 mm	1 mm	0.5 mm	0.25 mm	0.125 mm
% PASSING	100	94.3	78.8	61.9	41.1	15.3	4.7

Table 3.9. Granulametrical requirements for masonry sand [36]

TYPE		% Passing by Weight		
		Fine Sand 0/2	Medium Sand 0/4	Course Sand 0/8
Sieve Size	8	-	-	100
	4	-	100	90 – 100
	2	100	90 - 100	70 – 95
	1	90 – 100	40 - 85	35 – 75
	0.500	*	*	25 – 55
	0.250	*	*	10 – 30
	0.125	10 – 25	10 – 25	2 – 10
Fineness Modulus		1.40 - 2.30	1.80 - 2.90	-
* Not Limited				

Two mortar batches of 30 dm^3 were prepared using the mix proportions given in Table 3.10. Each batch was used within 3 hours to insure the necessary workability of the mortar being used.

Table 3.10. Mix proportions by weight and volume

	Weight per 1 m^3 (kg)	Volume (m^3)	Density (kg/dm^3)
Cement	400	333.33	1.20
Sand	1300	1000	1.30
Water	250	250	1.00

Six 4.00 x 4.00 x 16.00 cm^3 specimens were cast for each mortar batch in order to obtain 28 day compressive strength of the mortar. TS 2848 [35] specifies minimum compressive strength for mortar Type A as 14.71 MPa, which was conformed by mortar batch, H2. Compressive strength of H1 mortar specimens was lower than minimum strength for mortar Type A (Table 3.11). The twelve specimens of mortar were stored in steel moulds for 24 hours and then were cured in water. All of the mortar specimens were

tested at the 28th day after they had been cast. The compressive strength of mortar batches are listed in Table 3.12.

Table 3.11. Minimum compressive strength of mortar [35]

MORTAR	MINIMUM COMPRESSIVE STRENGTH	
	kgf/cm^2	N/cm^2
A	150	1471
B	110	1079
C	50	490
D	20	196
E	5	49

Table 3.12. Compressive strength of mortar specimens

SPECIMEN NO.		COMPRESSIVE STRENGTH, f_{mr}' (MPa)
H1 (C1, C2, C3)	1	11.65
	2	11.65
	3	12.26
	4	14.72
	5	18.39
	6	15.94
	AVERAGE	**14.10**
H2 (C4, C5, C6)	1	15.33
	2	15.94
	3	15.94
	4	17.78
	5	19.01
	6	19.01
	AVERAGE	**17.17**

3.1.4. Reinforcement

4Φ10 vertical bars and Φ8 lateral ties were used for the construction of columns which were all deformed reinforcing bars with the minimum yield strength value of 420 MPa.

According to ACI 530/ASCE 5/TMS 402 [14], the percentage of vertical column reinforcement should not be less than $0.0025A_n$ nor exceed $0.04A_n$ and the minimum number of bars should be 4. Vertical reinforcements of 4Φ10 deformed bars conform the stated requirements which also enable a comparison of strength characteristics with reinforced columns.

Lateral ties of Φ8 deformed bars were bent to 135° degree turn with an extension of 6 bar diameters at the free end of the bars conforming ACI standards [14]. Lateral tie detailing of masonry columns is given in Figure 3.6 and Figure 3.7.

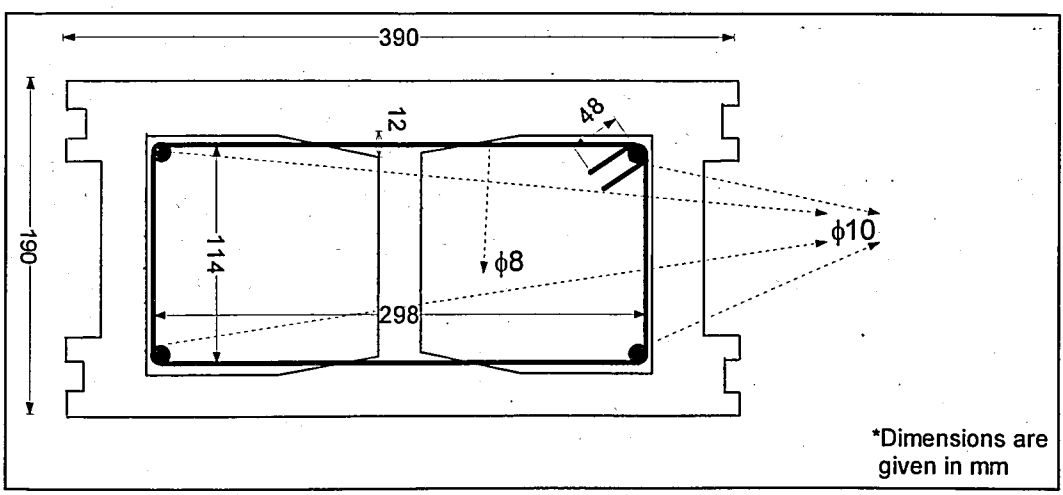

Figure 3.6. Lateral tie detailing of the columns

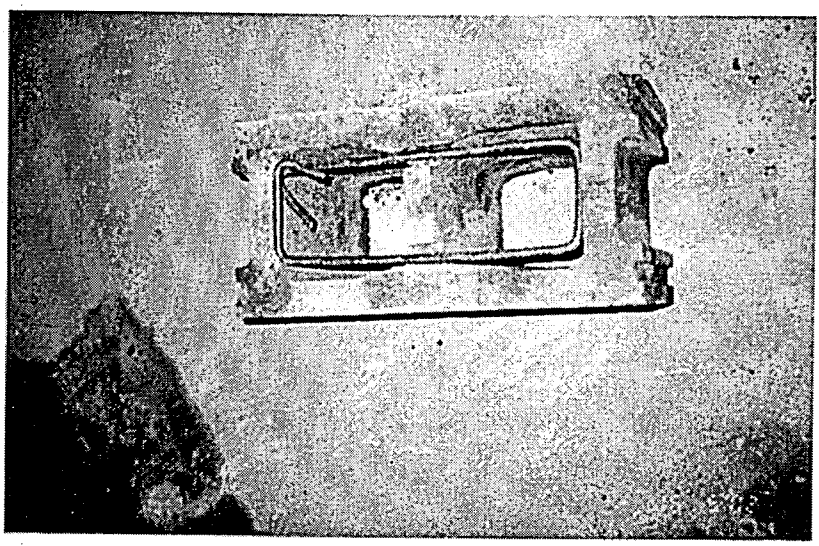

Figure 3.7. Placement of lateral ties into the hollow blocks

Lateral ties were embedded into the cores of the standard blocks whose midwebs were cut out by diamond saw to enable the lateral ties to be placed into the blocks. Thus, matching of mortar joints and the lateral ties was avoided [11] and lateral tie spacing was kept a constant distance of 190 mm throughout the height of each column. Additionally, vertical bars and lateral ties were connected to each other with wires. A previous study had shown that placing lateral ties at the mortar joints causes a high concentration of tensile splitting stresses around the ties, resulting in a reduction in the compressive strength of the masonry column [8].

The reason of reinforcing the columns with vertical bars was to increase the axial load carrying capacity of the columns. Also, lateral ties were used to provide confining effect to the infill concrete.

3.2. Column Fabrication

The reinforced blockwork masonry columns were constructed as fully bedded (entire cross-section of the concrete block units were covered with mortar) and stack bonded (placement of units is such that head joints in successive courses are vertically aligned) by an experienced mason. Six column specimens were prepared for the experiment by using 190 x 190 mm x 390 mm cross section standard load-bearing concrete hollow block units

and bond beam units. The reinforced masonry columns had mortar joints of 10 mm thickness and they were all 9 course high with an h/d ratio of 9.42. This value was satisfactory to ensure that the slenderness would not effect the test to be carried out under axial loading.

Each base block of the columns was a bond beam that did not have end shells and the midweb. The geometry of the bond beams made it possible to clear any mortar dropping during column construction and to fix the vertical bars to the first lateral tie. The rest of the blocks were standard two core hollow block units whose midwebs were cut 20 mm deep and 20 mm wide grooves. These grooves were necessary to fix lateral ties into the cores of the hollow blocks and to avoid lateral ties to match with the mortar joints [11].

The mortar used for the construction of the nine course high reinforced blockwork masonry columns was prepared as two identical mortar batches, H1 and H2 according to TS 2848 [35] with the details being described in Section 3.1.3.

Before adding the water needed for mortar paste, sand and cement had been mixed until obtaining a dry homogeneous mixture. The water was then added to the dry mixture gradually to obtain the consistency of the mortar paste. Block surfaces were prewetted in order to reduce water suction and to prevent premature stiffening of mortar [13].

After fixing the vertical bars and the first lateral tie into the bond beam, the mortar was laid on the end shell of the bond beam. The remaining eight hollow block units were laid one on other by;

- passing their cores through the fixed vertical bars,
- fixing the lateral tie into each block and to the vertical bars,
- laying the mortar with 10 mm thickness onto each block.

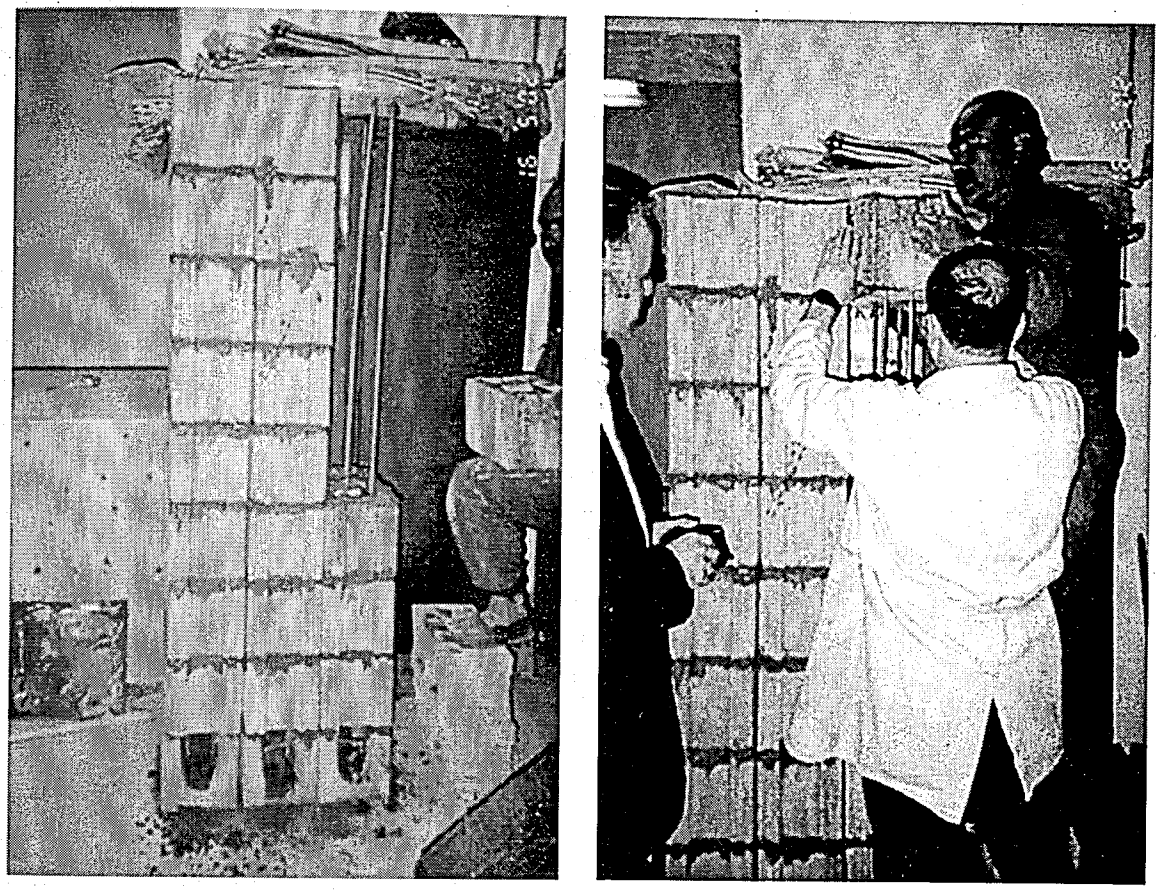

Figure 3.8. Construction of the columns

as given Figure 3.8. The lateral ties and the vertical bars were attached to each other with wires before the placement of the following block onto the other block units. The details of the reinforcements were as described in Section 3.1.4.

After construction of the nine course high reinforced hollow block columns, they were cured under ambient conditions for 7 days to allow the mortar joints to gain their strength.

The columns were then filled with 3 different types of infill concrete which were prepared in a 250 dm^3 capacity concrete mixer. After wetting the columns, the infill concrete being prepared according to TS 706 standards [32], was cast into the cores of the corresponding columns and compacted in layers within the hollow blocks.

While casting the infill concrete, U shaped steel bars were placed onto each column in order to assist the mobilization of the heavy columns by the crane. These steel bars were then cut off after placing each column under the testing pump. After casting, the columns were cured by water for 7 days and left under ambient laboratory conditions for the remaining 21 days.

Consequently, six reinforced blockwork columns were constructed with varying mortar and concrete properties but with the same reinforcement details. Configuration of each column is described in Table 3.13 briefly. A brief sketch of column specimens and dimensions are shown in Figure 3.9.

Table 3.13. Column configuration

COLUMN NO. PROPERTIES	C1	C2	C3	C4	C5	C6
INFILL CONCRETE TYPE	M1	M1	M2	M2	M3	M3
MORTAR TYPE	H1	H1	H1	H2	H2	H2
VERTICAL REINFORCEMENT	4Φ10	4Φ10	4Φ10	4Φ10	4Φ10	4Φ10
LATERAL TIE	Φ8	Φ8	Φ8	Φ8	Φ8	Φ8
LATERAL TIE SPACING	190 mm	190 mm	190 mm	190 mm	190 mm	190 mm

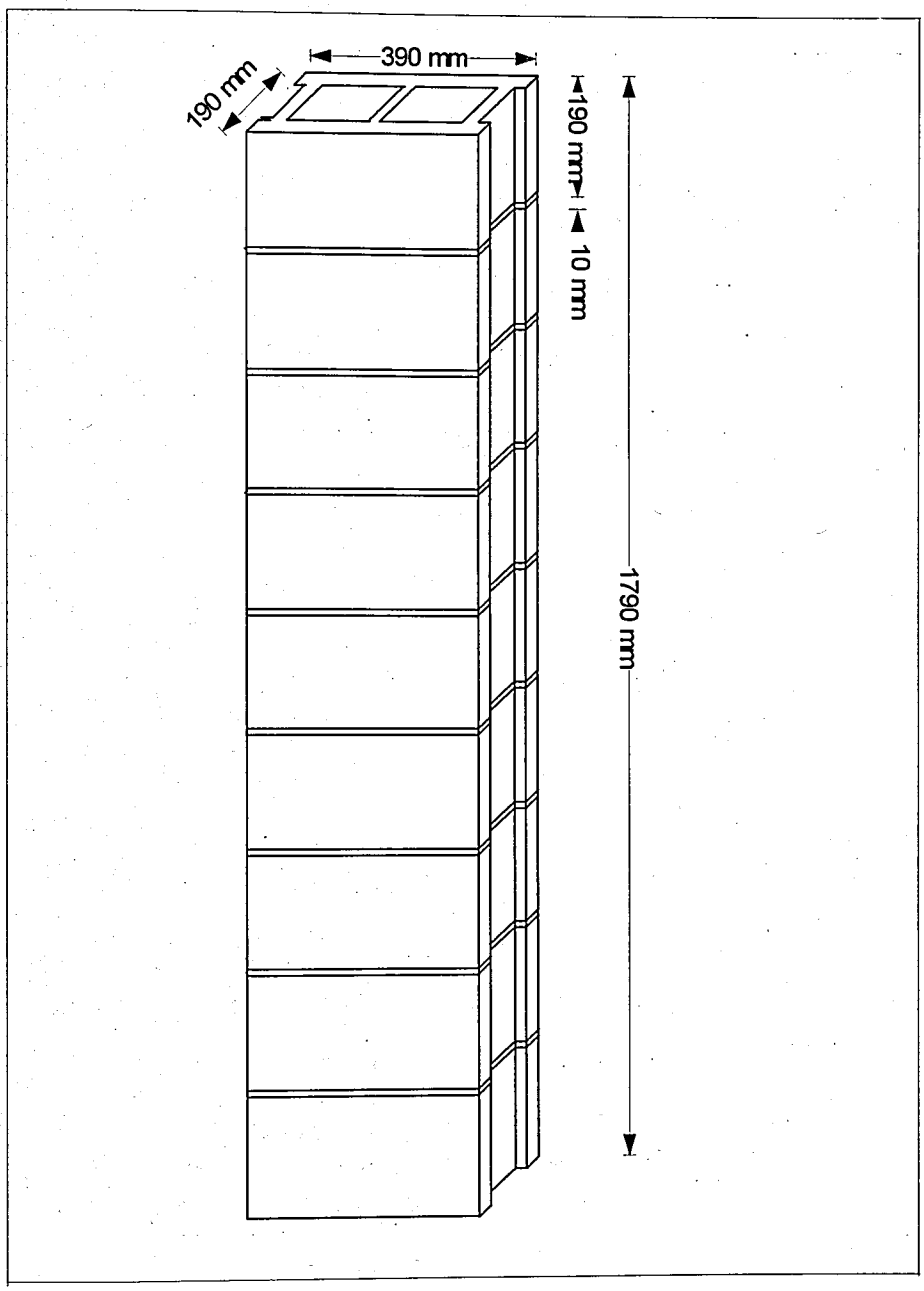

Figure 3.9. Column specimen dimensions

3.3. Instrumentation

The vertical deflections of the columns under incremental loading were recorded by the linear variable differential transducers (LVDTs) at every second. These transducers were fixed on pin supports, which were attached on midheight of third and seventh blocks with thin steel pipes about 80 cm in length. LVDT1 was mounted on the end webs and LVDT2 was mounted on the face shells of the block units.

After positioning the column under the testing machine with the help of the crane, the U shaped steel bars that were embedded on the top surface were cut using a disc grinder. A steel plate with 50 mm thickness was placed onto the column in order to provide the uniform distribution of incremental loading.

Vertical load was applied by two heads of 1000 kiloNewtons (kN) capacity hydraulic testing machine. Testing machine was operated through the hydraulic pump for which 20 bars of pressure corresponded to 70.70 kN of loading. At each level of load increments, the data collected by LVDTs were filed in computer.

To prevent any possible damage to the instruments, LVDTs were removed just before column failure. Test mechanism related to the experimental procedure is shown in Figure 3.10 and Figure 3.11.

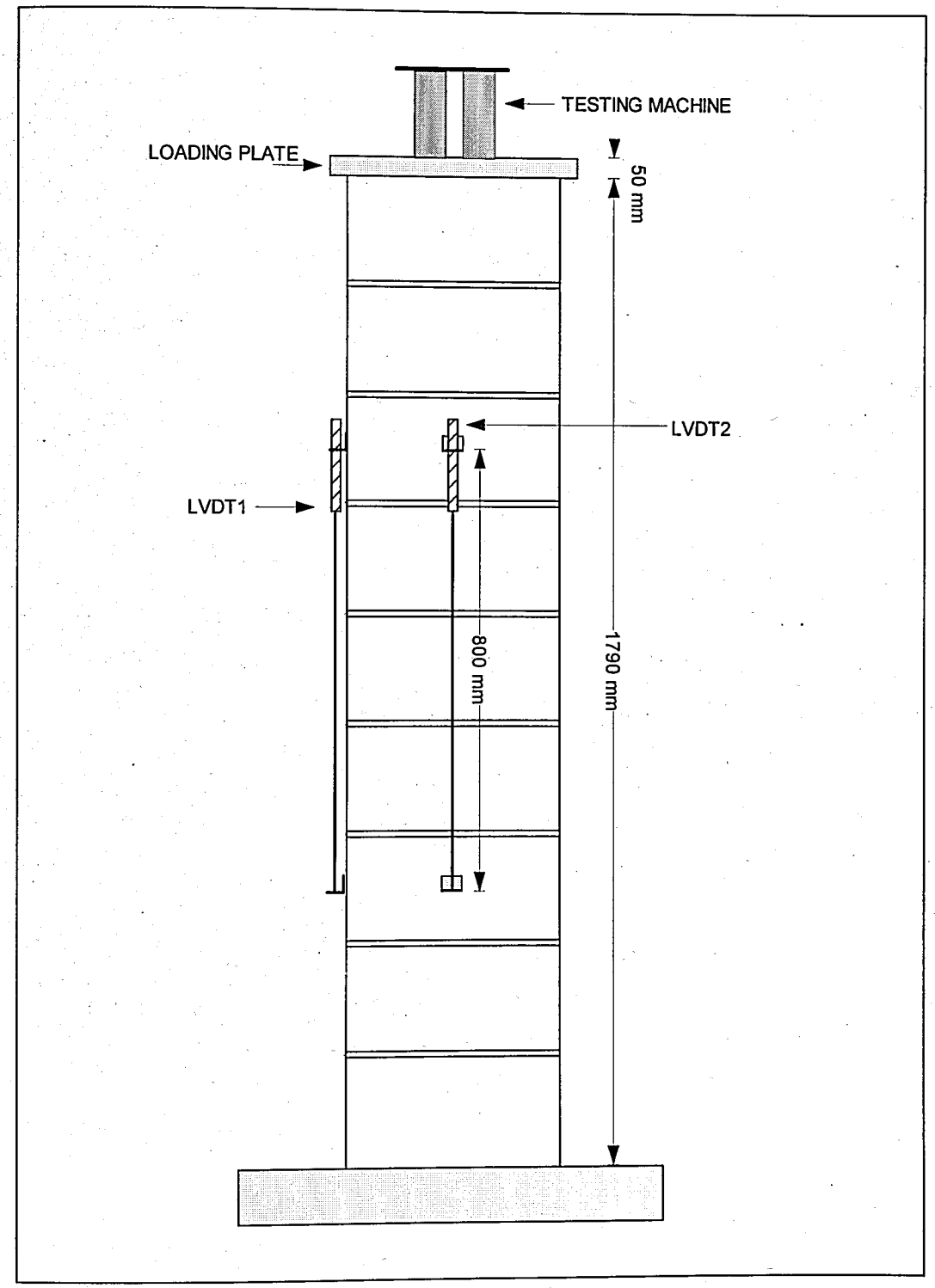

Figure 3.10. Test mechanism of the columns

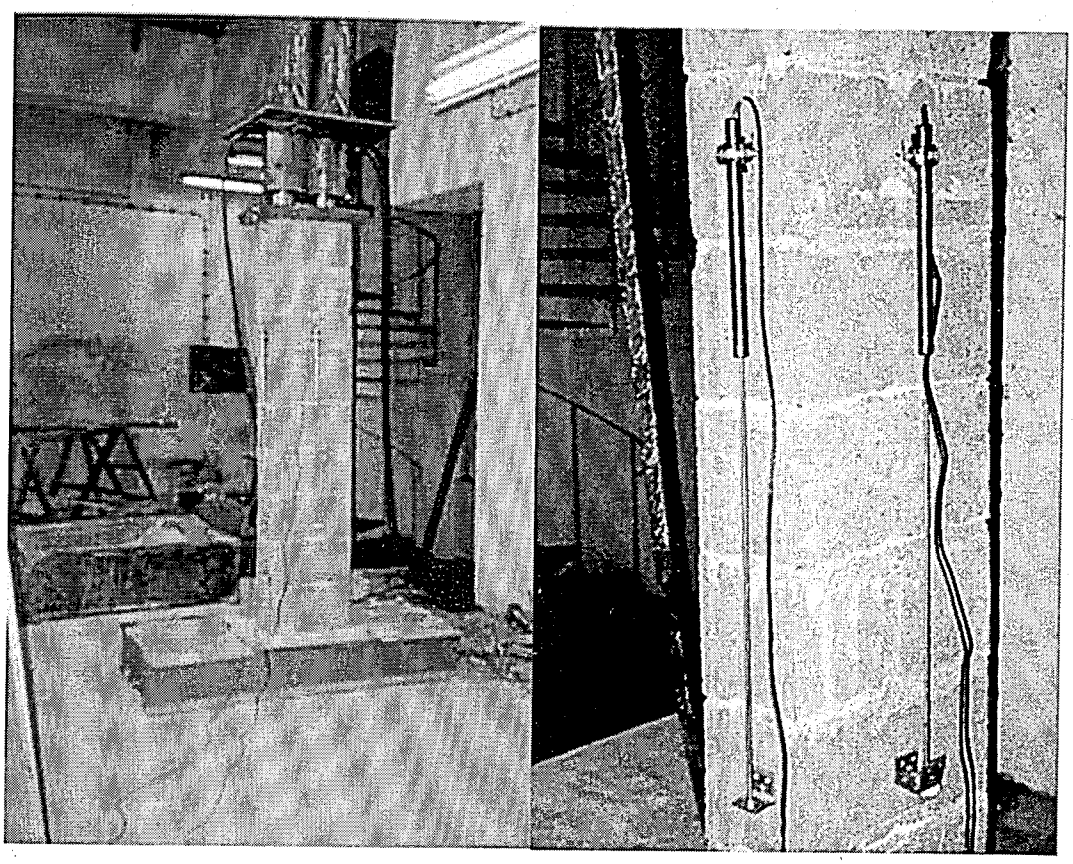

Figure 3.11. Instrumentation of the column specimens

4. NUMERICAL MODELLING OF REINFORCED CONCRETE BLOCKWORK MASONRY COLUMNS

4.1. Introduction

Nonlinear finite element modelling of the reinforced concrete masonry columns has been developed by using LUSAS 13.3 [37] which is an associative feature based modeller program. The model geometry is implemented in terms of features, which are subdivided into finite elements in order to perform the analysis by the program. [37].

The computer program used for modelling has the advantage of a preprocessor for meshing the system, assigning the material properties and models; and defining the loading conditions; and a postprocessor for graphical presentation of results.

The constituents of reinforced masonry column; concrete block, infill concrete, mortar and reinforcement were represented by different elements, which enabled material properties to be assigned separately within the model.

The generation of the finite element mesh was conducted with the assumptions that the fillets at the edges of cores were squared off and tapering of the block cross section was negligible in order to simplify the complexity of the geometry.

Three dimensional nonlinear finite element modelling of the columns was based on the failure models representing the nonlinear behavior of constituent materials that were available in the computer program. Actual behavior of concrete materials depends on the physical and mechanical properties of aggregates and cement paste; and nature of loading. Complicated mathematical models are necessary to describe the strength of real materials under various loading conditions. Section 4.2 describes the failure criteria of isotropic materials under various stress conditions.

4.2. Failure Surfaces and Models

The strength of concrete under multiaxial stresses is a function of the state of stress. The interaction of various components of state of stress should be considered in order to determine strength of concrete elements.

Failure criteria of isotropic materials based on state of stress are defined by functions of principal stresses, which are independent of the choice of coordinate system.

$$f(\sigma_1, \sigma_2, \sigma_3) = 0 \tag{4.1}$$

Equation (4.1) is inadequate to establish failure criteria concerning multiaxial state of stress due to the difficulties to supply a geometric and physical explanation of failure. Principal stress invariants I_1, J_2 and J_3 are used for expressing principal stresses σ_1, σ_2 and σ_3 in order to formulate various failure criteria of materials. Thus, Equation (4.1) can be replaced by;

$$f(I_1, J_2, J_3) = 0 \tag{4.2}$$

The principal-stress invariants can be expressed by the following equations;

$$I_1 = \sigma_x + \sigma_y + \sigma_z = \sigma_{ii} \tag{4.3}$$

$$J_2 = \tfrac{1}{2}(s_1^2 + s_2^2 + s_3^2) = \tfrac{1}{6}\left[(\sigma_1 - \sigma_2)^2 + (\sigma_2 - \sigma_3)^2 + (\sigma_3 - \sigma_1)^2\right] \tag{4.4}$$

$$J_3 = \tfrac{1}{3}(s_1^3 + s_2^3 + s_3^3) = s_1 s_2 s_3 \tag{4.5}$$

General shape of a failure surface for an isotropic material is described by its cross sections perpendicular to hydrostatic axis with ξ=constant and the intersection curves between failure surface and the meridian plane containing hydrostatic axis with θ=constant. Hydrostatic axis d is the diagonal axis making equal angles with the principal axes in the principal stress space (Figure 4.1).

The diagonal d axis is the hydrostatic stress state and the planes perpendicular to the d axis represent the pure shear state of the stress named as deviatoric planes. θ is the angle of similarity defining the projection of the deviatoric plane on σ_1 axis as shown in Figure 4.2.

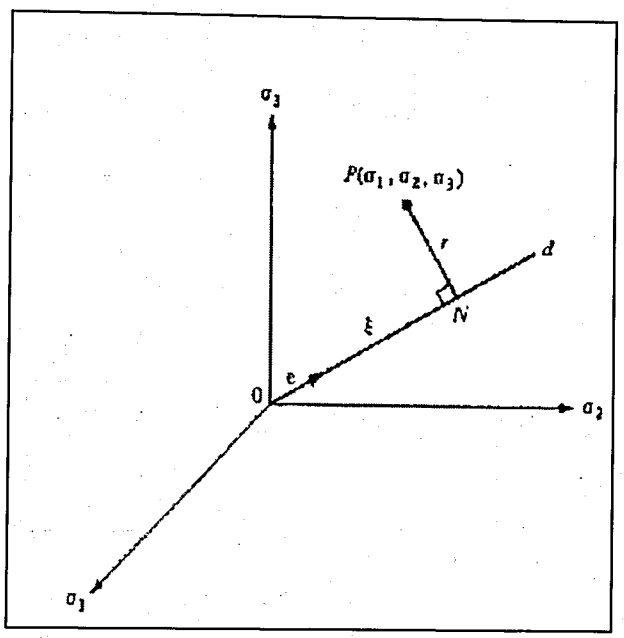

Figure 4.1. Representation of stress in principal stress state [38]

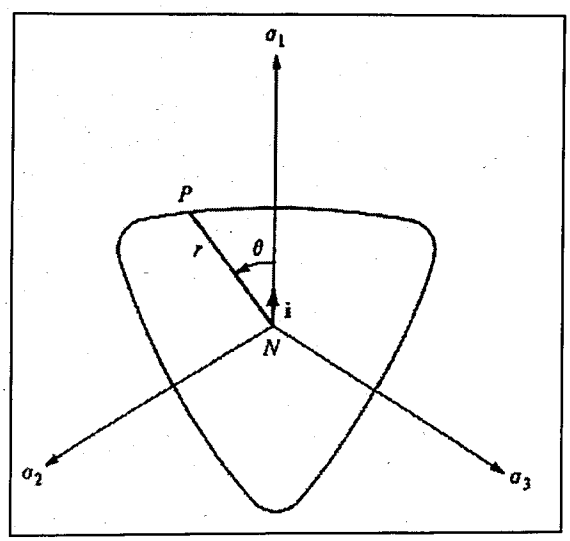

Figure 4.2. Deviatoric plane in the principal stress space [38]

Using the fact that the cross sectional shapes of the failure surface have threefold symmetry due to the material isotropy, it is necessary to perform experiments between $\theta=0$ and $\theta=60^0$ sectors.

$\theta=0^0$ and $\theta=60^0$ sectors are the two extreme conditions corresponding to tensile meridian and compressive meridian, respectively (Figure 4.3). The failure curve is nearly triangular for tensile and small compressive stresses (corresponding to small values of ξ near the π plane). It becomes increasingly more circular for higher compressive stresses (corresponding to high hydrostatic pressures or increasing ξ).

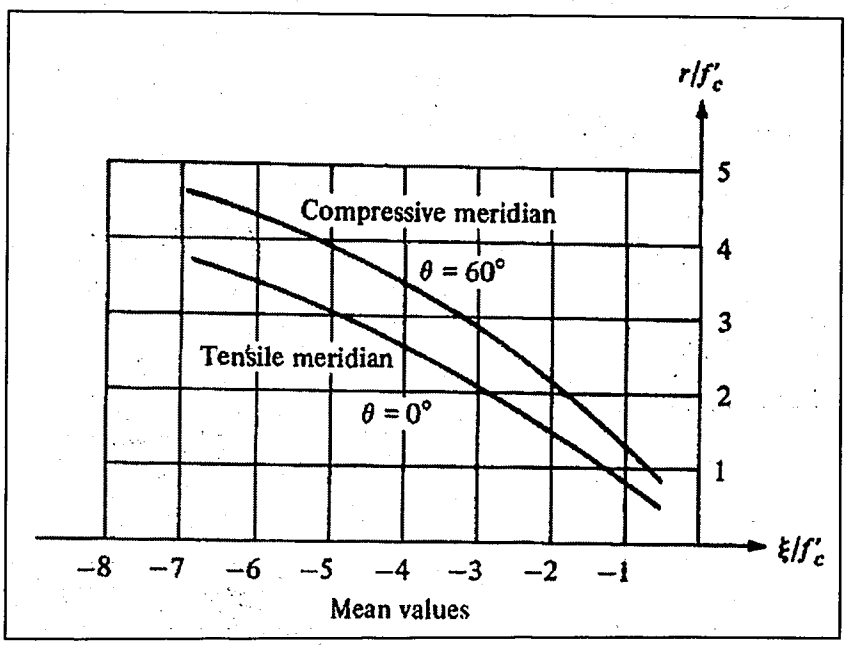

Figure 4.3. General character of meridians based on the experiments of Launay *et al.* [39]

4.2.1. Shearing-Stress Criteria

The effect of hydrostatic pressure on the yield value of the material is negligible for metals and concrete under high pressure. This condition causes the shearing stress to play the major role on yielding of the metals. Tresca and Von Mises are the failure criteria based on the key variable "maximum shearing stress".

Tresca yield criterion states that the yielding of the material starts when the maximum shearing stress at a point reaches a critical value k, which is determined experimentally as half of the yield stress σ_y for reinforcing steel. Mathematical definition of the criterion is given as;

$$\max(\tfrac{1}{2}|\sigma_1-\sigma_2|,\tfrac{1}{2}|\sigma_2-\sigma_3|,\tfrac{1}{2}|\sigma_3-\sigma_1|)=k \tag{4.6}$$

The k value is the yield stress in pure shear, which can be expressed as;

$$\frac{\sigma_1-\sigma_2}{2}=\frac{1}{\sqrt{3}}\sqrt{J_2}\left[(\cos\theta-\cos(\theta+\frac{2\pi}{3})\right]=k \tag{4.7}$$

for $0^0 \le \theta \le 60^0$. Also, Tresca criterion can be expressed as;

$$f(J_2,\theta)=\sqrt{J_2}\sin(\theta+\frac{\pi}{3})-k=0 \qquad \text{or} \tag{4.8}$$

$$f(r,\theta)=r\sin(\theta+\frac{\pi}{3})-\sqrt{2}k=0 \tag{4.9}$$

The maximum shear stress criterion corresponds to a prism whose cross section is a hexagon in three dimensional stress coordinate system as shown in Figure 4.4. Also, the projection of Tresca failure surface on (σ_1-σ_2) coordinate plane is the hexagon circumscribed by Von Mises ellipse as given in Figure 4.5.

Von Mises yield criterion differs from Tresca Yield Criterion that the critical value k is defined as;

$$\tau_{oct}=\sqrt{\tfrac{2}{3}J_2}=\sqrt{\tfrac{2}{3}}k \quad \text{and} \quad \sigma_y=\sqrt{3}k=1.732k \tag{4.10}$$

$$f(J_2)=J_2-k^2=0 \tag{4.11}$$

Von Mises yield curve is given by Equation (4.12).

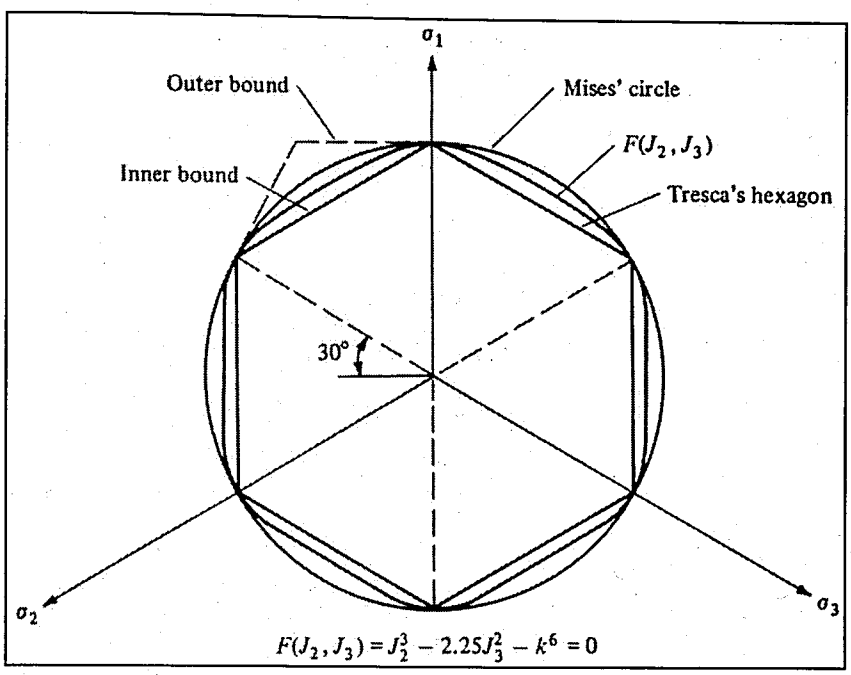

Figure 4.4. Shearing stress criteria on deviatoric plane [38]

The general yield criterion of an isotropic material on the deviatoric plane (Figure 4.4) is defined by the equation;

$$f(J_2, J_3) = J_2^3 - 2.25J_3^2 - k^6 = 0 \tag{4.12}$$

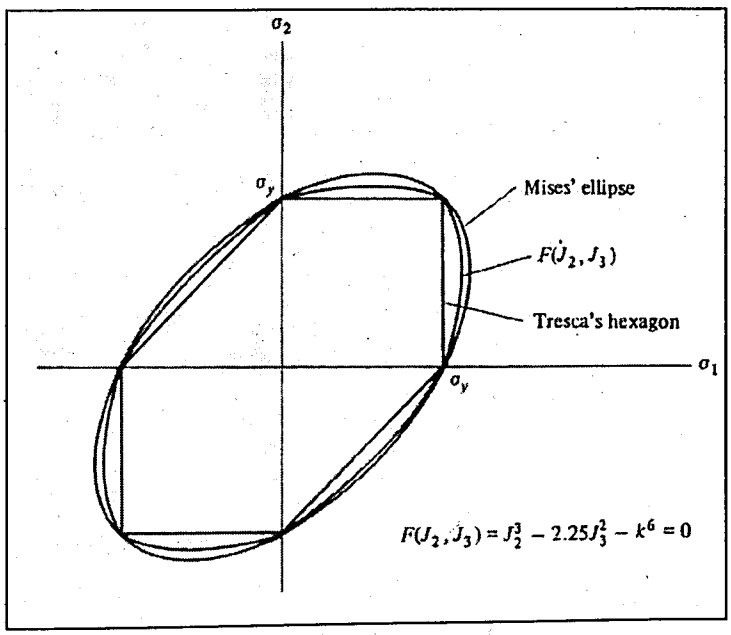

Figure 4.5. Shearing-stress criteria on the coordinate plane $\sigma_3 = 0$ [38]

4.2.2. Mohr-Coulomb Criterion

Mohr's criterion states that the failure is governed by the relation between the limiting shearing stress τ and the normal stress σ. The simplest form of Mohr's failure envelope is the straight line, given in Figure 4.6. The equation for the envelope is given by the general expression;

$$|\tau| = c - \sigma \tan\phi \tag{4.13}$$

where c is the cohesion and ϕ the internal friction angle of the material. Equation (4.14) is identical with the equations (4.15) and (4.16) which can be derived from Figure 4.6 for $\sigma_1 \geq \sigma_2 \geq \sigma_3$;

$$\sigma_1 \frac{1+\sin\phi}{2c\cos\phi} - \sigma_3 \frac{1-\sin\phi}{2c\cos\phi} = 1 \tag{4.14}$$

$$\frac{\sigma_1}{f_t'} - \frac{\sigma_2}{f_c'} = 1 \tag{4.15}$$

where; $f_c' = \dfrac{2c\cos\phi}{1-\sin\phi}$ and $f_t' = \dfrac{2c\cos\phi}{1+\sin\phi}$

Mohr-Coulomb failure criterion can be described by the following equations, alternatively;

$$f(I_1, J_2, \theta) = \tfrac{1}{3} I_1 \sin\phi + \sqrt{J_2}\sin(\theta + \frac{\pi}{3}) + \frac{\sqrt{J_2}}{\sqrt{3}}\cos(\theta + \frac{\pi}{3})\sin\phi - c\cos\phi = 0 \tag{4.16}$$

$$f(\xi, r, \theta) = \sqrt{2}\xi\sin\phi + \sqrt{3}r\sin(\theta + \frac{\pi}{3}) + r\cos(\theta + \frac{\pi}{3})\sin\phi - \sqrt{6}c\cos\phi = 0 \tag{4.17}$$

with $0^0 \leq \theta \leq 60^0$

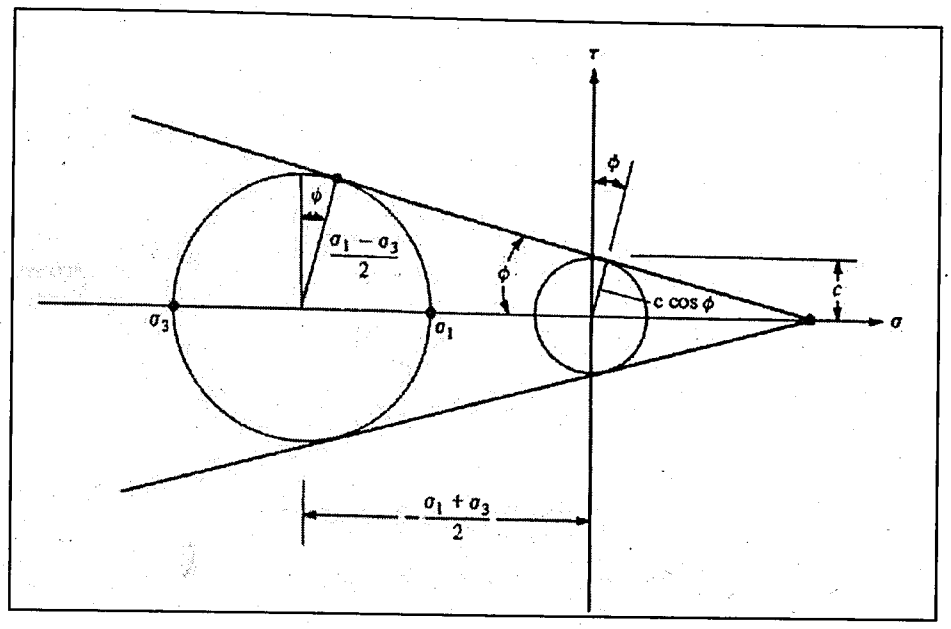

Figure 4.6. Mohr Coulomb criterion [38]

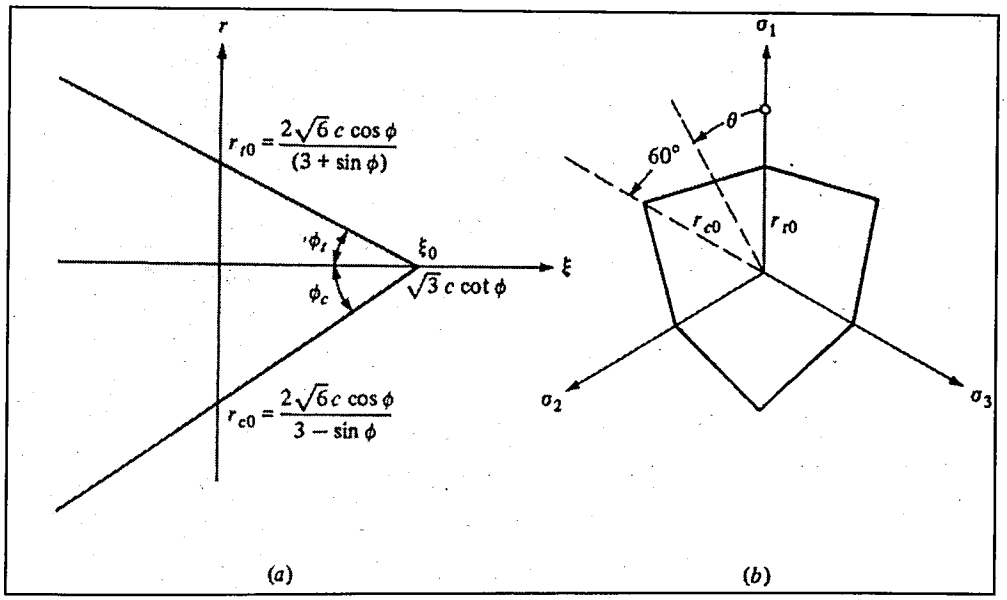

Figure 4.7. Mohr-Coulomb criterion: (a) meridian plane, $\theta = 0^0$ (b) π plane [38]

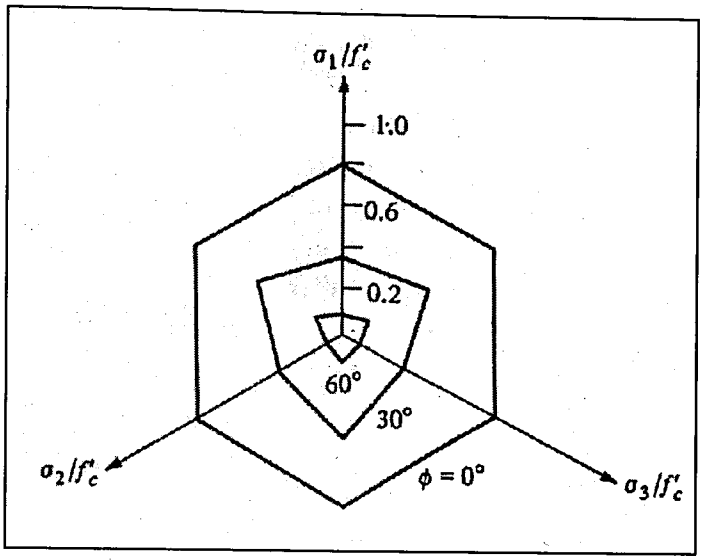

Figure 4.8. Mohr-Columb failure curves on the deviatoric plane [38]

The characteristic lengths r_{to} and r_{co} on the π plane corresponding to $\theta = 0^0$ and 60^0 in Figure 4.7 can be derived from Equation (4.17) for $\xi = 0$, $r = r_{t0}$, $\theta = 0^0$ and $\xi = 0$, $r = r_{c0}$, $\theta = 60^0$ as given by the following equations;

$$r_{t_0} = \frac{2\sqrt{6}c\cos\phi}{3+\sin\phi} = \frac{\sqrt{6}f_c'(1-\sin\phi)}{3+\sin\phi} \tag{4.18}$$

$$r_{c_0} = \frac{2\sqrt{6}c\cos\phi}{3-\sin\phi} = \frac{\sqrt{6}f_c'(1-\sin\phi)}{3-\sin\phi} \tag{4.19}$$

$$\frac{r_{t_0}}{r_{c_0}} = \frac{3-\sin\phi}{3+\sin\phi} \tag{4.20}$$

A family of Mohr Coulomb cross sections in the π plane for several values of ϕ is shown in Figure 4.8. For $\phi = 0$ ($f_c' = f_t'$) the hexagon becomes equivalent with Tresca's hexagon.

Mohr-Coulomb criterion can be combined with tensile strength cutoff for a better approximation in the tensile stress zone. In such a case, the maximum tensile strength, f_t' (experimental uniaxial tensile strength) for cutoffs is not the same with the fictitious tensile strength identified by Equation (4.16).

4.2.3. Drucker-Prager Criterion

Drucker-Prager criterion eliminates the difficulty and complications of numerical solutions of Mohr-Coulomb criterion which is caused by its hexagonal corners forming an outer bound to the general failure surface. The hexagonal pyramid shaped Mohr-Coulomb failure surface turns into a smooth conical shape for Drucker-Prager criterion in the deviatoric plane as shown in Figure 4.9. Equations expressing Drucker-Prager criterion are given as;

$$f(I_1, J_2) = \alpha I_1 + \sqrt{J_2} - k = 0 \qquad \text{or} \qquad (4.21)$$

$$f(\xi, r) = \sqrt{6}\alpha\xi + r - \sqrt{2}k = 0 \qquad (4.22)$$

where;

$\xi = I_1 / \sqrt{3}$ and $r = \sqrt{2J_2}$

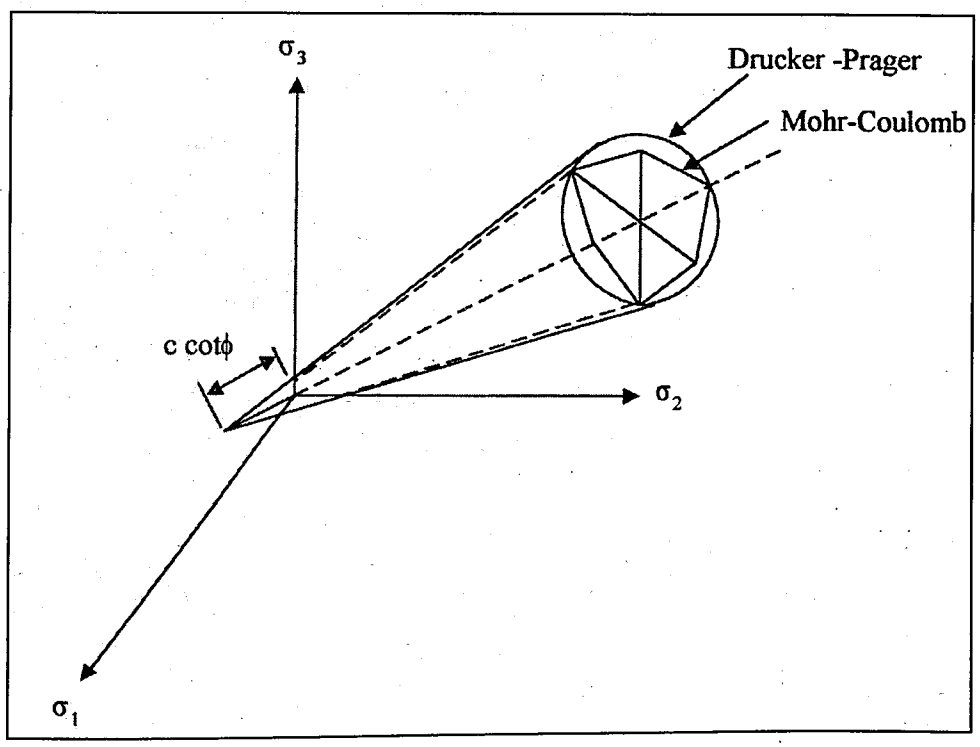

Figure 4.9. Drucker-Prager and Mohr-Coulumb criteria [37]

Drucker Prager criterion has mainly two shortcomings in connection with concrete modeling, the linear relation between ξ and r and the independence of the angle of similarity θ (Figure 4.10). Mohr-Coulomb hexagonal failure surface is approximated to Drucker-Prager cone by intersecting the failure curves along the compression meridian or the tensile meridian. The positive constants of Drucker Prager surface, α and k are derived as;

$$\alpha = \frac{2\sin\phi}{\sqrt{3}(3-\sin\phi)} \qquad k = \frac{6c\cos\phi}{\sqrt{3}(3-\sin\phi)} \tag{4.23}$$

for compressive meridian r_c, where $\theta = 60^0$ and

$$\alpha = \frac{2\sin\phi}{\sqrt{3}(3+\sin\phi)} \qquad k = \frac{6c\cos\phi}{\sqrt{3}(3+\sin\phi)} \tag{4.24}$$

for tensile meridian r_t, where $\theta = 0^0$.

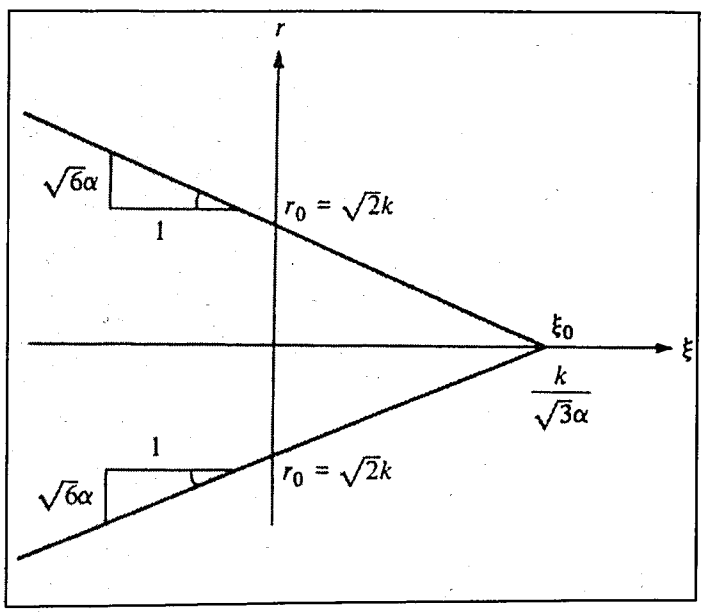

Figure 4.10. Meridian plane for Drucker-Prager criterion [38]

The previous experimental data [40, 41] show that the relation between ξ and r is nonlinear for the compression and tensile meridians. The internal friction angle of the concrete materials in the compression zone, ϕ_c has been stated to vary between 30^0 and 40^0 by plotting alternative slopes to the compressive meridian given in Figure 4.11 [42, 43]. Consequently, $\phi_c = 33.5^0$ has been used as the internal friction of the concrete blocks and the infill concrete for the implementation of the Drucker-Prager material model.

Both Mohr-Coulomb and Drucker-Prager failure criteria are applicable models for materials that exhibit volumetric plastic strains, such as concrete, rock and soils.

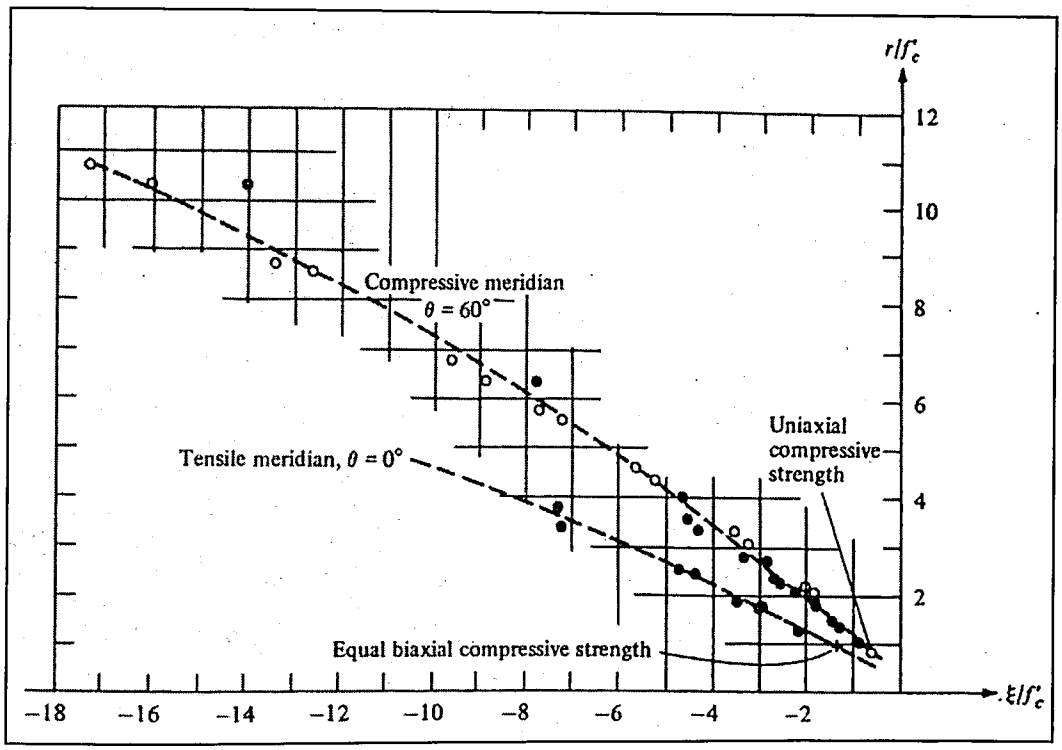

Figure 4.11. Test results along the tensile and compressive meridians [40, 41]

4.3. Solution Methods for Nonlinear Finite Element Analysis

Nonlinear analysis of materials for which the relation between the external load and the displacement is in the form of a first-order differential equation, involves a series of load increments $\{\Delta R\}_n$ and corresponding displacement increments, $\{\Delta\delta\}_n$.

The combination of the incremental method, in which the structure is loaded in small increments with an iterative process, is an optimal approach in order to satisfy the equilibrium conditions. Thus, for each incremental load on the system, the actual tangent stiffness matrix, $[K]_t$ is estimated by using the material elastoplastic tangent stiffness matrix $[D]^{ep}$ which is derived from the flow theory of plasticity. The relation is given by;

$$\{\Delta R\} = [K]_t \{\Delta\delta\} \tag{4.25}$$

After the completion of each incrementation, the residual force is calculated in order to evaluate whether the solution is completed or not. The residual force is the unbalance between internal force and the external load, which can be regarded as the part of the load that has not yet produced any displacement [37]. The residual force vector is calculated as;

$$\{\varphi(\delta)\} = \int_V [B]^T \{\sigma\} dV - \{R\} \tag{4.26}$$

The evaluation of the residual force vector and the correction of the solution are named as equilibrium iterations. The iteration procedure is carried out up to the point that the residual force is smaller than a prescribed negligible value.

Newton-Raphson iteration is one of the most favorable methods in order to achieve the convergence of each incremental load. During the iterative process, reevaluation of the stiffness matrix depends on the nonlinearity of the problem at given incrementation.

4.3.1. Solution Algorithm for the Nonlinear Finite Element Analysis

The solution of the nonlinear finite element problems consist of a series of load increments $\{\Delta R\}_n$ corresponding to the incremental displacement $\{\Delta\delta\}_n$ with the tangent stiffness matrix $[K_t]$. First incremental displacement $\{\Delta\delta\}_1$ is estimated by solving the system with a representative linear tangent stiffness matrix $[K_t]$ which does not conform the equilibrium state within the incrementation. The stress vector $\{\sigma\}_n$ and the hardening parameters ε_p^n and k^n are obtained at the end of the n^{th} loading increment. Each incremental process involves a number of iterations, which must be performed for the determination of the next point on the equilibrium path.

The evaluation of the stress vector $\{\sigma\}_{n+1}$ is summarized briefly by the following steps.

1. Incremental displacement $\{\Delta\delta\}_{n+1}$ is estimated by using the preceding tangent stiffness matrix $[K_t]_n$ and the incremental loading $\{\Delta R\}_{n+1}$ with the relation;

$$\{\Delta\delta\}_{n+1} = [K_t]_n^{-1} \{\Delta R\}_{n+1} \tag{4.27}$$

The corresponding strain vector $\{\Delta\varepsilon\}_{n+1}$ is calculated as;

$$\{\Delta\varepsilon\}_{n+1} = [B]\{\Delta\delta\}_{n+1} \tag{4.28}$$

where [B] is the strain matrix.

2. The incremental elastic stress $\{\Delta\sigma^e\}_{n+1}$ and the current elastic stress $\{\sigma^e\}_{n+1}$ is calculated as;

$$\{\Delta\sigma^e\}_{n+1} = [D]^e \{\Delta\varepsilon\}_{n+1} \tag{4.29}$$

$$\{\sigma^e\}_{n+1} = \{\sigma\}_n + \{\Delta\sigma^e\}_{n+1} \tag{4.30}$$

where $[D]^e$ is the elastic material stiffness matrix.

3. The stress invariants I_1, J_2, J_3 and θ, and the yield function $f(\{\sigma\}, \varepsilon_p, k)$ are evaluated for the stress vector $\{\sigma^e\}_{n+1}$. Using the hardening parameters ε_p^n and k^n, the yield function is expressed as;

$$f(\{\sigma^e\}_{n+1}, \varepsilon_p^n, k^n) = f_1 \tag{4.31}$$

The negative values of the yield function f_1, indicate the elastic state of stress whereas the positive values of the yield function correspond to the plastic state. The function being equal to zero defines the general form of yield surface.

4. If $f_1<0$, the system is in the elastic zone meaning that:

$$\{\Delta\sigma^p\}_{n+1} = 0 \tag{4.32}$$

$$\{\sigma\}_{n+1} = \{\sigma^e\}_{n+1} \tag{4.33}$$

The incremental $(n+1)^{th}$ solution is completed.

5. If $f_1>0$, the solution is followed by step 7 setting $f_0<0$.

6. The scaling factor r is a tool for the initiation of the iteration process involving the transition of the stress state from elastic to plastic. Figure 4.12 is a geometric interpretation of the transition. The stress state at C can be denoted as;

$$\{\sigma^c\} = \{\sigma^a\} + r\{\Delta\sigma^e\} \tag{4.34}$$

for which $r\{\Delta\sigma^e\}$ is the portion of the stress increment where the plastic behavior is first taken into account. The simplest approximate value of $r=r_1$ is;

$$r_1 = -\frac{f_0}{f_1 - f_0} \tag{4.35}$$

Evaluation of the yield function gives;

$$f(\{\sigma^a\} + r_1\{\Delta\sigma^e\}, \varepsilon_p^n, k^n) = f_2 \neq 0 \tag{4.36}$$

A better approximation of the scaling factor can be expressed as;

$$r = r_1 + \Delta r_1 = r_1 - \frac{f_2}{\left\{\frac{\partial f}{\partial \sigma}\right\}^T \{\Delta\sigma^e\}} \tag{4.37}$$

If $f_0=0$, the scaling factor r is set to zero and r_1 is calculated as;

$$r_1 = 1 - r = 1 \tag{4.38}$$

The solution is continued from step 8.

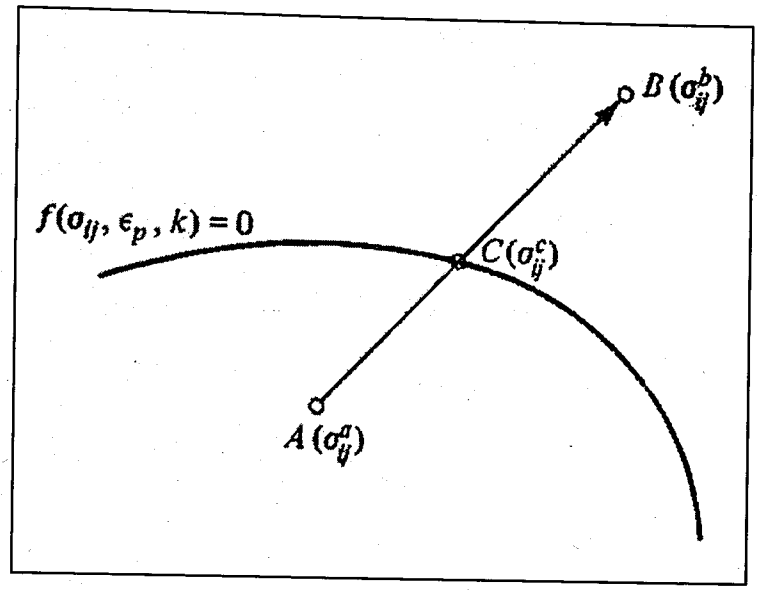

Figure 4.12. Transition from elastic to plastic state [38]

7. Scaling factor is evaluated according to equations (4.35) and (3.37).

8. The iterative value of the stress $\{\sigma\}_i$ is calculated as;

$$\{\sigma\}_i = \{\sigma\}_n + r\{\Delta\sigma^e\}_{n+1} \tag{4.39}$$

Sub-incremental stress and strain vectors are estimated by the division of the elastic stress and strain vectors into m smaller intervals as given by the following equations;

$$\{d\varepsilon\}_i = \left(\frac{1-r}{m}\right)\{\Delta\varepsilon\}_{n+1} \tag{4.40}$$

$$\{d\sigma^e\}_i = \left(\frac{1-r}{m}\right)\{\Delta\sigma^e\}_{n+1} \tag{4.41}$$

9. The stress invariants for $\{\sigma\}_i$ and the hardening parameter $H = d\sigma_e / d\varepsilon_p$ are calculated by using ε_p^n from the uniaxial stress-strain curve.

10. The plastic material stiffness matrix $[D]^p$ is calculated using the elastoplastic material model in order to evaluate the plastic portion of the iterative stress state.

11. Using the plastic material stiffness matrix $[D]^p$;

$$\{d\sigma\}_i = \{d\sigma^e\}_i - [D]^p \{d\varepsilon\}_i \tag{4.42}$$

is calculated and the stress vector is updated as;

$$\{\sigma\}_{i+1} = \{\sigma\}_i + \{d\sigma\}_i \tag{4.43}$$

12. The plastic work done per unit volume and the plastic strain increment are calculated for the current stress value.

13. The stress vector $\{\sigma\}_{i+1}$ is corrected by the stress correction vector $\{\delta\sigma\}$ which is given as;

$$\{\delta\sigma\} = -\frac{\left\{\frac{\partial f}{\partial \sigma}\right\} f_3}{\left\{\frac{\partial f}{\partial \sigma}\right\}^T \left\{\frac{\partial f}{\partial \sigma}\right\}} \tag{4.44}$$

f_3 is the final value of the yield function which is the small deflection from the yield surface. The correction vector $\{\delta\sigma\}$ prevents the cumulative increase of deflection from the yield surface at the forward steps of the analysis.

14. The consecutive steps starting from 9 up to 14 are reevaluated for $\{\sigma\}_{i+1}$. This loop is carried out up to the stress value $\{\sigma\}_{m+1}$ where the iteration is finalized for the $(n+1)^{th}$ incremental load.

15. $$\{\sigma\}_{m+1} - \{\sigma\}_n = \{\Delta\sigma\}_{n+1} \quad (4.45)$$

is the total change in the stress vector for the $(n+1)^{th}$ incrementation. The change in plastic stress vector $\{\sigma^p\}_{n+1}$ is evaluated by;

$$\{\Delta\sigma^p\}_{n+1} = \{\Delta\sigma\}_{n+1} - \{\Delta\sigma^e\}_{n+1} \quad (4.46)$$

The 15 steps described above are reapplied to the next incremental loading until the total load {R} is completed. For every load step, the residual force vector {φ(δ)} is also evaluated up to the level where the residual reaches to the negligible value for the termination of the total nonlinear solution.

4.4. Description of the Finite Element Model

4.4.1. Meshing Elements

The three dimensional column geometry was generated by meshing the constituent materials; blocks, infill concrete, mortar and reinforcement. Meshing of the three dimensional materials; blocks, infill concrete and mortar was developed by using eight noded isoparametric solid continuum elements. Vertical and lateral reinforcements were meshed by using two noded three dimensional isoparametric bar elements [37] (Figure 4.13).

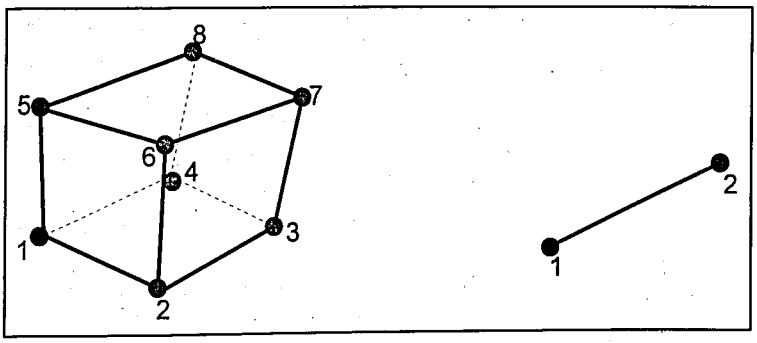

Figure 4.13. Eight noded hexagonal element and two noded bar element

Eight noded three dimensional continium elements are generally applicable to the cases where the stress field is fully three dimensional, that is, it cannot be approximated with two dimensional elements. Eight noded hexagonal continium elements enable the solution of normal and shear stresses and strains in three dimensional global system. Moreover, principal stresses and strains with their corresponding direction cosines may be obtained.

Two noded bar elements are suitable for modelling reinforcements and truss elements. Two noded isoparametric bar elements utilize the solution of axial stresses and strains, which are the main solution parameters of the reinforcement.

Combination of eight noded continium elements with two noded bar elements is attained through matching of the nodes facing one another.

Modelling of the concentrically loaded reinforced masonry column was developed by constituting one forth of the column geometry using the advantage of symmetry and uniform loading of the system (Figure 4.14). Nodes of the surfaces on the planes of symmetry perpendicular to x and y directions were restrained for x and y displacements, respectively. Top surface of the column was subjected to incremental distributed loading in $-z$ direction. Degrees of freedom on the bottom surface of the column were fully restrained in all directions whereas translation in vertical direction of top surface was kept free.

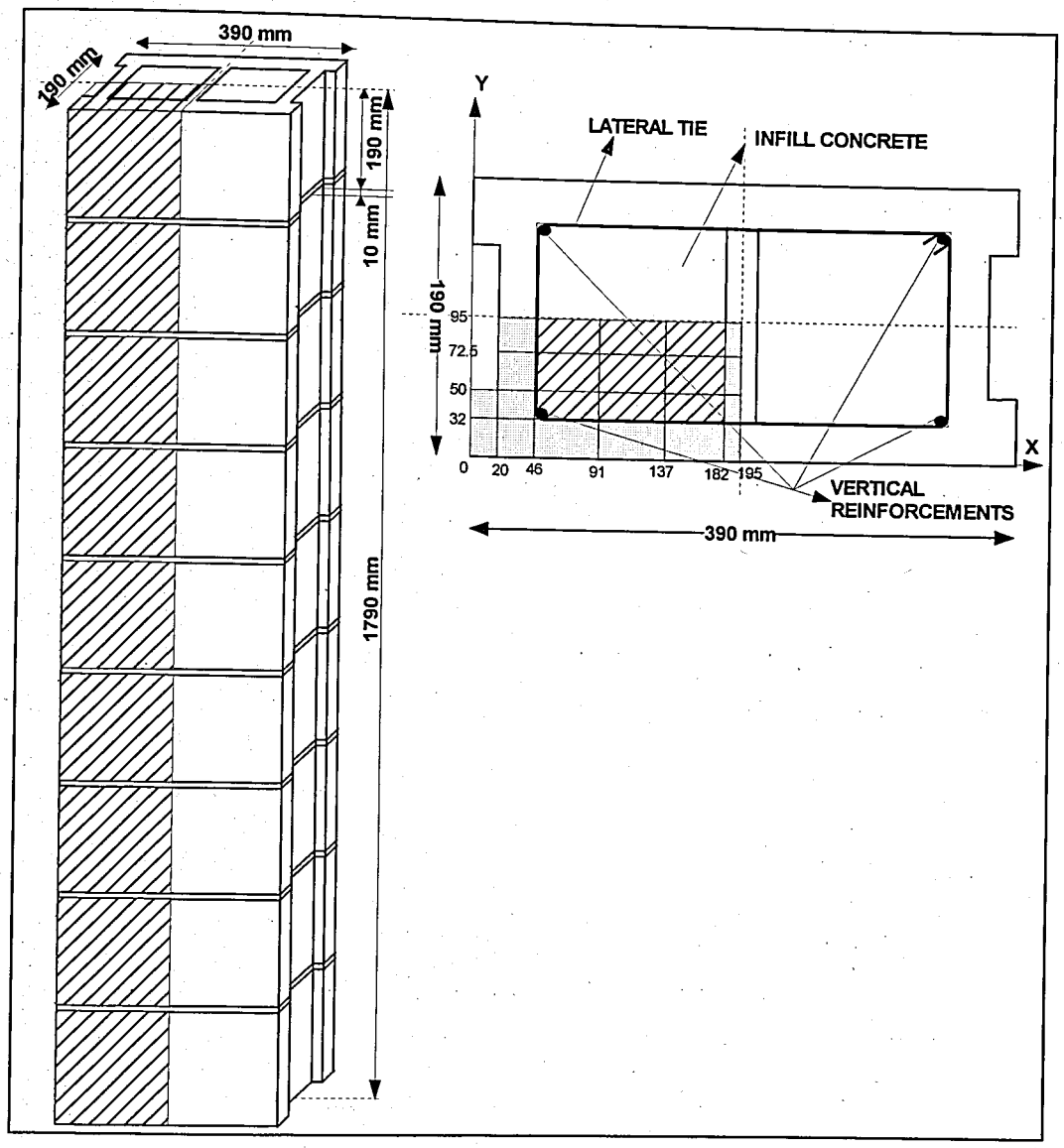

Figure 4.14. Column and block geometry

4.4.2. Material Properties

Material properties of constituents were defined and assigned to the corresponding meshes by using the material characteristics listed in Table 4.1.

Table 4.1. Material characteristics used for nonlinear modeling

MATERIAL CHARACTERISTICS	INFILL CONCRETE	BLOCK	MORTAR	REINFORCING STEEL
Elastic modulus E (MPa)	$500f_c'$ * $1000f_c'$ **	$500f_{bl}'$ * $1000f_{bl}'$ **	$500f_{mr}'$ * $1000f_{mr}'$ **	200 000
Poisson's ratio ν	0.2	0.2	0.2	0.3
Plastic material model	Drucker Prager	Drucker Prager	Drucker Prager	Von Mises
Initial yield strength of reinforcement f_y (MPa)	-	-	-	420
Initial cohesion c (MPa)$^{+}$	$0.25f_c'$	$0.25\ f_{bl}'$	$0.25\ f_{mr}'$	-
Initial friction angle ϕ (MPa)$^{++}$	33.5	33.5	$1.519\ f_{mr}'$	-

$^{+}$ The expressions for c is based on the previous studies [44]
$^{++}$ The expression for ϕ is based on the previous studies [42, 43]
* Elastic modulus for model columns M3b and M4b
** Elastic modulus for model columns M3a and M4a

where;

f_c': Specified cylinder compressive strength of infill concrete

f_{bl}': Compressive strength of concrete block

f_{mr}': Compressive strength of mortar

Isotropic plastic material models, Drucker-Prager and Von Mises were used for nonlinear analysis of the column [6, 38]. Drucker-Prager model was applied to the eight noded solid elements corresponding to infill concrete, block and mortar whereas Von Mises model was used for the two noded bar elements referring to vertical and lateral reinforcement. As previously discussed in Section 4.2.3, Drucker-Prager criterion is applicable to materials which exhibit volumetric plastic straining such as soil, concrete and rock. The yield surface defining Drucker-Prager criterion was expressed by Equation (4.22) with the positive material constants α and k where;

$$\alpha = \frac{2\sin\phi}{\sqrt{3}(3-\sin\phi)}$$

$$k = \frac{6c\cos\phi}{\sqrt{3}(3-\sin\phi)}$$

for the materials under compression. Therefore, the internal friction angle, ϕ and the cohesion, c are the main parameters necessary for the implementation of Drucker-Prager isotropic material model.

Von Mises criterion discussed in Section 4.2.1 is the most universally accepted yield criterion for metals. The yield surface defined by the criterion was expressed by Equation (4.10) with the constant k, which is the yield stress in pure shear. Yielding of metals under uniaxial tension occurs when $\sigma_1 = \sigma_y$ and $\sigma_2 = \sigma_3 = 0$. Thus, substitution of the principal stresses in equation (4.8) results with the expression;

$$\sigma_y = \sqrt{3}k$$

where σ_y is the tensile yield strength of the metal. The reinforcement elements of the columns were modelled using Von Mises criterion.

4.5. Application of the Model

Among masonry columns tested under axial loading, column specimens C3 and C4 were modeled by using the nonlinear finite element analysis program. The model columns named as M3a, M3b and M4a, M4b had the same type and percentage of vertical reinforcement with 190 millimeters (mm) constant tie spacing as described in the experimental program. Lateral ties were meshed at the top surface of each concrete block, also having contact with the bottom surface of each mortar layer.

Model columns M3a, M3b and M4a, M4b had the same material properties with C3 and C4 columns, respectively. Elastic modulus of the infill concrete, the concrete block and the mortar was defined by;

$$E_c = 500 f_c'$$
$$E_{bl} = 500 f_{bl}'$$
$$E_{mr} = 500 f_{mr}'$$

for the column models, M3b and M4b. The lower bound of the stress strain curves obtained from the experimental data are developed by the column models M3b and M4b. Columns M3a and M4a were modelled by using the elastic modulus;

$$E_c = 1000 f_c'$$
$$E_{bl} = 1000 f_{bl}'$$
$$E_{mr} = 1000 f_{mr}'$$

which form the upper bound of the stress strain curves. Details of the model columns M3a, M3b and M4a, M4b are described in Table 4.2.

Table 4.2. Description of the model columns M3a, M3b and M4a, M4b

MODEL PROPERTIES			M3a	M3b	M4a	M4b
Compressive strength of concrete blocks	f_{bl}'	(MPa)	17.11	17.11	17.11	17.11
Compressive strength of infill concrete	f_c'	(MPa)	21.96	21.96	21.96	21.96
Compressive strength of mortar	f_{mr}'	(MPa)	14.10	14.10	17.17	17.17
Tensile yield strength of reinforcements	f_y	(MPa)	420	420	420	420
Area of lateral ties	A_{s1}	(mm^2)	50.27	50.27	50.27	50.27
Area of vertical reinforcement	A_{s2}	(mm^2)	78.54	78.54	78.54	78.54
Elastic modulus of concrete blocks	E_{bl}	(MPa)	17 110	8555	17 110	8555
Elastic modulus of infill concrete	E_c	(MPa)	21 960	10980	21 960	10980
Elastic modulus of mortar	E_{mr}	(MPa)	14 100	7050	17 170	8585
Elastic modulus of reinforcements	E_s	(MPa)	200 000	200 000	200 000	200 000
Initial cohesion of concrete blocks	c_{bl}	(MPa)	4.28	4.28	4.28	4.28
Initial cohesion of infill concrete	c_c	(MPa)	5.49	5.49	4.49	4.49
Initial cohesion of mortar	c_{mr}	(MPa)	3.53	3.53	4.29	4.29
Internal friction of concrete blocks	ϕ_{bl}		33.50	33.50	33.50	33.50
Internal friction of infill concrete	ϕ_c		33.50	33.50	33.50	33.50
Internal friction of mortar	ϕ_{mr}		21.42	21.42	26.08	26.08
Poisson's ratio of concrete blocks	ν_{bl}		0.2	0.2	0.2	0.2
Poisson's ratio of infill concrete	ν_c		0.2	0.2	0.2	0.2
Poisson's ratio of mortar	ν_{mr}		0.2	0.2	0.2	0.2
Poisson's ratio of reinforcements	ν_{sl}		0.3	0.3	0.3	0.3

5. DISCUSSION OF ANALYTICAL AND EXPERIMENTAL RESULTS

5.1. Failure Behavior of Columns Tested under Axial Loading

The concentrically loaded masonry columns were observed to fail in various modes depending on the concrete core strength characteristics and degree of compaction during filling process. Detailed observations of failure modes of each column are explained as below.

Column C1: Before reaching the failure load, minor cracks were observed at first and third block end webs which propagated through the fourth block shell up to the failure load level. The column failure was dominated by splitting and separation of face shells of second and third blocks from concrete core. The concrete core was observed to crush under the separated block shells at the failure load (Figure 5.1). Although the concrete core possessed the highest strength among the concrete specimens, the column C1 exhibited premature failure. The tapering of the block cross section changing through the block height prevented the penetration of fresh concrete within the cavities causing the premature column failure.

Also, buckling of vertical reinforcements could be observed between lateral ties within the second block unit. Additionally, crushing of upper parts of block shells were observed under the steel loading plate.

Column C2: Failure of column C2 took place by complete splitting of the face shells and the end webs from sixth block to ninth block. Minor cracks initiating from lower block shells propagated through the fifth and sixth blocks up to 50 percent of the failure load. These cracks widened and caused sudden splitting of block shells at the failure load. Local crushing of block shells was observed under steel loading plate for column C2. Extensive buckling of vertical reinforcements could be clearly seen between the lateral ties of seventh

block causing sudden splitting of face shells. Crushing of the concrete core inside could be inspected clearly.

Both columns C1 and C2 having low slump values of concrete exhibited premature failure. The penetration of the fresh concrete within the reinforcement and the blocks was prevented by the block geometry causing the premature failure.

Column C3: The vertical cracks of the block shells initiating about 65 percent of the failure load were observed to propagate through the fourth block shell before reaching the ultimate load. Failure mode was dominated by complete splitting of face shells and end webs from second block to fifth block (Figure 5.2). It is noted that the block shell, concrete core and reinforcement interface bond was best achieved in this column. Buckling of the vertical reinforcement was observed at the fifth block region for which crushing of the concrete core could be seen under the block shells (Figure 5.3).

Column C4: Failure of the column C4 occurred with splitting of face shells of eighth and ninth blocks. At 70 percent of the failure load, vertical cracks were formed at the corners of seventh block shells, which widened and propagated through the eighth block shell causing the failure of the column. Buckling of vertical reinforcement was observed between lateral ties inside the eighth block unit (Figure 5.4). Similar to the observations from column C3, concrete core and block shell interface bond was successfully achieved for this column.

Column C5: The column failure was caused by splitting of face shells and end webs from second block to fourth block. Extensive buckling of vertical reinforcement was observed at the region of fourth block shell. The vertical cracks originating from the first and fourth block shells propagated and joined vertically causing the separation of intermediate block shells from the concrete core. Concrete core and block shell interface bond could not be achieved successfully at the region of the block shells that split outwards (Figure 5.5). This behavior is a foreseeable result of tapering of the web shells that hinder the penetration of the infill concrete between the reinforcement and the block shells.

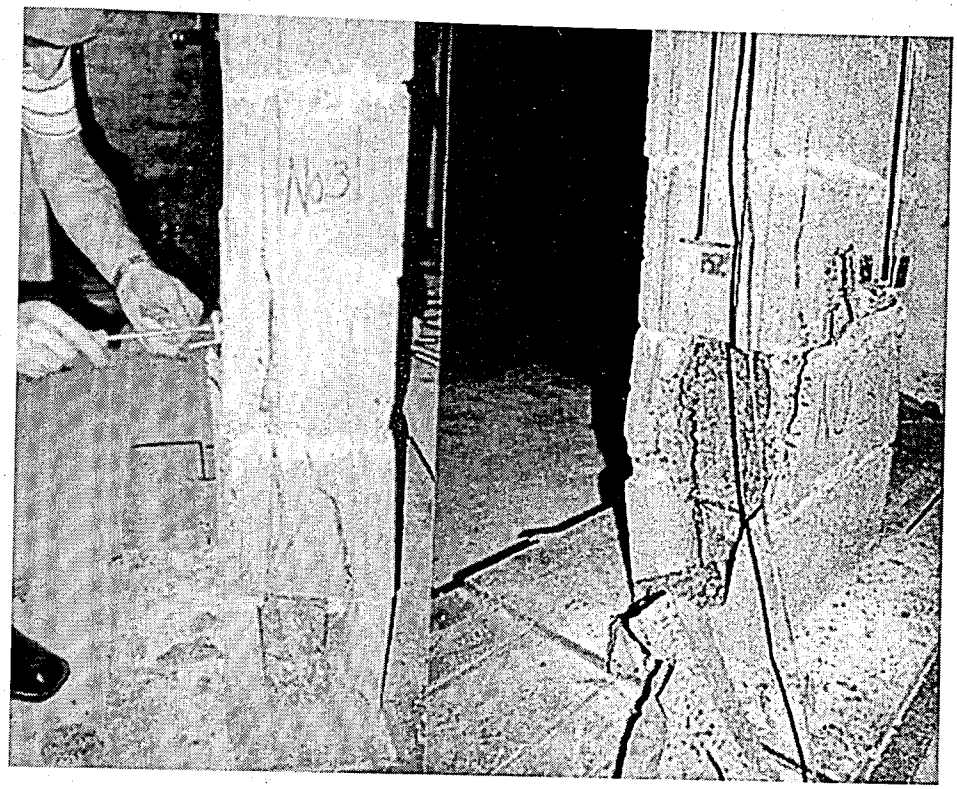

Figure 5.1. Vertical cracks at the block shells of column C1

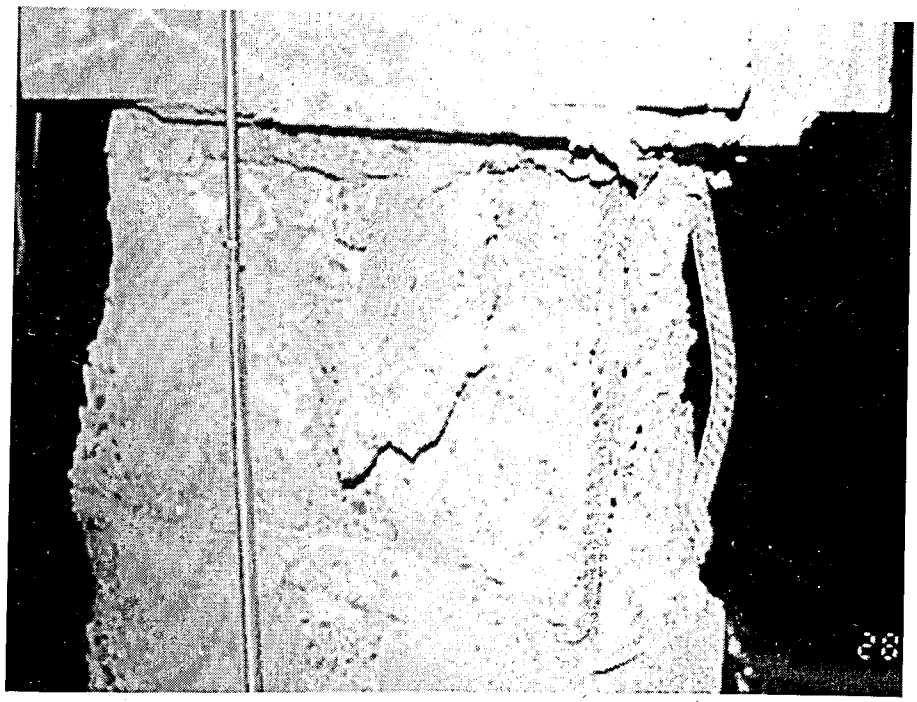

Figure 5.2. Buckling of the reinforcement and crushing of the concrete core (C3)

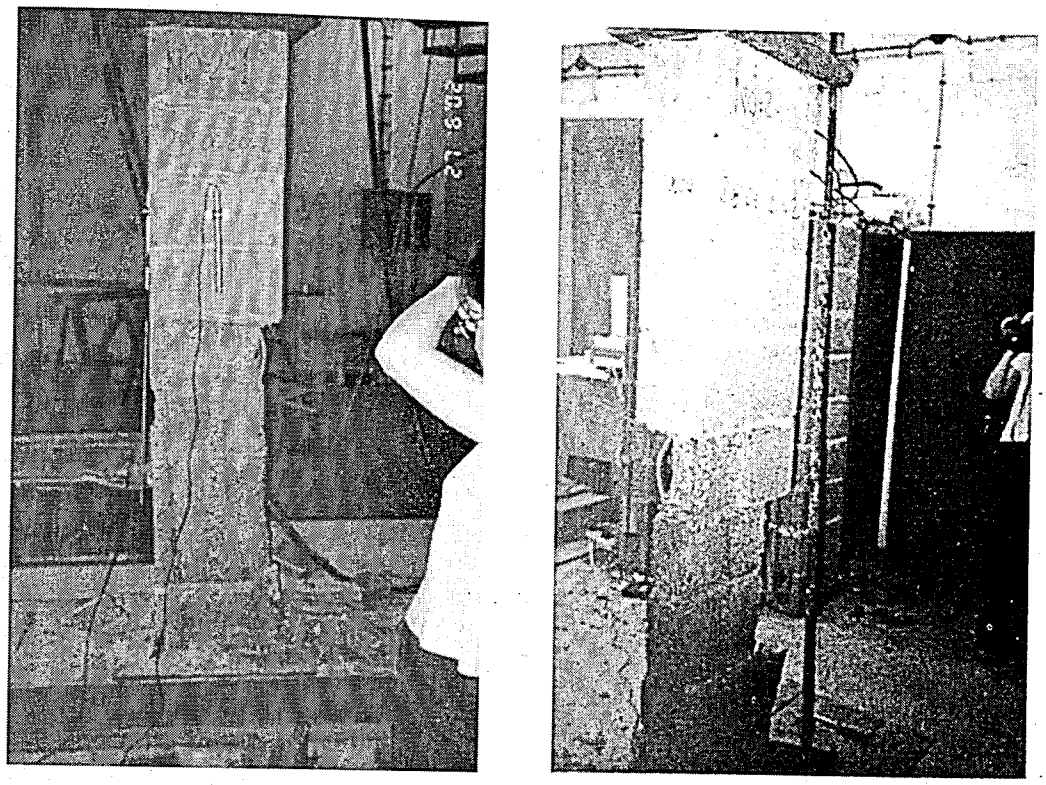

Figure 5.3. Failure of C3 and vertical reinforcement buckling

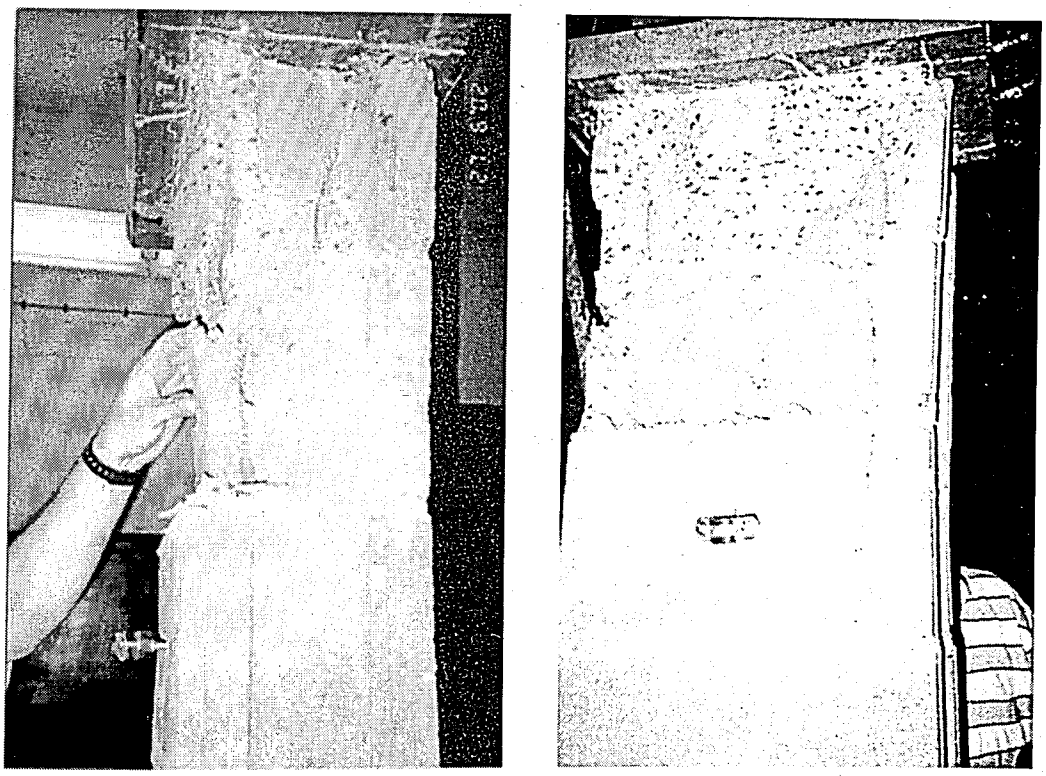

Figure 5.4. Splitting of shells and vertical reinforcement buckling (column C4)

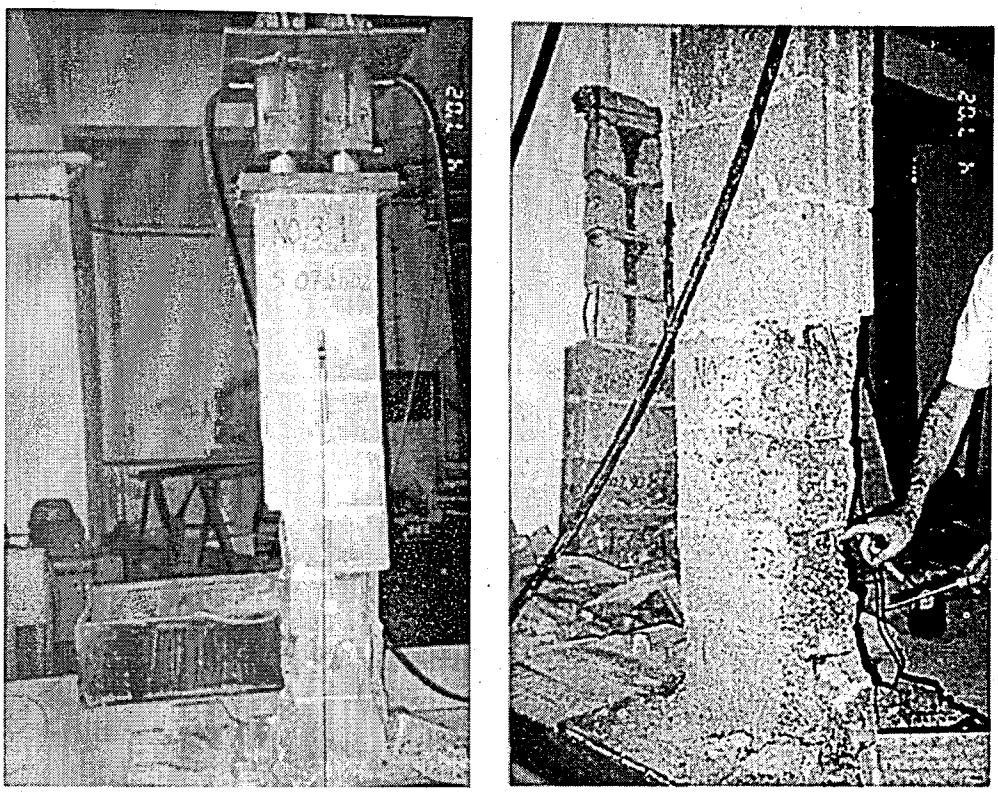

Figure 5.5. Failure of column C5

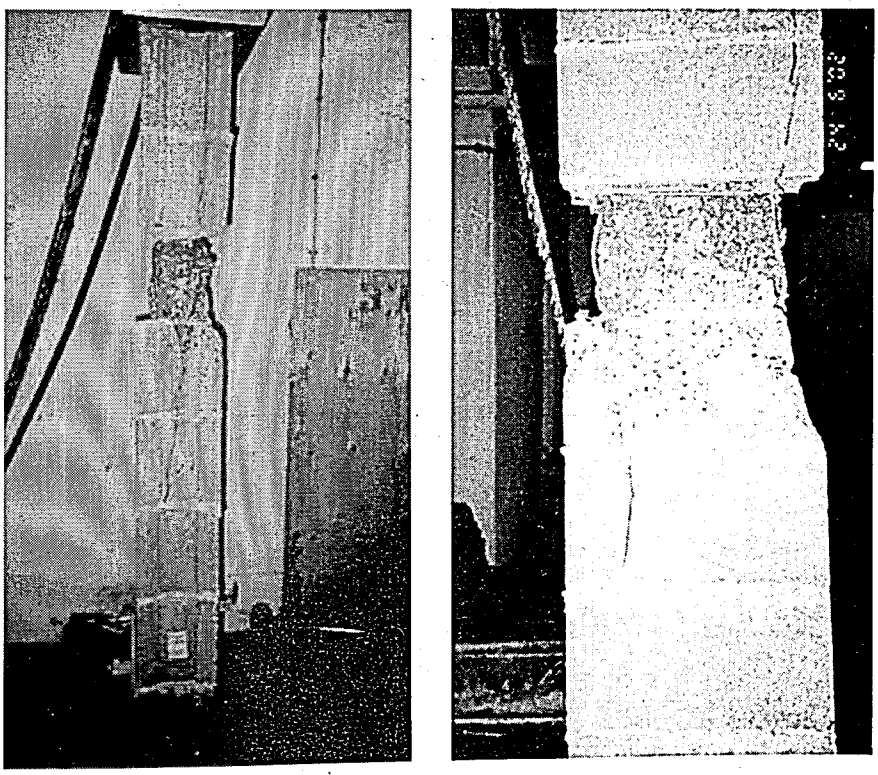

Figure 5.6. Vertical cracks at end web and face shell of column C6

Column C6: Vertical major cracks on the face shell corners of second block forming at about 90 percent of the failure load propagated at upward direction. Failure was caused by complete separation of the sixth to the seventh block shells from the concrete core. Also, vertical reinforcement buckled extensively at the region of seventh block. Similar to column C5, interface bond between concrete core and block shells could not be achieved successfully for this column (Figure 5.6).

General remarks on the failure modes of columns can be summarized as below;

- The major crack propagation on columns under axial loading was observed at block shell corners along the vertical reinforcement. The main reason for this type of crack formation is the differences in stiffness and Poisson's ratio between the steel and the masonry. As the cracks propagate, the localized lateral tensile stresses in masonry shells are relieved.
- Failure modes of columns were dominated by simultaneous separation of the block shell and the grout; and buckling of vertical reinforcement between lateral ties at the region of splitting block shells. Thus, it can be deduced that sudden splitting of the block shells was also caused by buckling of reinforcement at outward directions and the lateral tie spacing of 190 mm was not adequate to prevent buckling of vertical reinforcement.
- Ultimate load reached by the columns C3 and C4 was higher than the load levels reached by the other column specimens, even though they possessed the lowest strength of infill concrete with the maximum slump value of 15 cm. among the column specimens. The failure load results underline the effect of the concrete slump on the failure behavior and strength of the columns besides the effect of infill concrete strength.
- The concrete block units were manufactured with a tapering cross section through the height of the unit preventing the full penetration of the fresh concrete in the voids especially for the columns C1, C2, C5 and C6.
- Most of the column block shells had the tendency to split along the end webs causing separation of the face shells from the concrete core.

- Even for the columns exhibiting premature failure, no complete collapse of the columns was observed at ultimate load.
- Penetration of the concrete between vertical reinforcement and block shell could be best achieved by 15 cm slump concrete which was used for C3 and C4 columns.

5.2. Ultimate Strength of Concentrically Loaded Reinforced Masonry Columns

Ultimate load carrying capacity of a reinforced concrete masonry column mainly depends on the infill concrete, the block unit and the mortar compressive strength and the percentage of vertical reinforcement within the masonry column. The contribution of the lateral ties was not included directly to the previous equations expressing the ultimate strength. However, previous studies on reinforced masonry columns [10] show that the lateral tie detailing and existence of lateral reinforcement confining the longitudinal bars have increasing effects on the ultimate strength and ductility of the concentrically loaded reinforced masonry columns.

Compressive strength of the infill concrete being used in this study was the main variable of the experiments. The masonry columns were classified in three categories with respect to the infill concrete compressive strength varying from 21.96 MPa to 31.48 MPa.

The ultimate strength equations proposed by Khalaf, Hendry. Fairbairn [11] and Sturgeon, Longworth, Warwaruk [10] suggest that increasing infill concrete compressive strength results in increased ultimate load carrying capacity of reinforced masonry columns. However, the column test results contradicted with this statement since the highest ultimate strength was achieved by C3 and C4 columns which possessed the lowest infill concrete compressive strength value (Table 5.1).

Table 5.1. Column test results

Column No.	Steel Area A_s (mm^2)	Concrete Strength f_c' (MPa)	Ultimate Load P_u (kN)	Ultimate Strain ε_u (LVDT1)	Ultimate Strain ε_u (LVDT2)
C1	314.16	31.48	760.03	0.0018	0.0028
C2	314.16	31.48	1201.90	0.0019	0.0033
C3	314.16	21.96	1325.63	0.0021	0.0036
C4	314.16	21.96	1307.95	0.0020	0.0038
C5	314.16	28.23	954.45	0.0012	0.0024
C6	314.16	28.23	848.40	0.0016	0.0018

Column specimens C3 and C4 having the lowest strength concrete and the highest slump gave the most consistent results with the ultimate strength values obtained using empirical formulas given in Table 5.2. Thus, the nonlinear numerical analysis of reinforced masonry columns was conducted using the material and physical properties of C3 and C4 columns in order to simulate the column behavior under axial loading.

Table 5.2. Ultimate strength of the reinforced masonry columns

Ultimate Load P_u (kN)	C1	C2	C3	C4	C5	C6
ACI 531/ASCE 5*	388.35	388.35	350.59	400.59	425.45	425.45
Khalaf, Hendry,Fairbairn**	1634.28	1634.28	1467.24	1688.44	1798.46	1798.46
Sturgeon, Longworth, Warwaruk***	995.19	995.19	721.38	721.38	901.72	901.72
Experimental Result	760.03	1201.90	1325.63	1307.95	954.45	848.40

* ACI 531/ASCE 5 [14], $P_u = (0.225 f_m' A_g + 0.65 A_s f_s)/1000$ where, $f_s = 166$ MPa

** Khalaf, Hendry, Fairbairn [11], $P_u = (f_m'(A_g - A_s) + (f_y A_s)/2)/1000$ where, $f_y = 420$ MPa

***Sturgeon, Longworth, Warwaruk [10], $P_u = [0.85 f_c'(A_c - A_s) + E_s A_s/700]/1000$

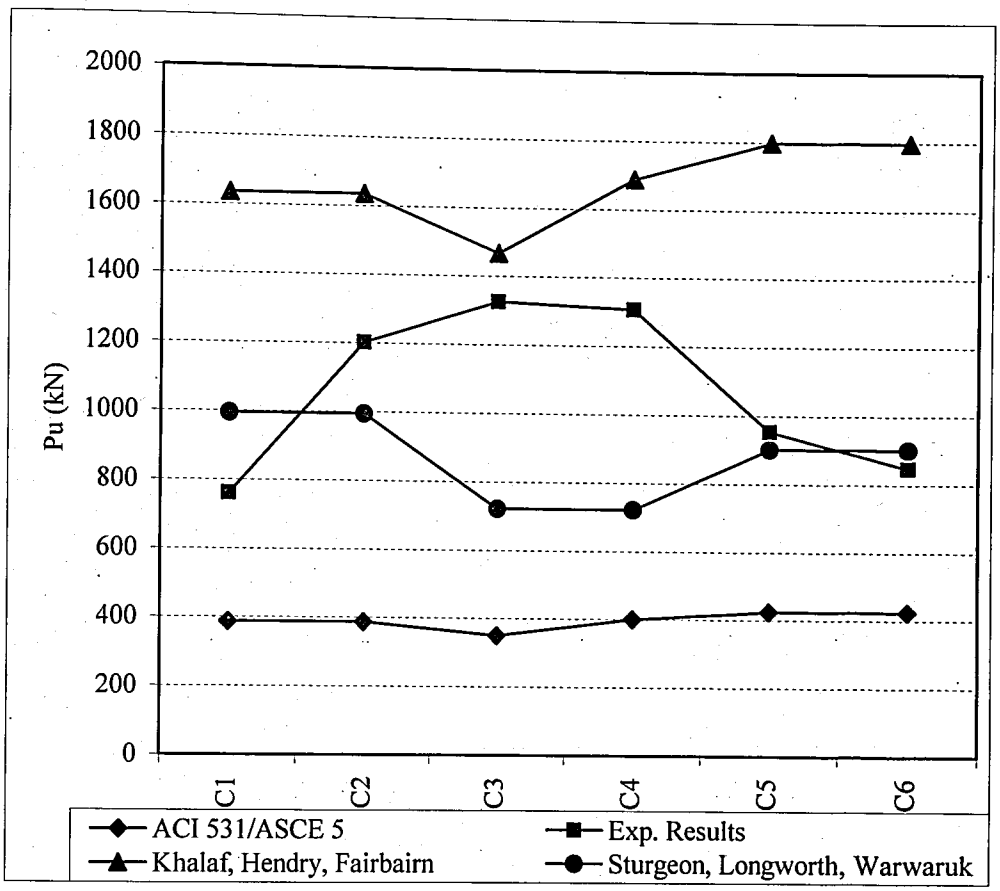

Figure 5.7. Ultimate strength of the reinforced masonry columns

Table 5.2 and Figure 5.7 summarize the results obtained using three different ultimate strength equations. Ultimate strength equation given by ACI 531/ASCE 5 [14] is mainly based on the specified prism compressive strength of the blockwork masonry, f_m' and the allowable axial compressive stress of the vertical reinforcement, f_s [14]. By comparing the test results with the values calculated from the equation given by ACI 531/ ASCE 5 [14], it can be deduced that the proposed equation underestimates the ultimate strength of the columns tested. Ultimate strength values obtained by the equation proposed by Sturgeon, Longworth and Warwaruk [10] correlate with the experimental results of C1, C2, C5 and C6 but the equation underestimates the ultimate strength of the columns C3 and C4. The ultimate strength equation proposed by Sturgeon, Longworth and Warwaruk [10] mainly depends on the compressive strength of the infill concrete omitting the compressive strength of the mortar and the block unit being used.

Ultimate strength predicted by Khalaf, Hendry and Fairbairn [11] is mainly a function of the specified compressive strength of masonry prism, f_m'. The experimental study did not include the estimation of compressive strength of masonry prisms, f_m' experimentally. Thus, prism compressive strength, f_m' values were obtained by the expression proposed by Khalaf, Hendry and Fairbairn [16]. Although test results of masonry columns filled with high strength concrete do not correlate with the predicted results, the results of the columns C3 and C4 are in good agreement with the values calculated by the proposed equation.

Load deformation curves created by the data collected from LVDT1 (which was fixed at the end webs of the columns) and LVDT2 (fixed to the face shells of the columns) are given in Figure 5.8, Figure 5.9 and Figure 5.10. The curves based on LVDT2 data indicate that the nonlinear behavior of masonry columns starts about 40 percent of the ultimate load in spite of the premature failure observed during the tests of columns C1, C2, C5 and C6.

The mean value of strains obtained from LVDT1 just before failure is 0.0018; which is lower than the mean strain value calculated from LVDT2 data; which is 0.0030. The load deformation curves plotted from the results of LVDT1, which was fixed at the end webs show linear behavior up to higher load levels than the curves plotted using the results of LVDT2 that was fixed to the face shells of the columns.

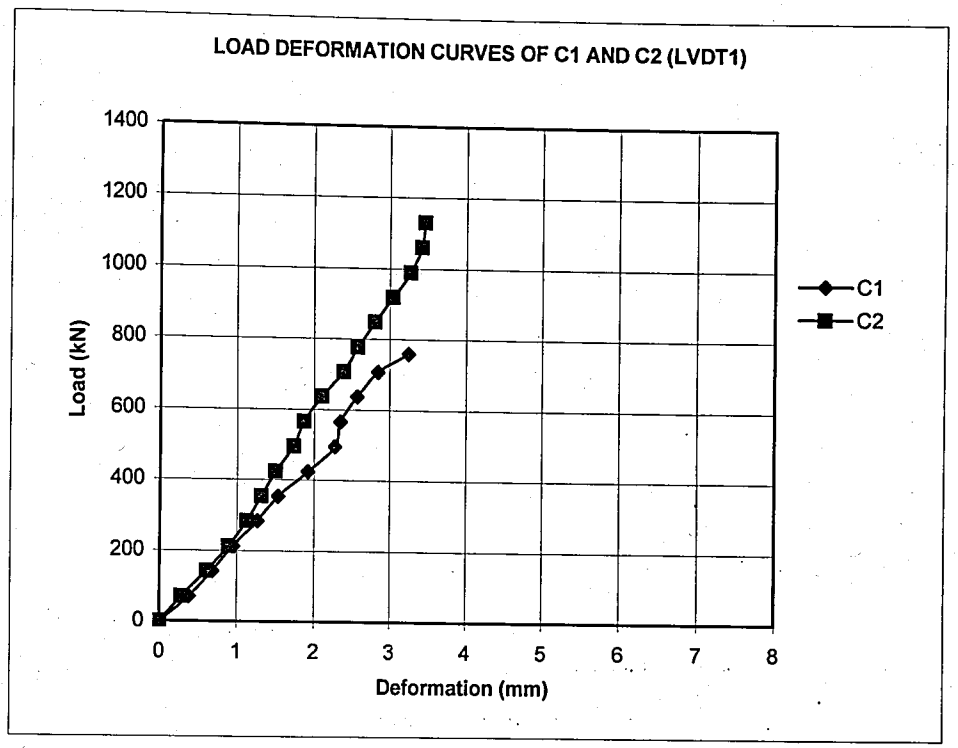

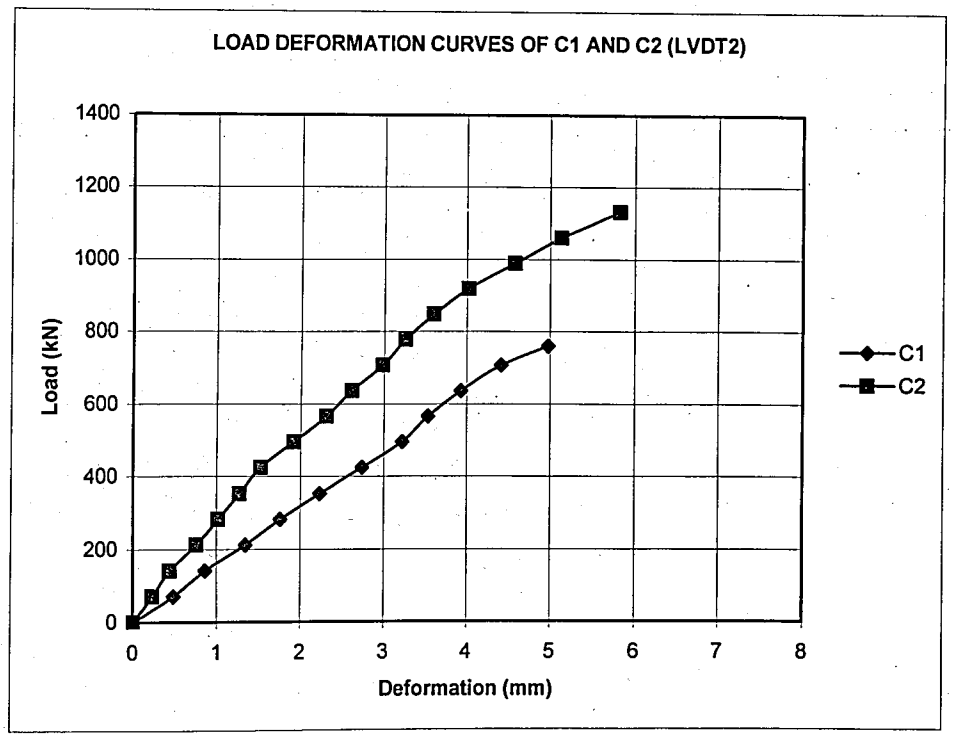

Figure 5.8. Load deformation (axial shortening) curves of C1 and C2

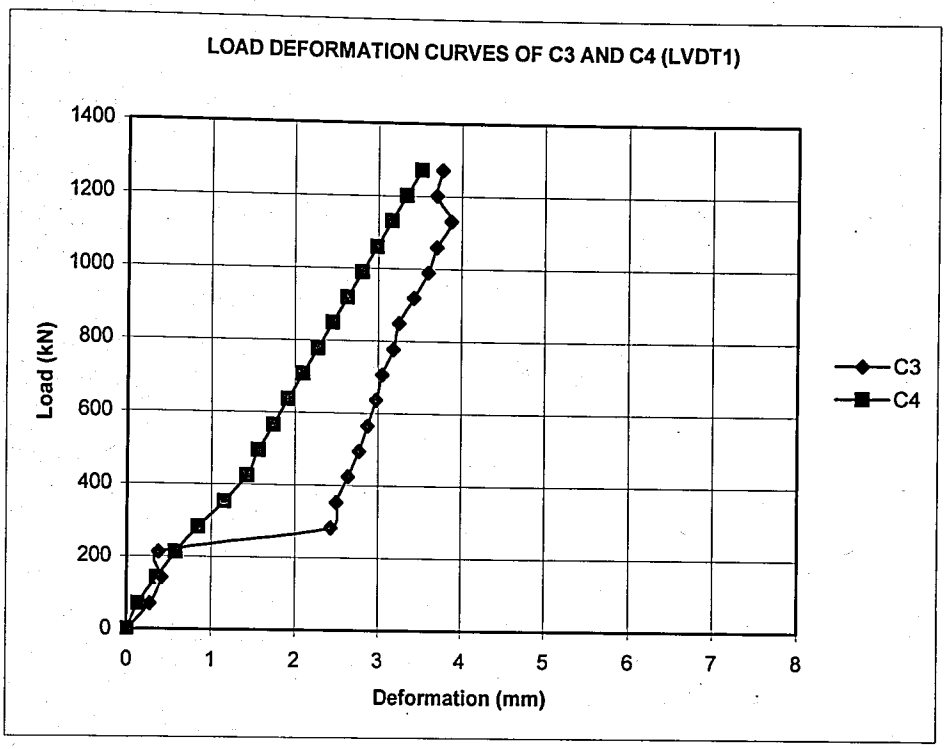

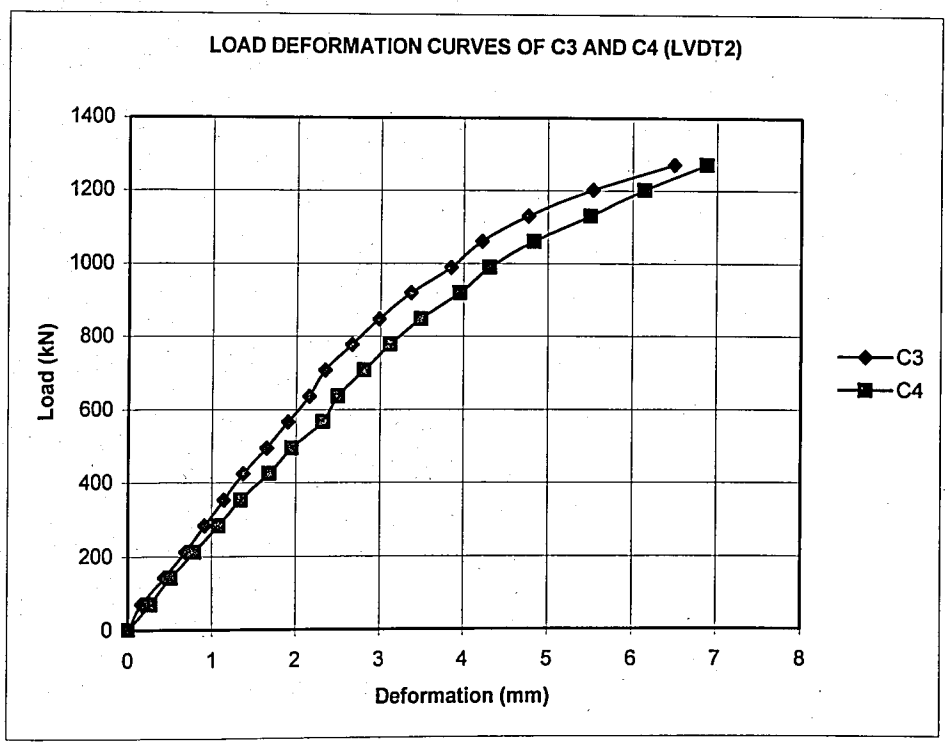

Figure 5.9. Load deformation (axial shortening) curves of C3 and C4

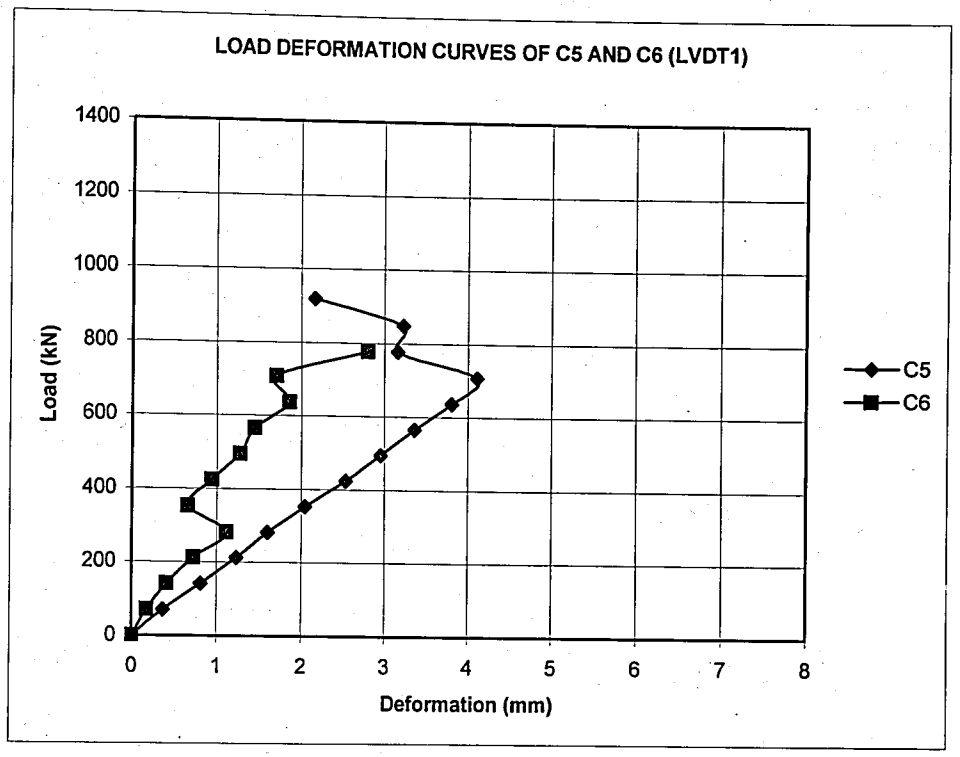

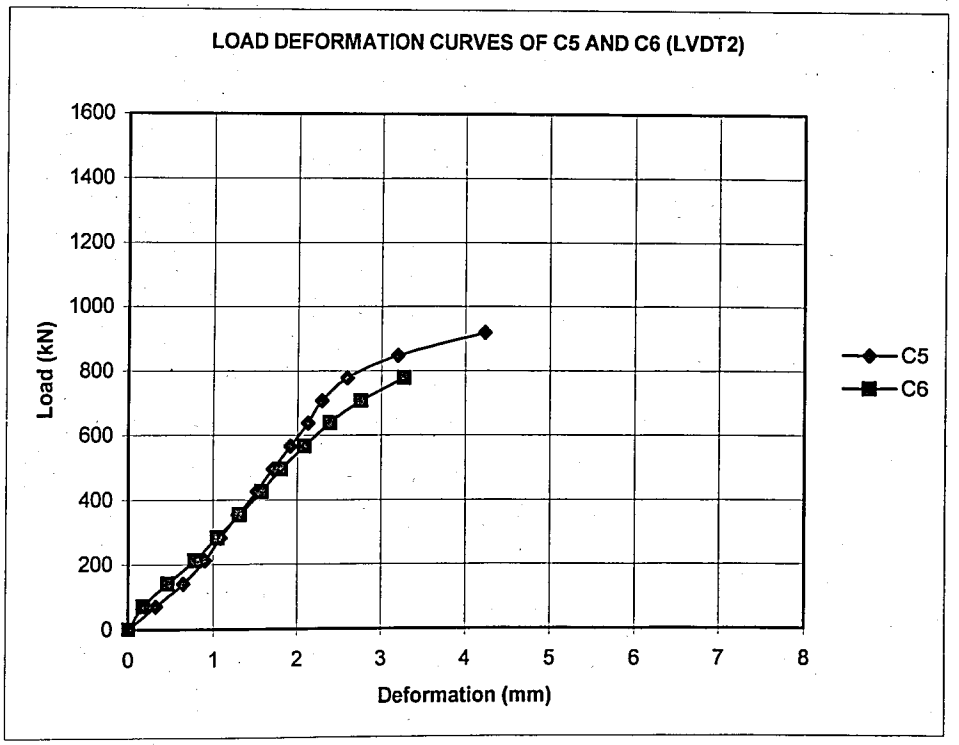

Figure 5.10. Load deformation (axial shortening) curves of C5 and C6

5.3. Elastic Modulus of Reinforced Masonry Columns

Using the experimental data obtained from LVDT1 and LVDT2, stress strain curves of each column are plotted as shown in Figure 5.11, Figure 5.12 and Figure 5.13. The stress strain curves of the columns plotted using LVDT1 data are generally linear up to the failure point or the curves deviate back at some load levels, which is not the expected behavior of the tested columns. Major cracks of the columns causing the separation of the block face shells were observed to originate and propagate along the centerline of the end webs through the height of each column. LVDT1 was also fixed along the centerline of the end webs coinciding with the direction of the crack propagation, which could be the main reason for the deviations of the collected data.

However, stress strain curves obtained from LVDT2 data exhibit the expected behavior of masonry columns under axial loading. The linear behavior can be observed up to about 40 percent of the compressive strength, f_m' and the plastic zone exists from 40 percent of the compressive strength up to the column failure.

Therefore, it can be deduced that stress strain curves and elastic modulus obtained from LVDT2 data are more representative of the reinforced masonry column behavior under axial loading.

The experimental, theoretical and proposed values of the column elastic modulus are listed in Table 5.3. Elastic modulus of each column was obtained by calculating the slope of each stress strain curve below the stress value of $0.33f_m$', where f_m' was the experimental value of column compressive strength.

Theoretical and proposed elastic modulus values were calculated for upper and lower bound elastic modulus values of the constituent materials, E_c, E_{bl} and E_j. Upper and lower bound values of E_c, E_{bl} and E_j were estimated by multiplication of each material compressive strength with 500 and 1000, respectively.

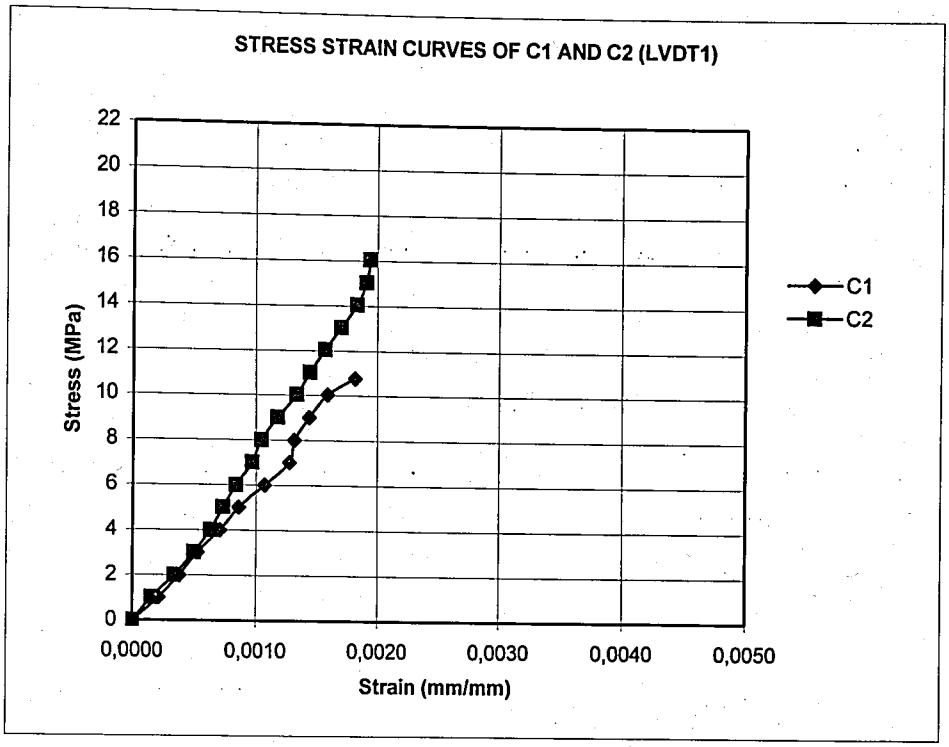

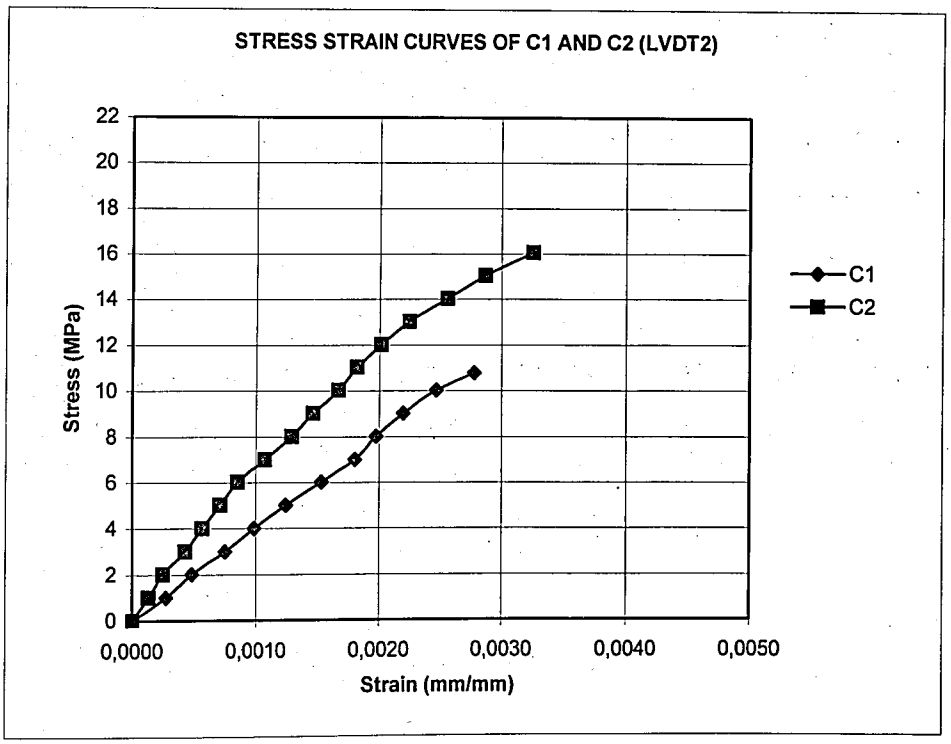

Figure 5.11. Stress strain curves of C1 and C2

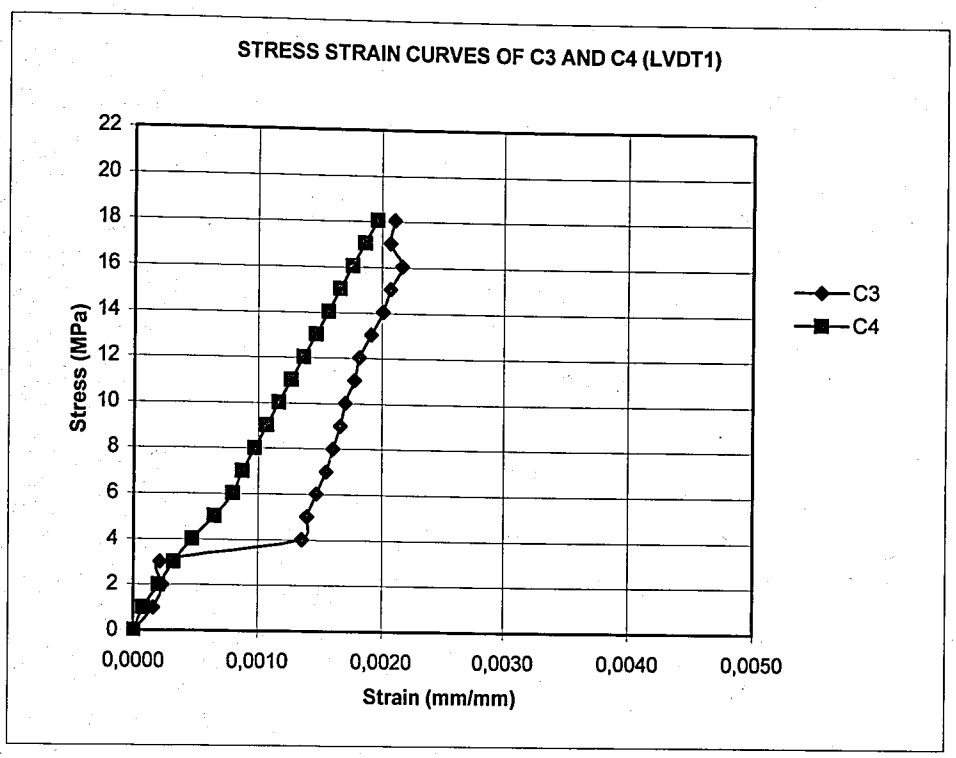

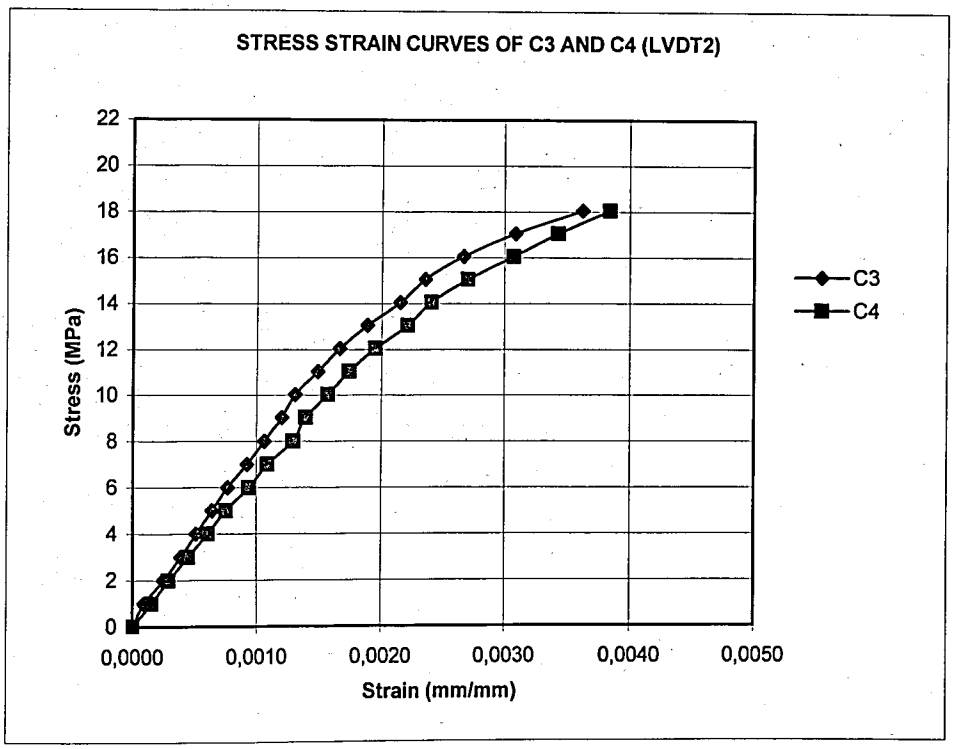

Figure 5.12. Stress strain curves of C3 and C4

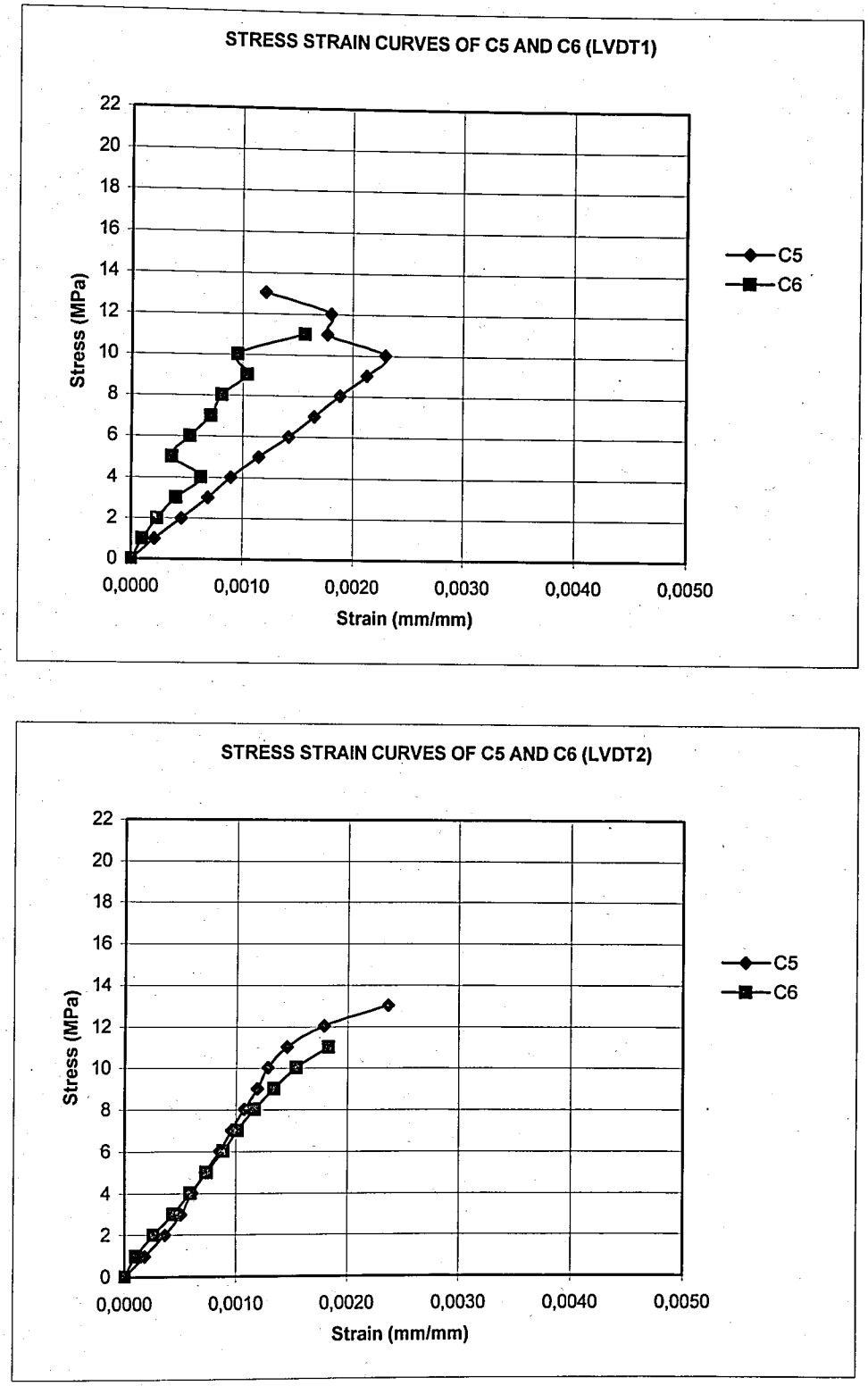

Figure 5.13. Stress strain curves of C5 and C6

Table 5.3. Elastic modulus of reinforced masonry columns

Column No.	E_m (LVDT1) (MPa)	E_m (LVDT2) (MPa)	E_m (Theo.)* (MPa)	E_m (Theo.)** (MPa)	E_m (Prop.) § (MPa)	E_m (Prop.) §§ (MPa)
C1	5782.9	4076.6	11994.08	23988.17	11471.50	22051.76
C2	7030.5	6930.1	11994.08	23988.17	11471.50	22051,76
C3	8325.9	7615.9	9687.69	19375.38	9525.16	18159.08
C4	7293.2	6452.3	9730.44	19460.88	9525.16	18159.08
C5	4276.3	7128.1	11249.04	22498.07	10807.04	20722.85
C6	6310.9	6543.4	11249.04	22498.07	10807.04	20722.85

*,**Theoretical elastic modulus calculated using lower and upper bound elastic modulus of concrete, mortar and block, respectively [21, 22]

$$E_m = \frac{1}{\delta/[(1-\eta)E_c + \eta E_{bl}] + 1/[(1-\eta)E_c + \eta E_j]}$$

§,§§Elastic modulus proposed by Sturgeon, Longworth, Warwaruk [10] calculated using lower and upper bound values of concrete, mortar and block.

$$E_m = \frac{0.85E_c(A_c - A_s) + E_{bl}A_{bl} + E_sA_s}{A_g}$$

Comparing the experimental results with the values obtained from theoretical [21, 22] and proposed formula [10], it is noted that the experimental values obtained from LVDT2 data are even below the lower bound estimations. Elastic modulus results of the theoretical and proposed equations are in good agreement with each other. Examining the values calculated from the experimental data, an expression of the column elastic modulus can be suggested as;

$$E_m = 422 f_m' \tag{5.1}$$

where f_m' is the compressive strength of masonry columns tested (Figure 5.14). The correlation coefficient; R of the predicted relation is 0.60; which indicates that the reliability of the predicted linear relationship is not high.

Elastic modulus calculated from LVDT1 data were closer to the lower bound theoretical and proposed values of elastic modulus, which varied between 4276.3 MPa and 8325.9 MPa.

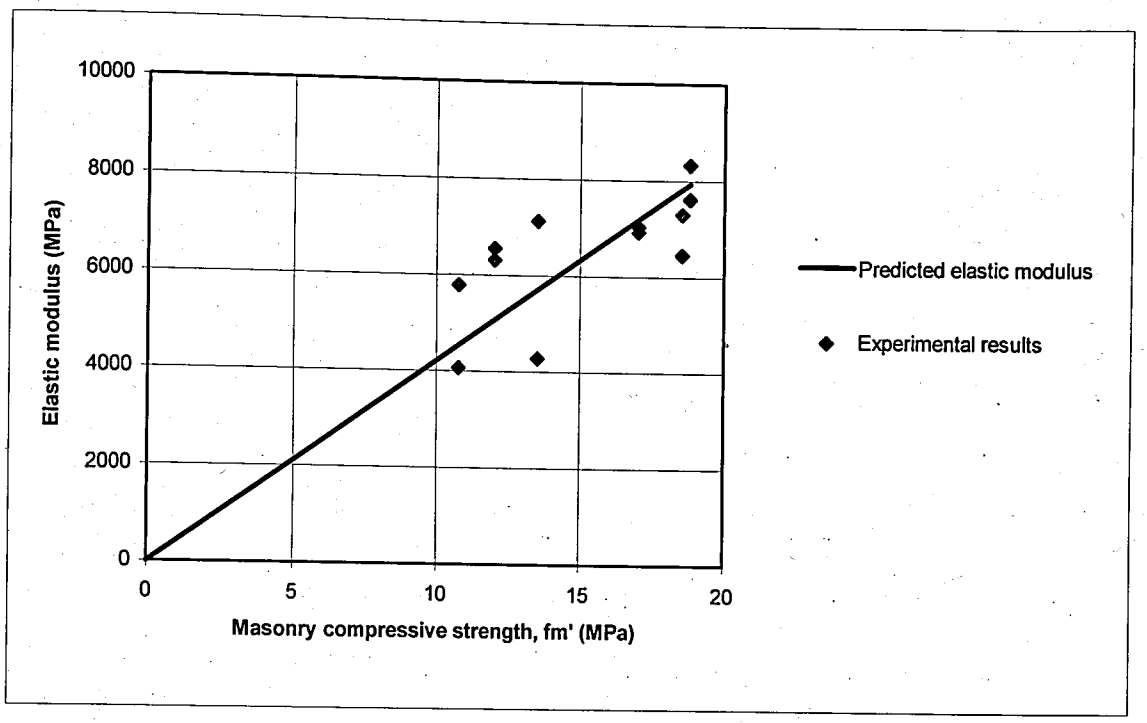

Figure 5.14. Predicted elastic modulus (Equation (5.1))

5.4. Discussion of the Analytical Results

In this study, the experimental behavior of reinforced masonry columns under axial loading was simulated by nonlinear finite element modeling of columns C3 and C4 which exhibited the expected behavior of masonry columns compared with the previous investigations. The model columns M3a and M3b were developed using the same material properties with C3. The behavior of column C4 was simulated by the analytical models, M4a and M4b. As it was discussed in Chapter 4, analyses of column models, M3b and M4b were performed using the lower bound values of elastic modulus of the materials composing masonry column. The models, M3a and M4a were developed by implementing the upper bound values of material elastic modulus.

Nonlinear finite element analyses of the models M3a and M4a were performed in eleven load increments whereas the solution of the models M3b and M4b were performed in eight and nine load increments, respectively.

Observing the analytical results, model column M3a has with an ultimate load of -1508.72 kN whereas ultimate load of model column M3b is -1501.65 kN. Similarly, the column models M4a and M4b reach the ultimate load values of -1519.84 and -1509.56 kN, respectively. Despite variable elastic modulus of the constituent materials for each column model, the ultimate load values attained by the columns are nearly the same.

Maximum vertical deformation values of the column models are observed at the center of the top column cross section, which decrease at the lower block levels as given in Figure 5.19 and Figure 5.20. Also, lateral deformations of the columns in x and y directions reach the maximum values at the center of end webs and face shells of the sixth and seventh block units. The observations imply that the failure of column models would result with the splitting of the seventh and the sixth block shells in outward direction under actual loading (Figure 5.15 to Figure 5.18).

Vertical stress of the three dimensional hexagonal elements reaches to its maximum value of –28 MPa approximately at the concrete core center regions within the eighth block shells. It is observed that the block shells and the concrete core within the lateral ties are exposed to lower vertical stress values varying from -8 to -22 MPa (Figure 5.21 and 5.22). In addition, maximum vertical shortening is observed at the mortar joints of the columns as given in Figure 5.23 and Figure 5.24. The lateral tensile stresses of the columns reach to the maximum values at the block face shells of the seventh to ninth block units.

The vertical bars of the columns are under compression with the average value of stress varying from -406 to -415 MPa. The strain results of the vertical bars show that most of the bar elements have yielded especially at the region of the sixth and seventh lateral tie elements (Figure 5.25 and Figure 5.28). The lateral ties of the column models are under tension with the maximum of average stress values varying from 366 to 400 MPa which occurs at the seventh lateral tie. The stress on the lateral ties decreases at the lower block units as given by Figure 5.29 and Figure 5.30.

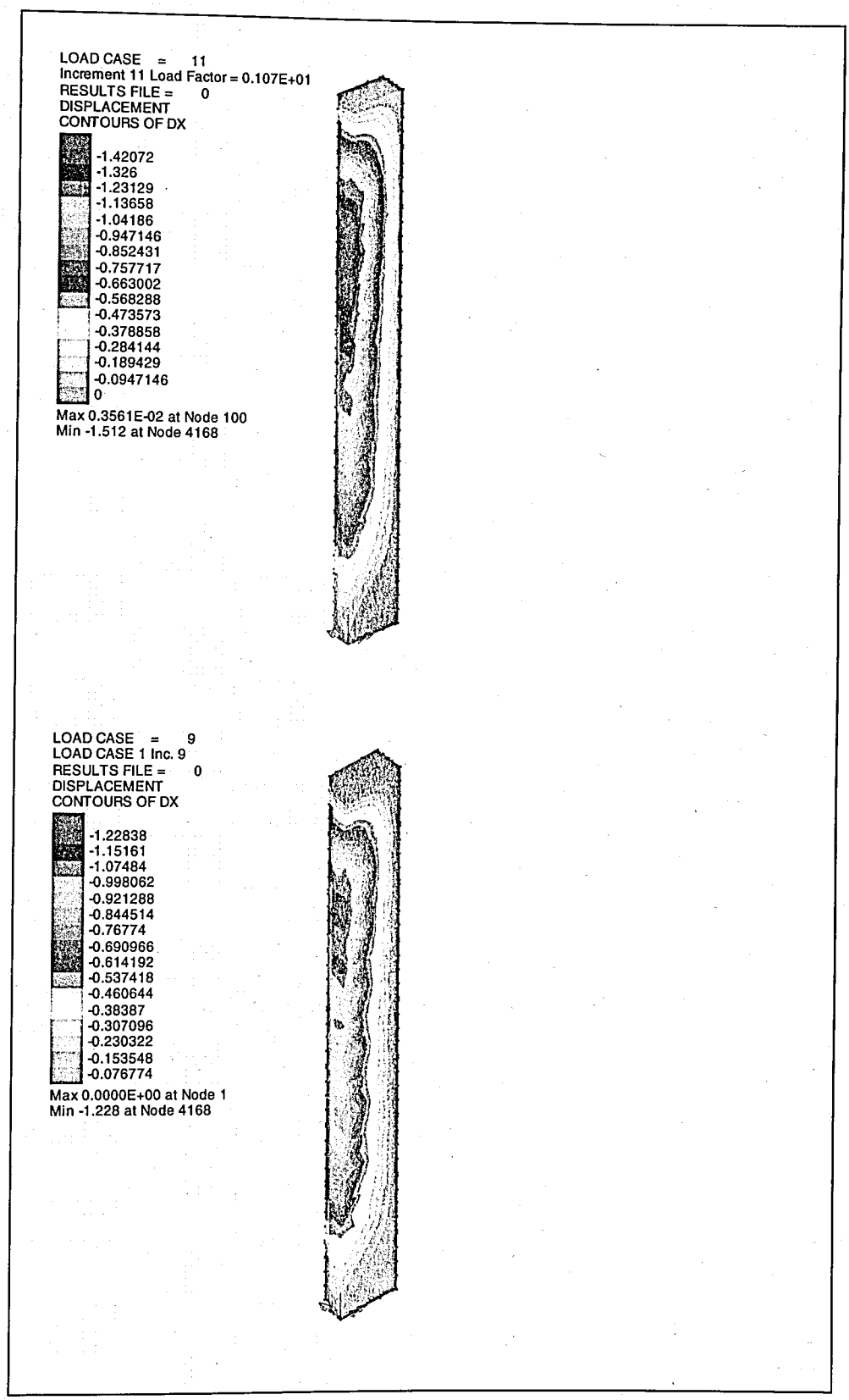

Figure 5.15. Lateral deformations in x direction for M3a and M3b

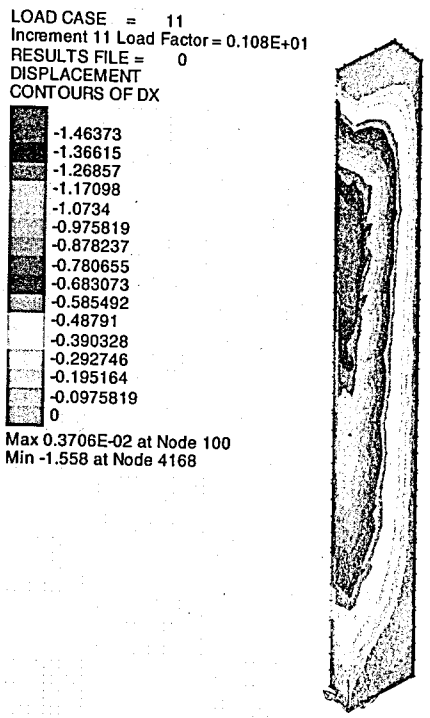

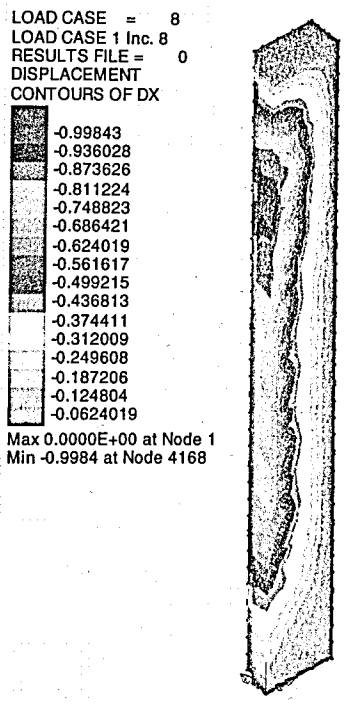

Figure 5.16. Lateral deformations in x direction for M4a and M4b

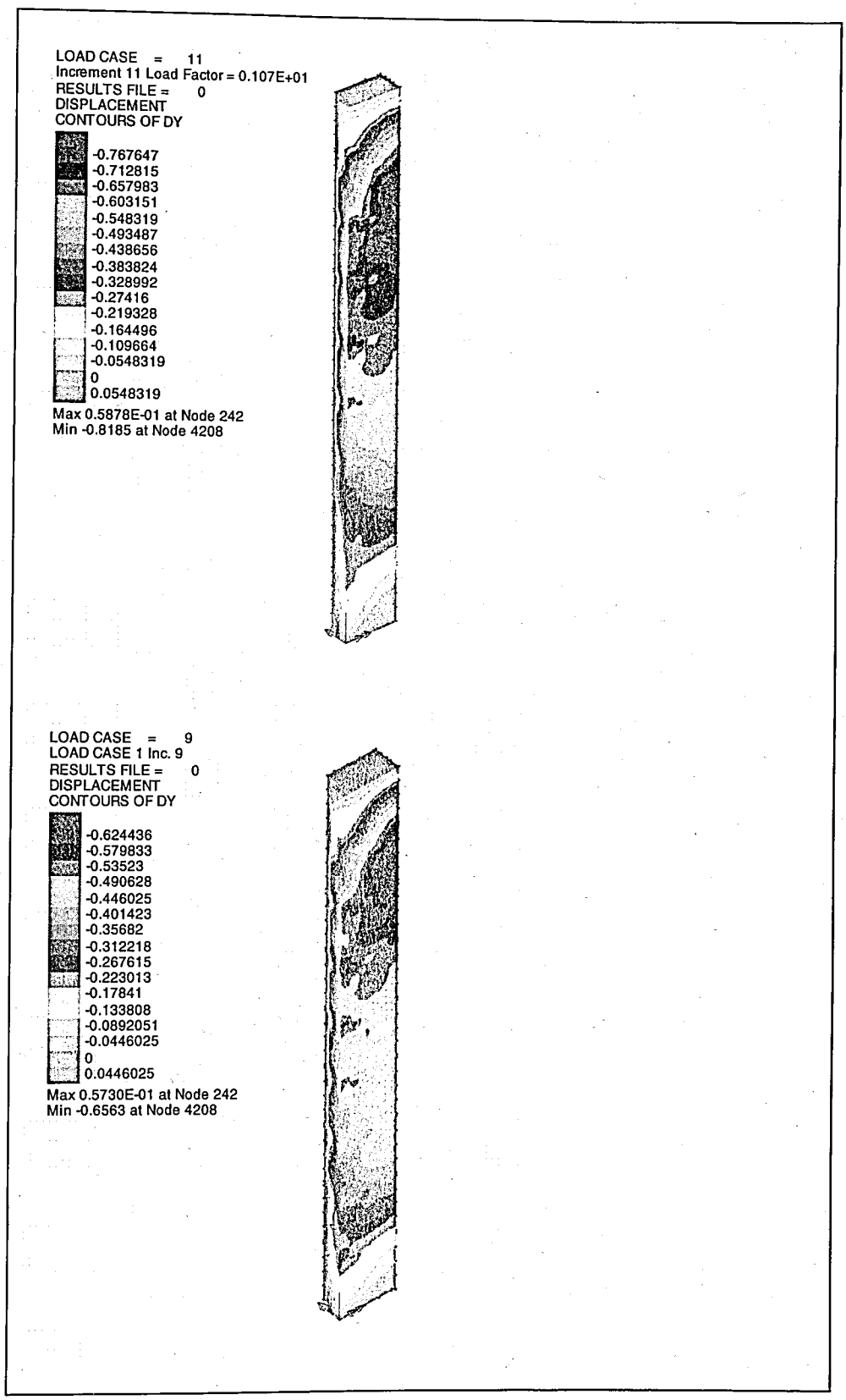

Figure 5.17. Lateral deformations in y direction for M3a and M3b

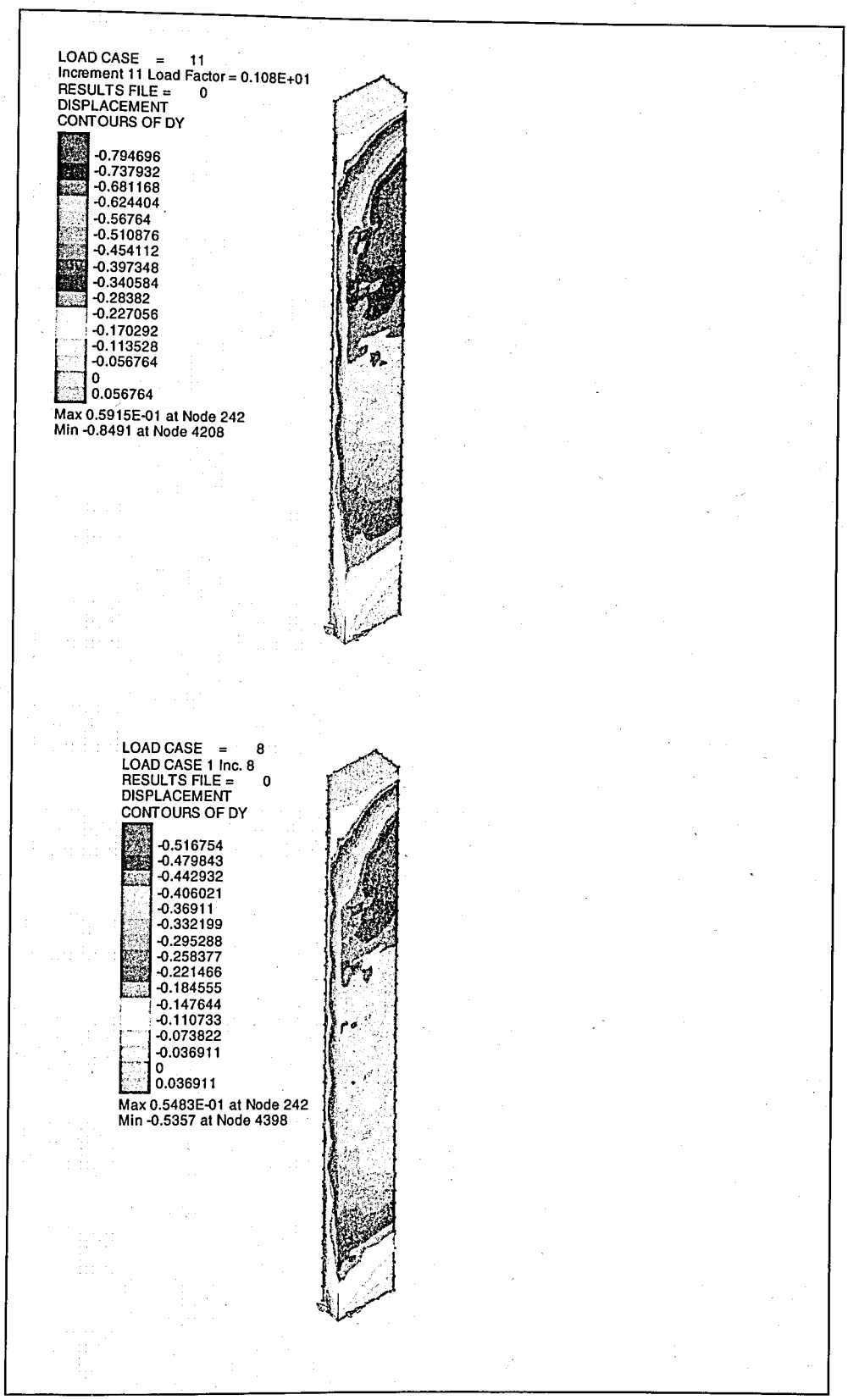

Figure 5.18. Lateral deformations in y direction for M4a and M4b

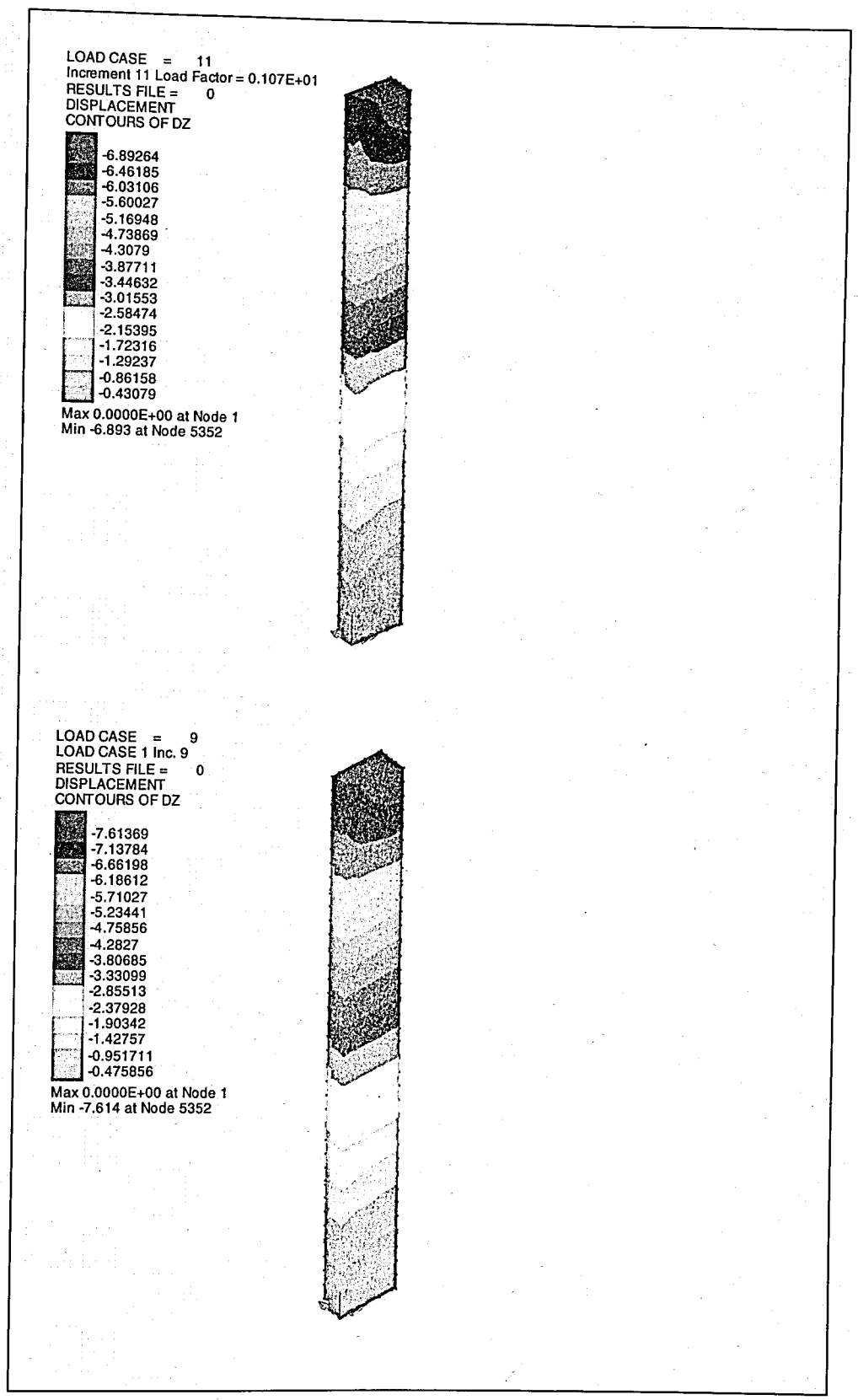

Figure 5.19. Lateral deformations in z direction for M3a and M3b

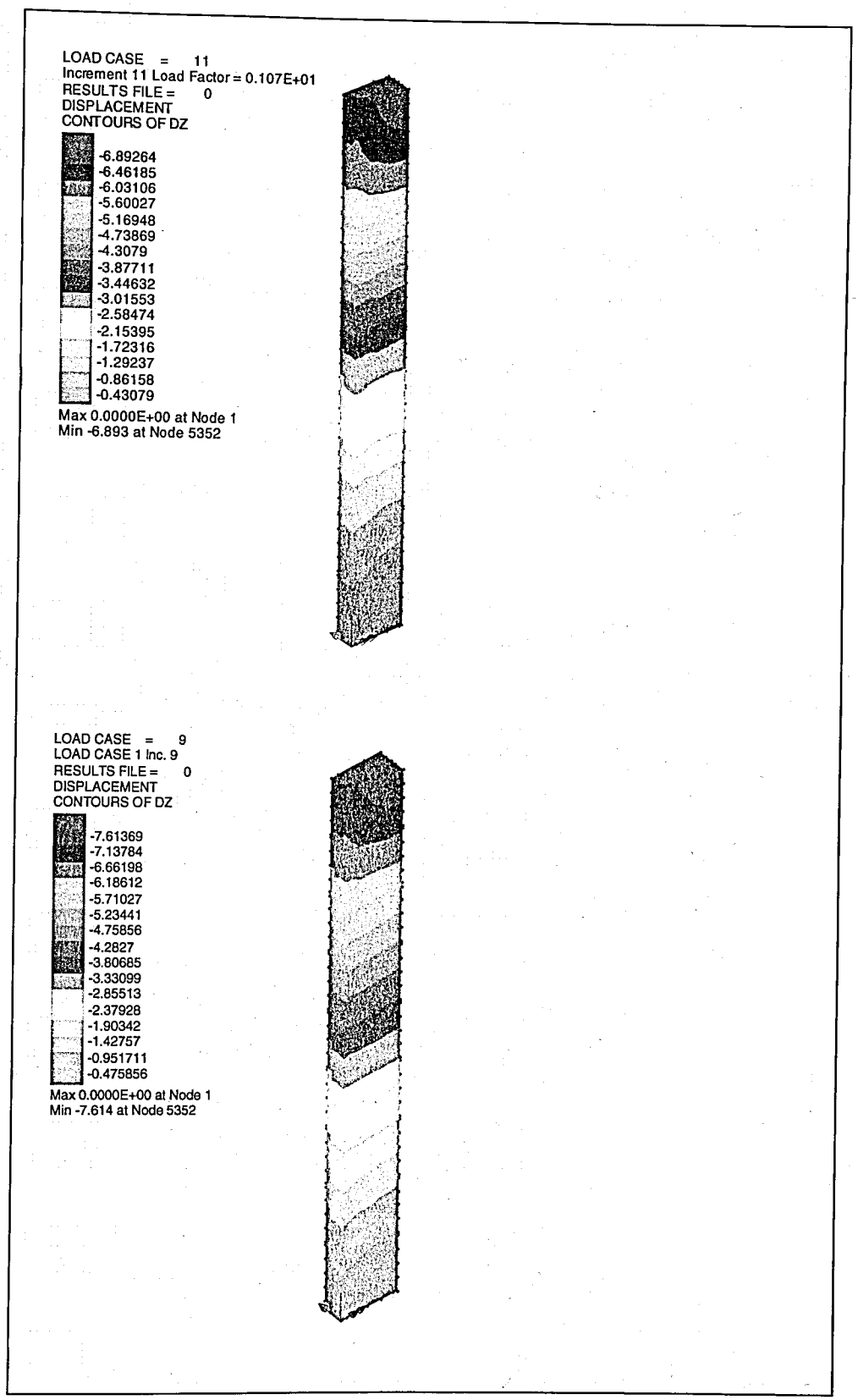

Figure 5.20. Lateral deformations in z direction for M4a and M4b

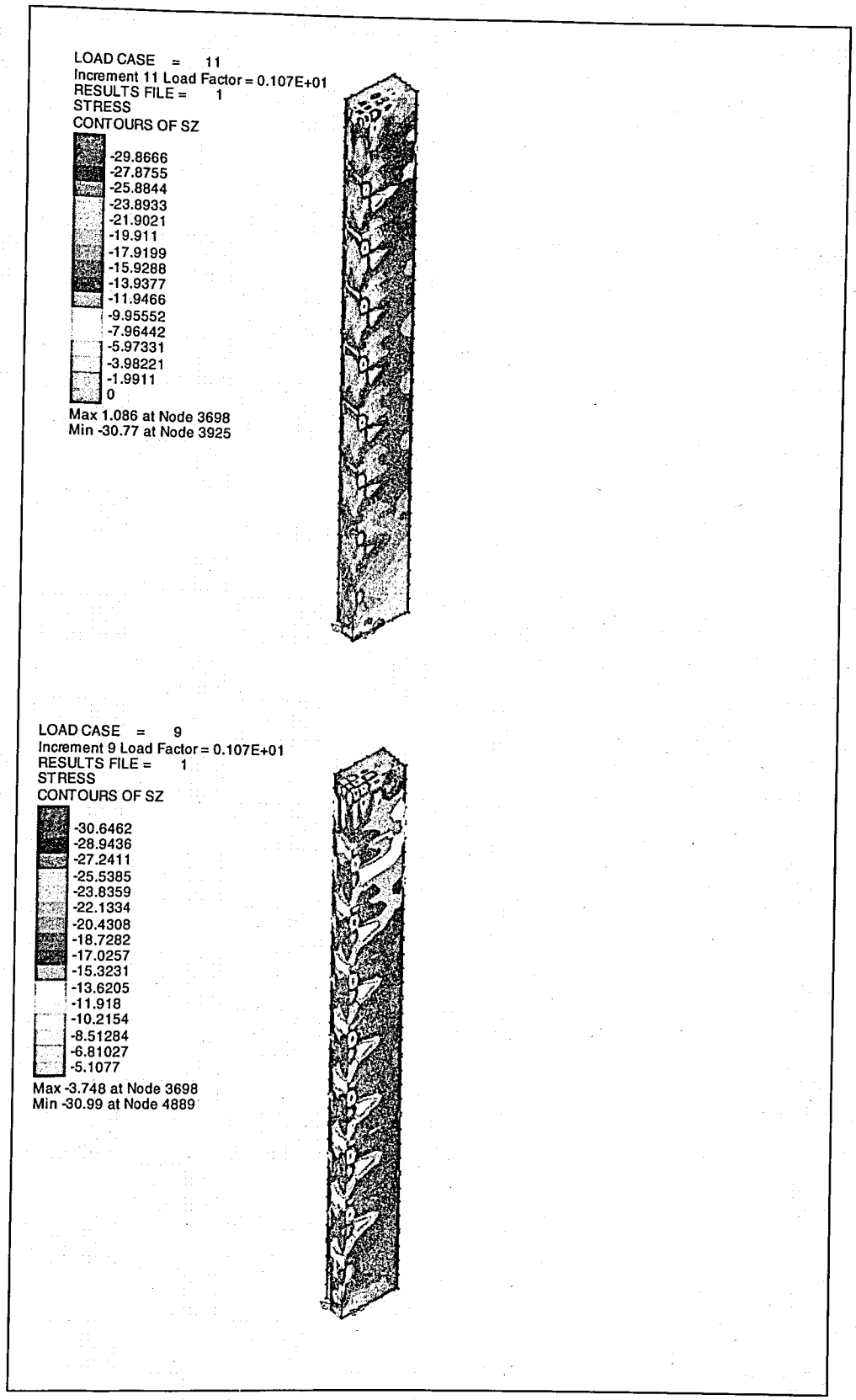

Figure 5.21. Vertical stress results for M3a and M3b

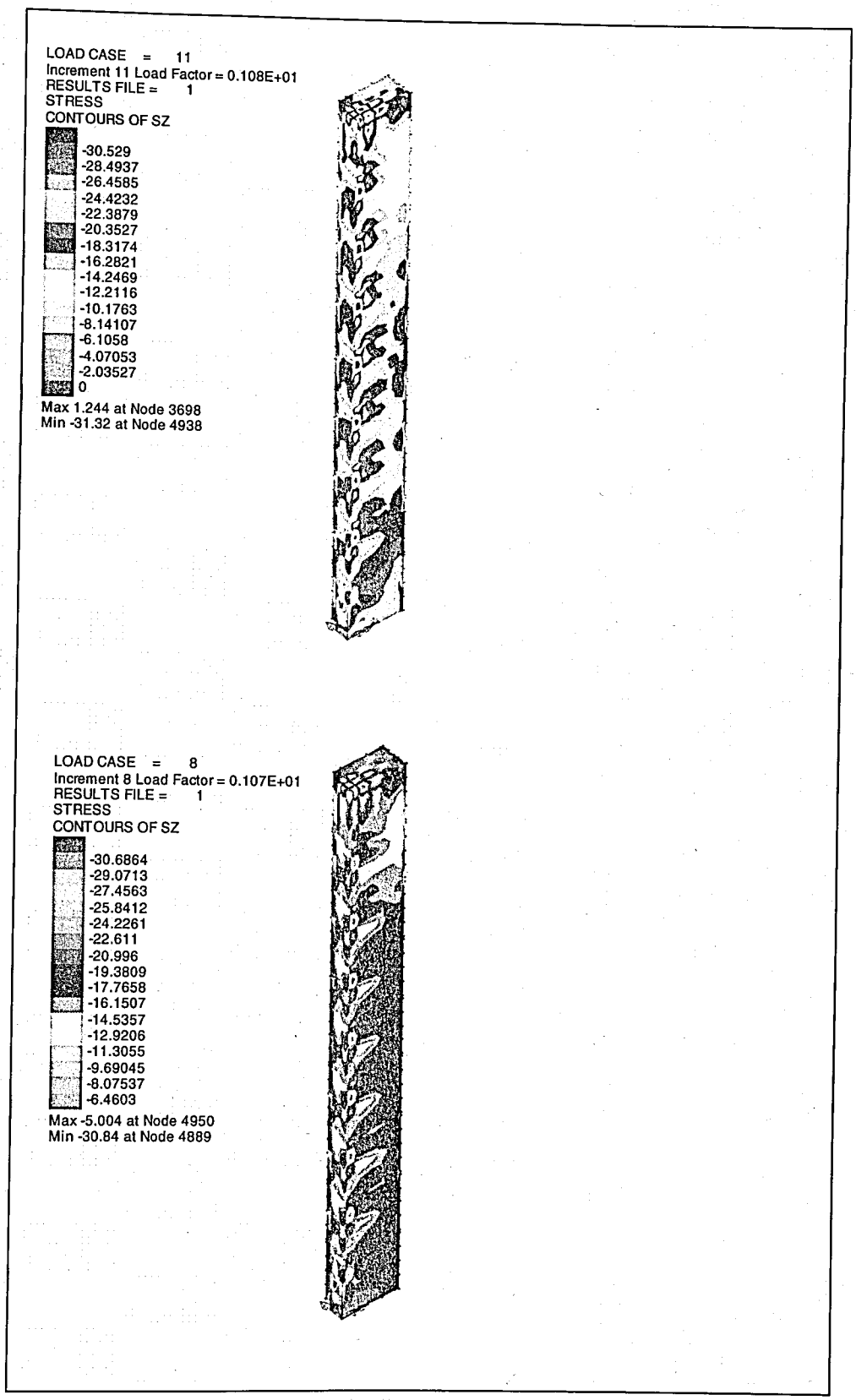

Figure 5.22. Vertical stress results for M4a and M4b

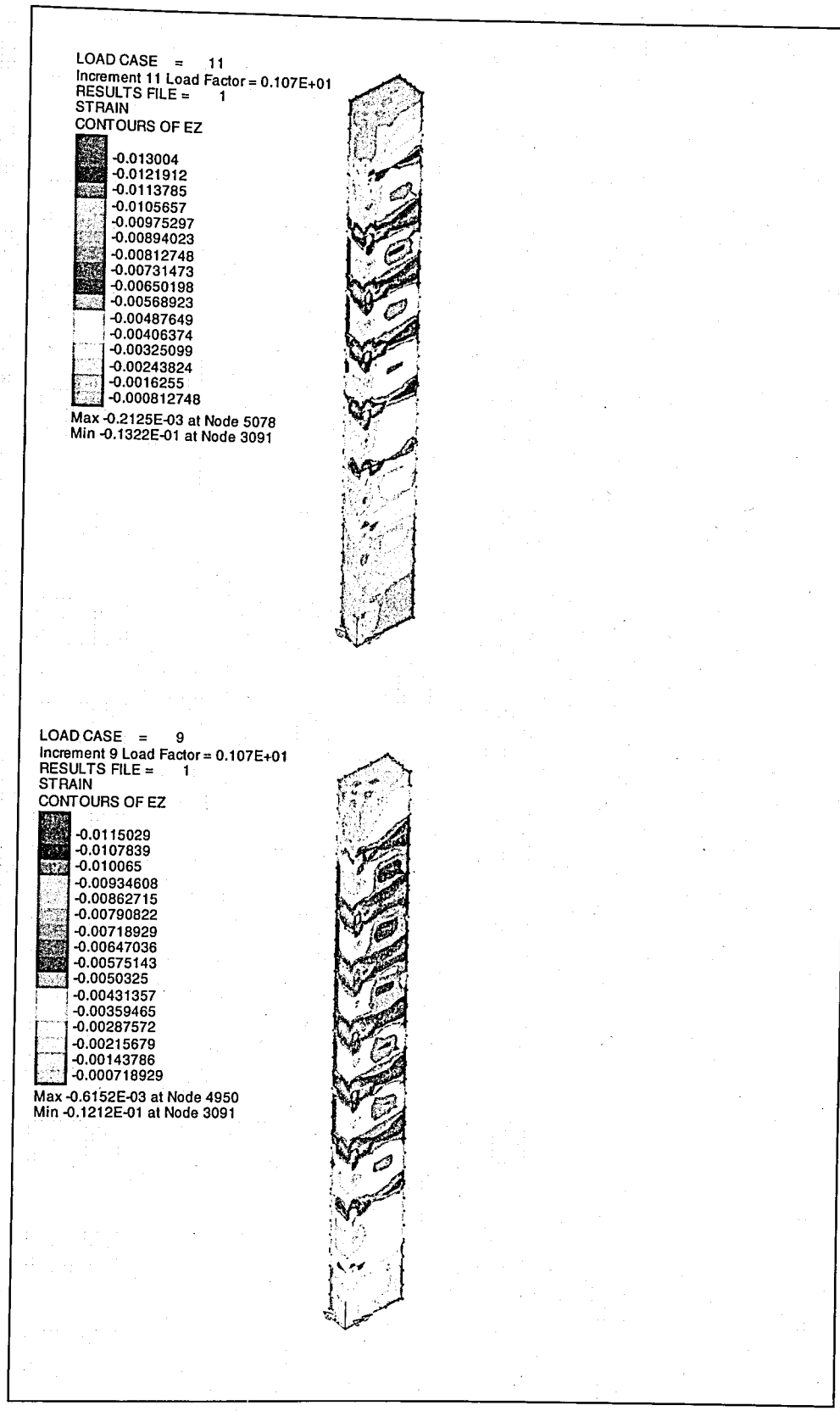

Figure 5.23. Vertical strains for M3a and M3b

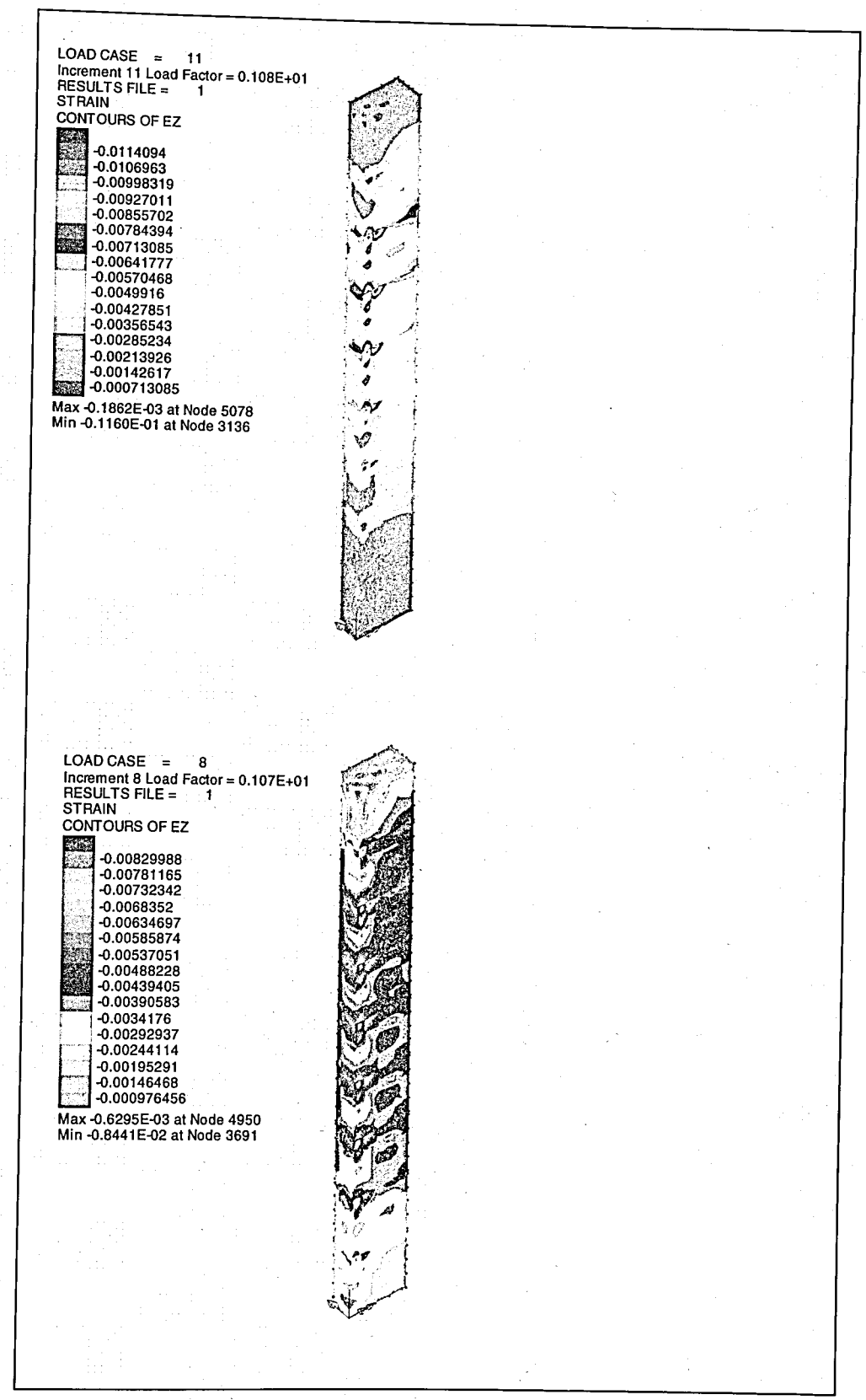

Figure 5.24. Vertical strains for M4a and M4b

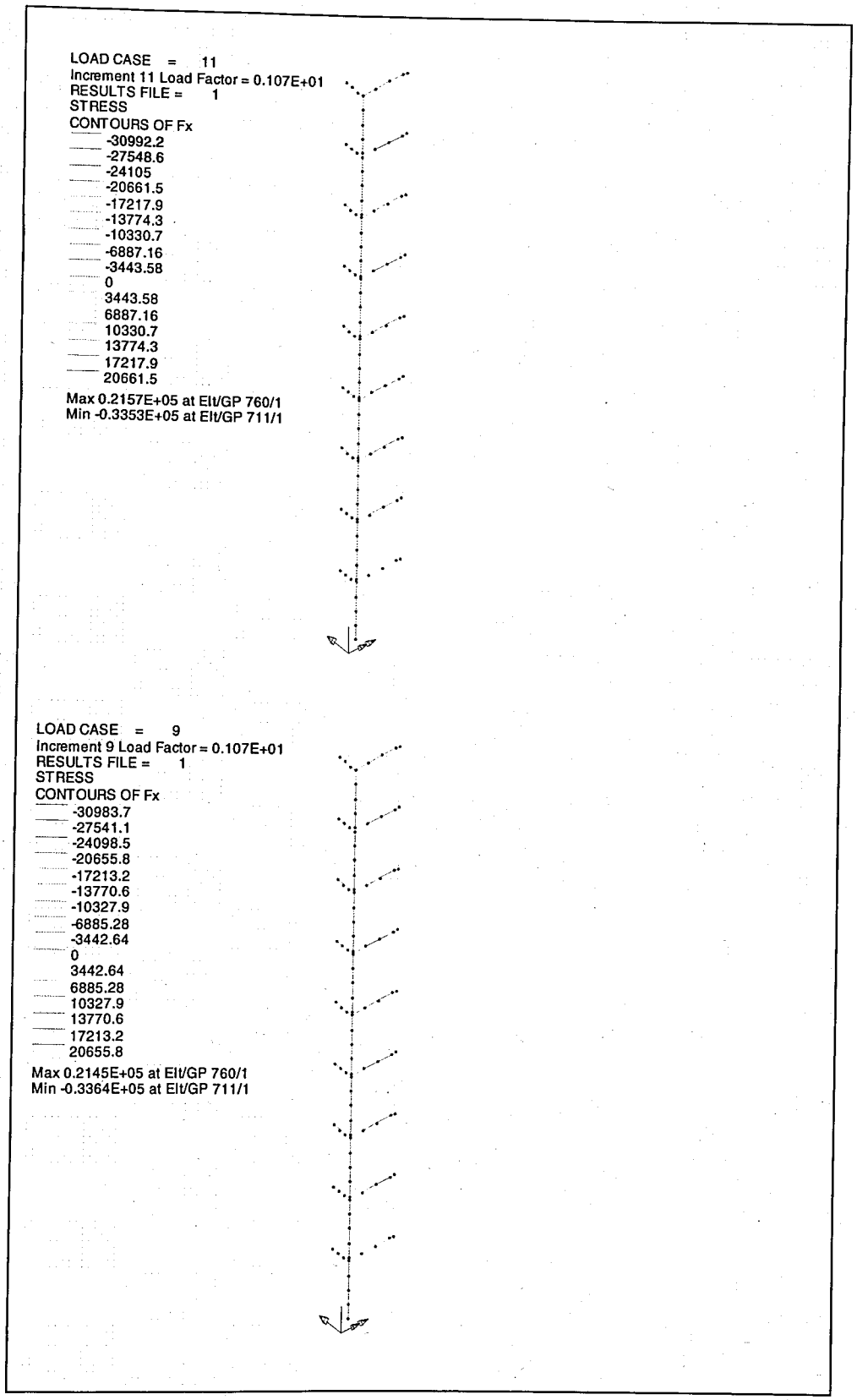

Figure 5.25. Forces on the reinforcement elements for M3a and M3b

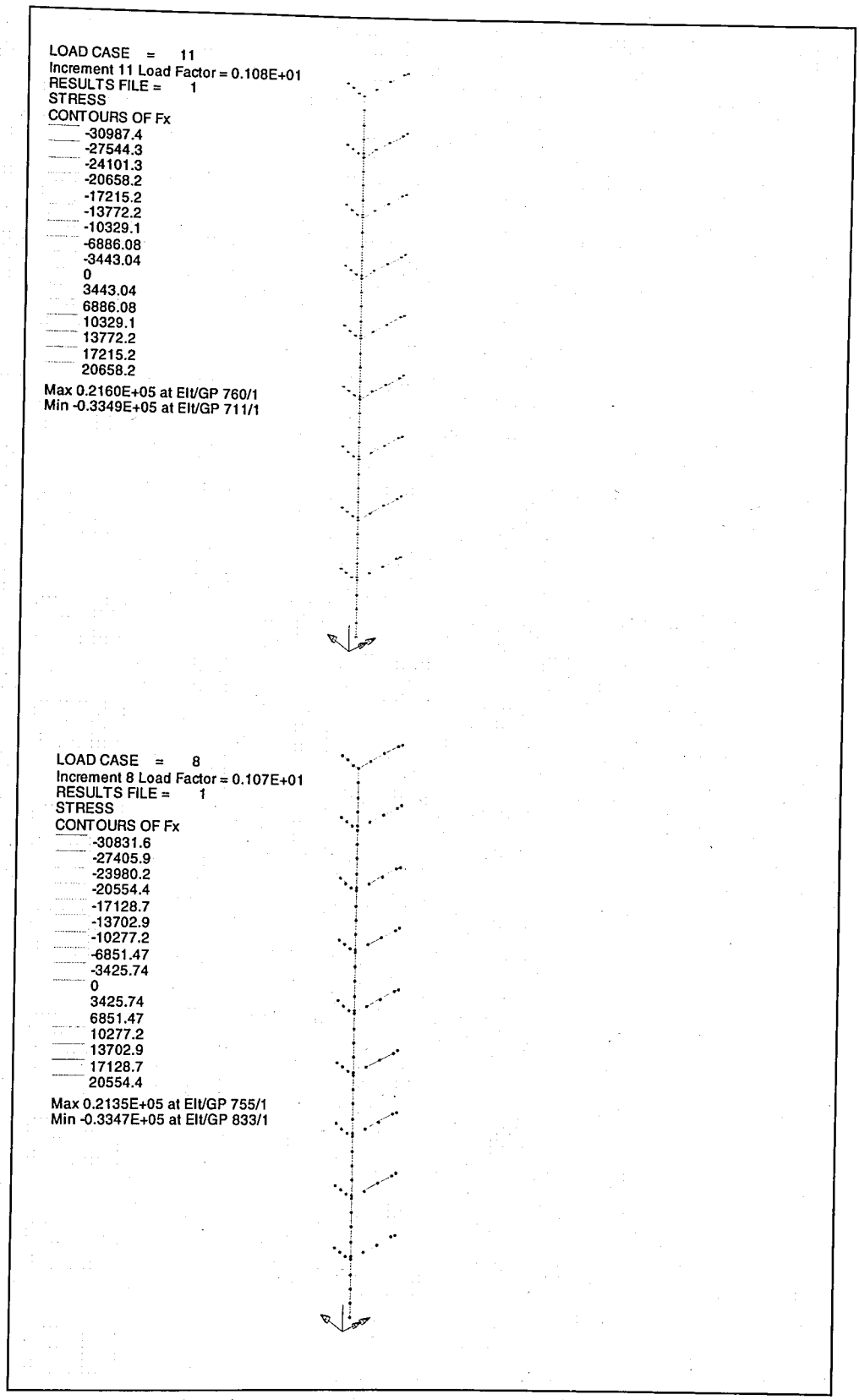

Figure 5.26. Forces on the reinforcement elements for M4a and M4b

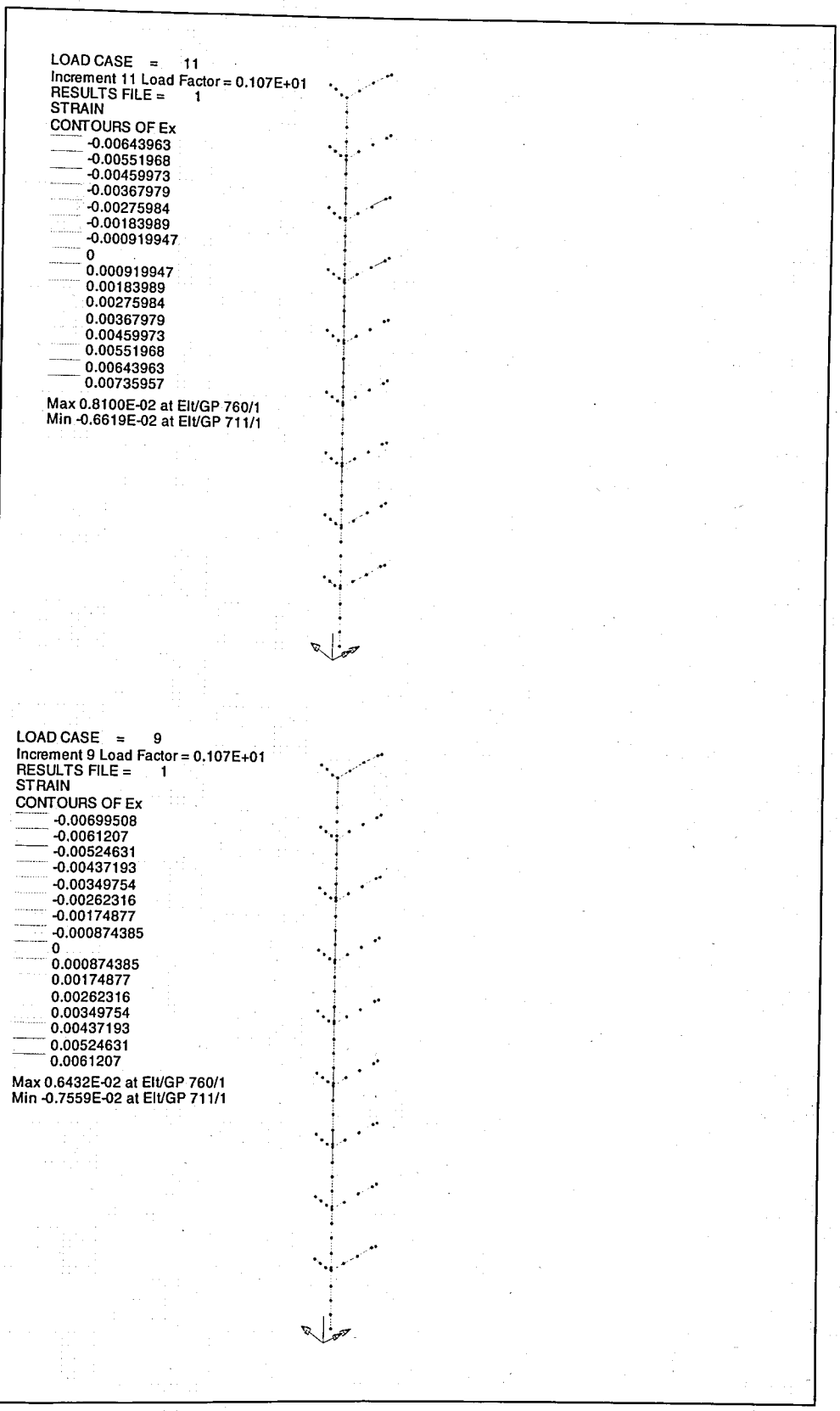

Figure 5.27. Strain results of the reinforcement elements for M3a and M3b

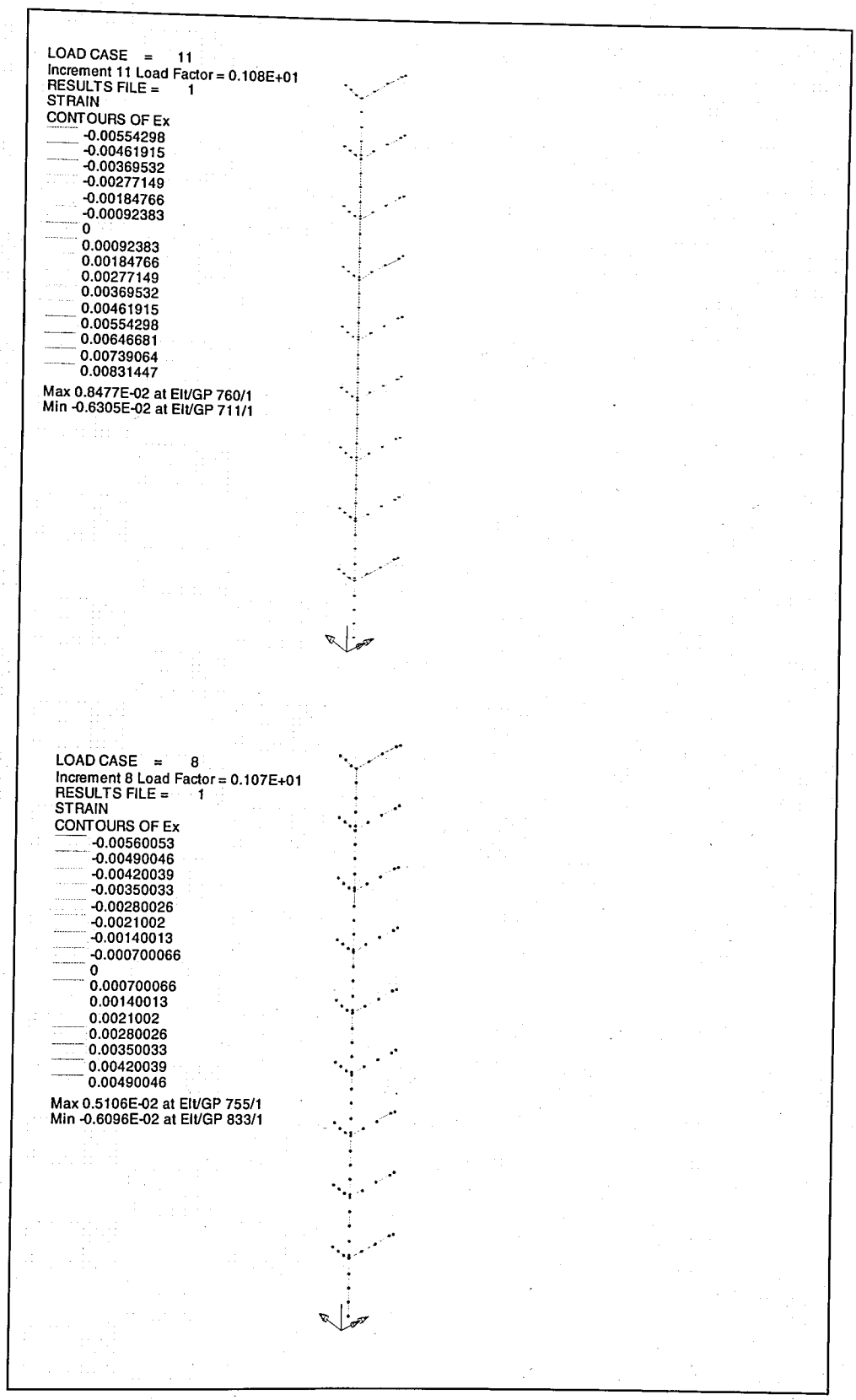

Figure 5.28. Strain results of the reinforcement elements for M4a and M4b

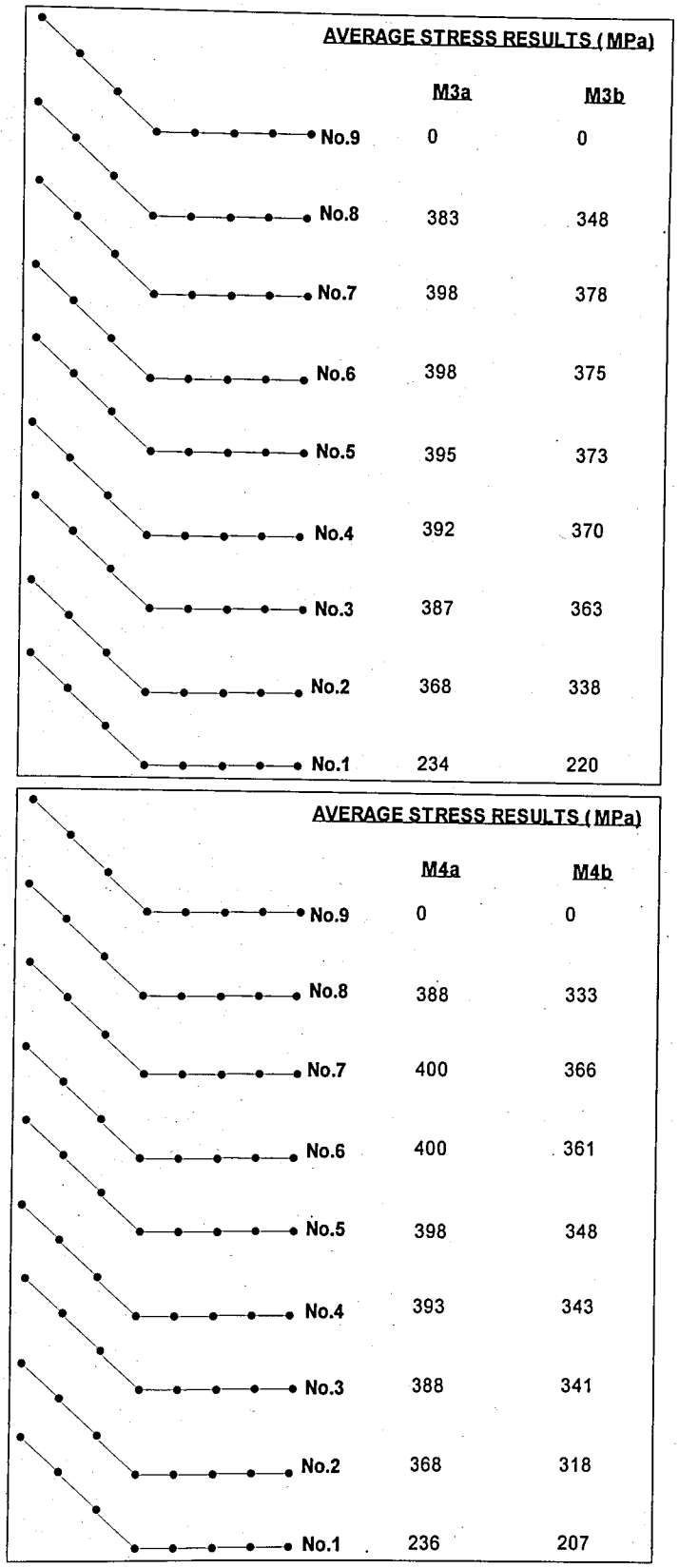

Figure 5.29. Average stress results of the lateral ties for M3a, M3b, M4a and M4b

Examining the results of the model columns, it is observed that locations of maximum displacements, stresses and forces; deformed shapes of the entire columns and reinforcements at the end of the solution process are very similar with each other. According to the analytical results, the failure of the masonry columns occur by crushing of concrete core, yielding of the vertical and lateral reinforcements and splitting of the block shells as a result of the concrete core expansion at the seventh to ninth block unit regions which correspond to the upper part of the masonry columns. However, the location of the column failure was observed at various block levels for the columns tested under axial loading. The failure modes of the tested columns still resemble with the conclusions derived from the analytical case.

Results of the analytical model of the columns are summarized in Table 5.4 which reflect the nonlinear analytical solutions of the full cross section of the reinforced masonry columns. The nonlinear solution of the analytical models is compared with the experimental results in Figure 5.30 and Figure 5.31.

Table 5.4. Summary of the analytical results

ANALYTICAL RESULTS			M3a	M3b	M4a	M4b
Ultimate load of the column	P_u	**kN**	1508.72	1501.65	1519.84	1509.56
Average stress on the longitudinal bar elements	σ_{av}	**MPa**	-405.94	-415.16	-406.36	-416.28
Average strain on the longitudinal bar elements	ε_{av}		-0.0038	-0.0042	-0.0037	-0.0037
Maximum stress of the lateral ties	σ_{av}	**MPa**	398	378	400	366
Maximum vertical deflection of the column	δ_z	**mm**	-6.89	-7.61	-6.97	-6.84
Average vertical stress of the column	σ_{zav}	**MPa**	-18.46	-18.42	-18.74	-18.64

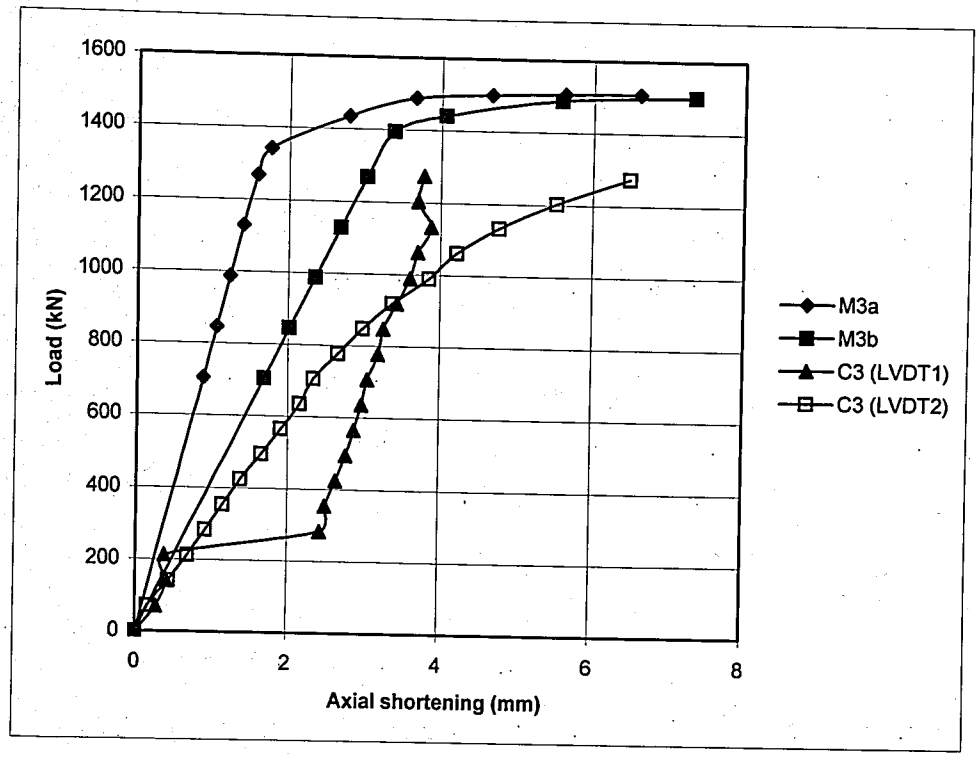

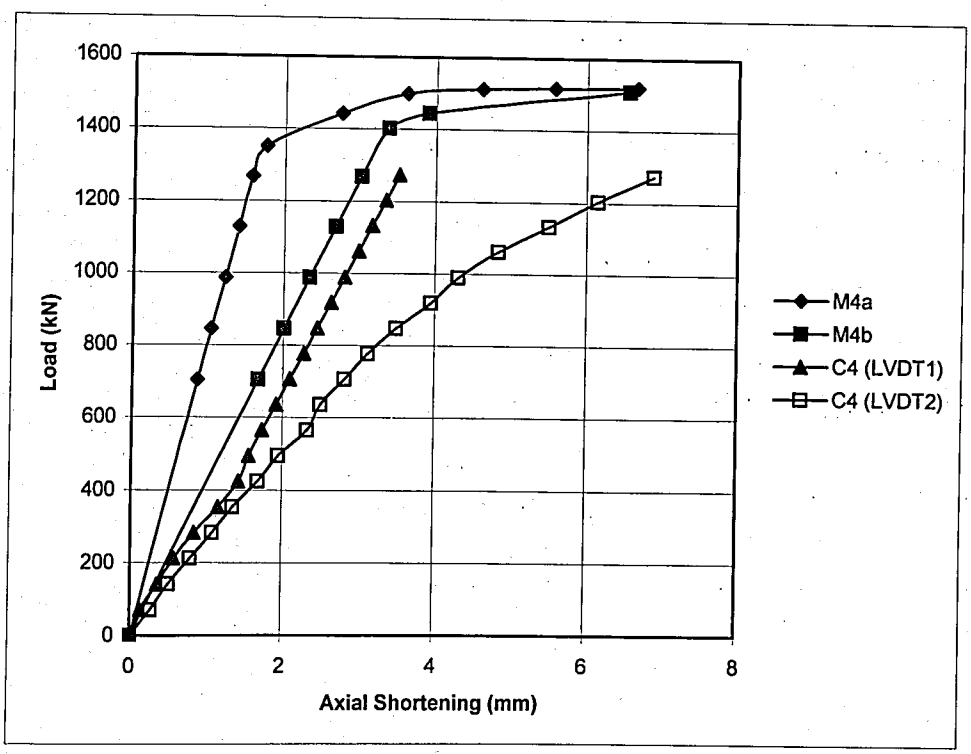

Figure 5.30. Load deformation (axial shortening) curves of the columns

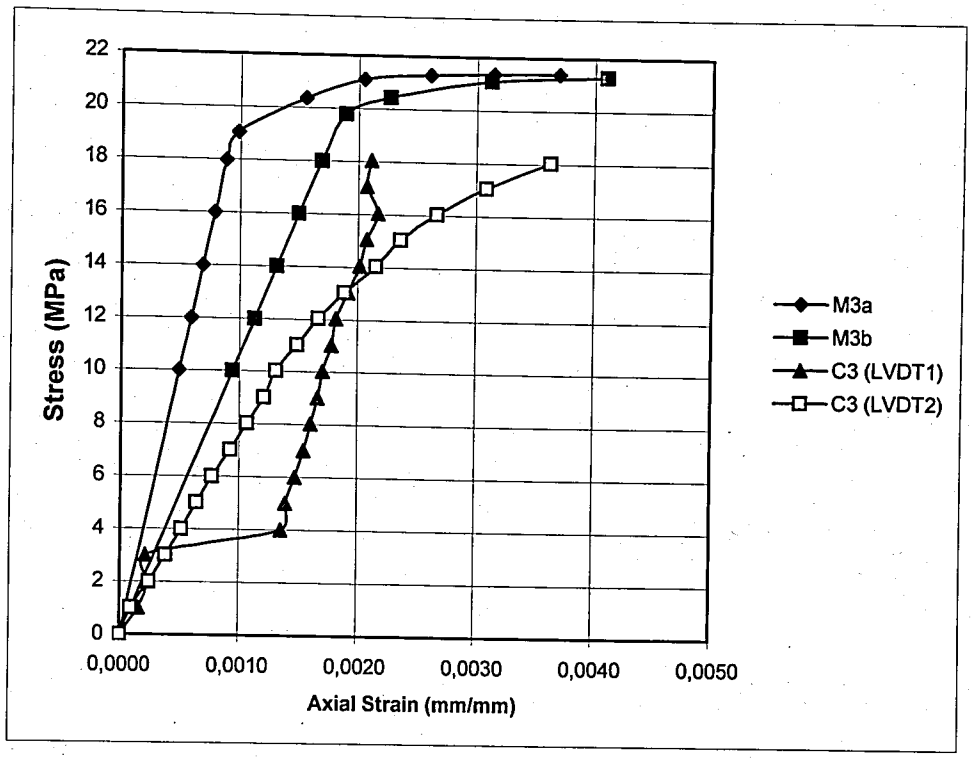

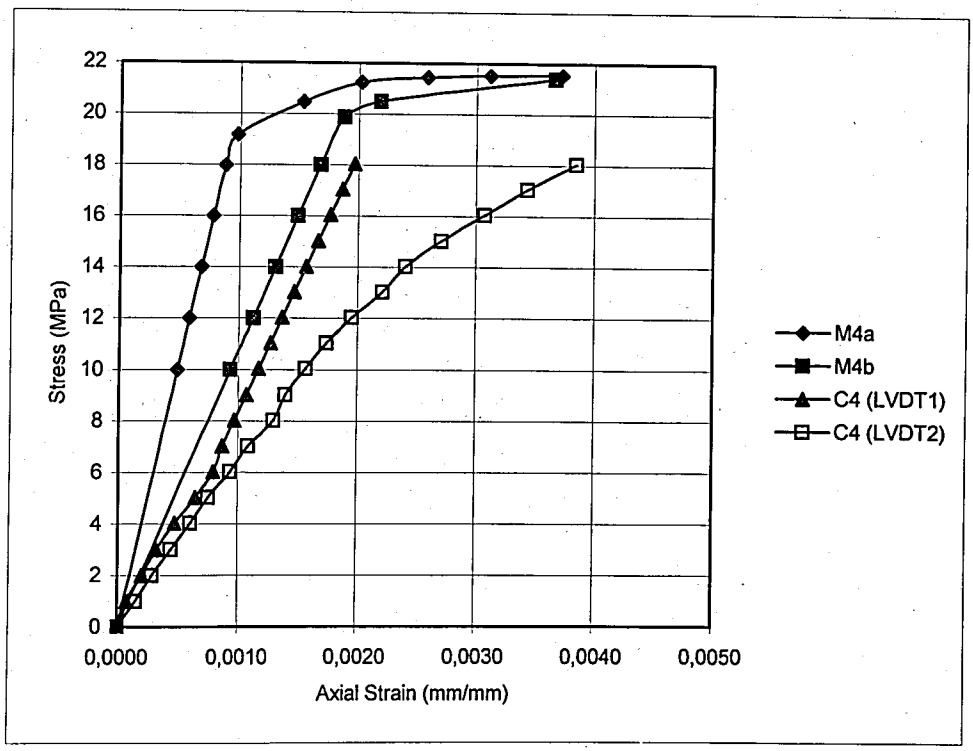

Figure 5.31. Stress strain curves of the columns

Table 5.5. Experimental and analytical results of columns

Column No.	Elastic Modulus E_m (MPa)	Ultimate Load P_u (kN)
Experimental column C3 (LVDT1)	8325.9	1325.6
Experimental column C3 (LVDT2)	7615.9	1325.6
Model column M3a	20410.0	1508.7
Model column M3b	10662.0	1501.7
Experimental column C4 (LVDT1)	7293.2	1308.0
Experimental column C4 (LVDT2)	6452.3	1308.0
Model column M4a	20490.0	1519.8
Model column M4b	10701.0	1509.6

As a whole, the analytical models reproduce the nonlinear behavior of the actually loaded masonry columns. It is noted that the ultimate load values derived from the analytical model columns are in good agreement with the experimental results. But the elastic modulus and vertical deformations derived from the analytical results exceed the experimental values. However the elastic modulus of the masonry columns which are obtained from analytical models are in good agreement with the values calculated theoretically in Section 5.3. The experimental stress strain curves of the columns C3 and C4 are even below the lower bound model curves, M3b and M4b but the curves obtained from LVDT1 data are much closer the lower bound curves of the analytical solutions.

6. CONCLUSIONS AND RECOMMENDATIONS

6.1. Conclusions

The results and discussions of the experimental study and analytical modelling lead to the following conclusions;

- Observed failure of columns tested under axial loading occurred by simultaneous vertical splitting of face shells and buckling of vertical reinforcement between lateral ties within one of the blocks that separated from concrete core.
- Vertical cracks were observed to originate at block shell corners and propagate vertically up to the failure load. Vertical crack propagation at block shell corners is caused by the differences of stiffness and Poisson's ratio between reinforcing steel and masonry. Localized tensile stresses in masonry shells are relieved by propagation of major cracks along the vertical reinforcement.
- Buckling of vertical reinforcement was generally observed over one course of block where pulling of lateral tie hooks did not occur at the region of buckling. This shows that, 135^0 degree lateral tie detailing is sufficient to restrain vertical reinforcement but 190 mm constant spacing of lateral ties is insufficient to prevent buckling of $4\phi10$ vertical reinforcements.
- Columns C1, C2, C5 and C6 that had higher strength of infill concrete but lower slump values exhibited premature failure behavior. Columns C3 and C4 with lowest concrete strength and highest slump resulted with highest ultimate load among the columns. This is a result of tapering of the block unit, which has been manufactured with variable cross section through the block unit height. The block geometry prevents penetration of the concrete within the cavities between the block shells and the reinforcement for the columns that possess lower slump infill concrete.
- None of the columns collapsed completely at failure load. This is a contribution of the reinforcements forming a cage to the concrete core and supporting the intact form of the masonry column even after the failure.

- The ultimate load results of the analytical solution are in good agreement with the experimental results whereas the elastic modulus of the column models is higher than the experimental values. Therefore, Drucker Prager failure criterion, being used for nonlinear modelling of concrete, mortar and concrete block units, is a representative material model for the estimation of reinforced masonry column ultimate strength.
- The analytical results indicate that reinforced masonry columns under axial loading fail with splitting of block shells and buckling of reinforcement at the upper block units exhibiting the maximum lateral deformations at the outward directions. However, the location of block shell splitting of tested columns was observed at various block units.
- Ultimate load of the columns were also calculated using equations given by ACI 530/ASCE 5 [14]; Khalaf, Hendry and Fairbairn [11]; and Sturgeon, Longworth and Warwaruk [10]. Both experimental and analytical results show that equation given by ACI 530/ASCE 5 [14] underestimates ultimate load of a reinforced masonry column. In addition, ultimate load values calculated using the equation proposed by Khalaf, Hendry and Fairbairn are in good agreement with the experimental and analytical results obtained from columns C3 and C4.
- Equation (5.1) was proposed in order to represent the elastic modulus of the reinforced masonry columns tested under axial loading in this study.

6.2. Recommendations

- The concrete block units used for the column construction have a tapering geometry which prevent the full penetration of the infill concrete between reinforcement and block shells. It is suggested that high slump value of infill concrete be used for experimental studies on reinforced concrete block masonry columns in order to ensure the necessary workability and flowability of fresh concrete. In addition, the concrete block units being used for this study should be manufactured with uniform cross section and special reinforcement grooves in order to provide proper concrete filling process and placement of reinforcement within the block units.
- Further study on concentrically loaded reinforced masonry columns should be carried out with varying percentage of vertical reinforcement and lateral tie diameter,

which will lead to define the effects of vertical and lateral reinforcement on strength more accurately.

- Drucker-Prager material model which is used for the nonlinear finite element analysis of the columns provides representative results for the ultimate strength but it overestimates the deformations of the columns tested. Therefore, further research should be conducted on nonlinear finite element modelling of reinforced masonry columns in order to simulate the nonlinear behavior of columns under axial loading and to obtain more consistent formulations expressing elastic modulus and ultimate load of reinforced masonry columns.

REFERENCES

1. Ramamurthy, K., *Studies on the Behavior of Concrete Hollow Block Masonry Prisms and Wall Panels*, Ph.D. Thesis, Indian Institute of Technology, 1991.

2. Hamid, A. A. and A. O. Chukwunenye., "Compression Behavior of Concrete Masonry Prisms", *Journal of Structural Engineering, ASCE*, Vol. 112, No. 3, pp. 605-613, March 1986.

3. Cheema, T. S. and R. E. Klingner, "Compressive Strength of Concrete Masonry Prisms", *ACI Journal*, Vol. 83, No. 1, pp. 88-97, January-February 1986.

4. Khalil, M., N. G. Shrive and P. Ameny, "Three-dimensional Stress Distribution in Concrete Masonry Prisms and Wall", *Magazine of Concrete Research,* Vol. 39, No. 139, pp. 73-82, 1987.

5. Afshari, F. A. and M. J. Kaldjan, "Finite Element Analysis of Concrete Masonry Prisms", *ACI Materials Journal*, Vol. 86, No. 5, pp. 525-530, September-October 1989.

6. Sayed-Ahmed, E. Y. and N. G. Shrive, "Nonlinear Finite-Element Model of Hollow Masonry", *Journal of Structural Engineering, ASCE*, Vol. 122, No. 6, pp. 683-690, June 1996.

7. *Compressive Strength of Masonry Assemblages (ASTM E447-84)*, American Society for Testing and Materials, Philadelphia, 1984.

8. Hatzinikolas, M., J. Longworth and J. Warwaruk, *Concrete Masonry Walls,* Structural Engineering Report, No. 70, Department of Civil Engineering, University of Alberta, 1978.

9. Feeg, C., J. Longworth and J. Warwaruk, *Effects of Reinforcement Detailing for Concrete Masonry Columns,* M.S. Thesis, University of Alberta, 1979.

10. Sturgeon, G. R., J. Longworth and J. Warwaruk, *An Investigation of Reinforced Concrete Block Masonry Columns,* Structural Engineering Report, No. 91, Department of Civil Engineering, University of Alberta, 1980.

11. Khalaf, F. M., A. W. Hendry and D. R. Fairbairn, "Reinforced Blockwork Masonry Columns", *ACI Structural Journal,* Vol. 90, No. 5, pp. 496-504, September-October 1993.

12. Chanine, G. N., *Behavior Characteristic of Face Shell Mortared Block Masonry Under Axial Compression,* M.S. Thesis, McMaster University, 1978.

13. Drysdale, R. G., A. A. Hamid and L. R. Baker, *Masonry Structures: Behavior and Design,* Prentice Hall, New Jersey, 1993.

14. Masonry Standards Joint Committee, *Building Code Requirements for Masonry Structures (ACI 530-92/ASCE 5-92/TMS 402-92),* American Concrete Institute and American Society of Civil Engineers, Detroit, New York, 1992.

15. Drysdale, R. G. and A. A. Hamid, "Behavior of Concrete Block Masonry Under Axial Compression", *ACI Journal Proceedings,* Vol. 76, No. 6, pp. 707-721, June 1979.

16. Khalaf, F. M., A. W. Hendry and D. R. Fairbairn, "Study of the Compressive Strength of Blockwork Masonry", *ACI Structural Journal,* Vol. 91, No. 4, pp. 367-375, July-August 1994.

17. Ganesan, T. P. and K. Ramamurthy, "Behavior of Concrete Hollow Block Prisms Under Axial Compression", *Journal of Structural Engineering, ASCE,* Vol. 118, No. 7, pp. 1751-1769, July 1992.

18. *Compressive Strength of Grouted Hollow Brick Prisms, Masonry: Materials, Properties and Performance (ASTM STP 728),* American Society for Testing and Materials, Philadelphia, 1982.

19. *Masonry Design for Buildings (CSA-CAN3-S304-M84),* Canadian Standards Association, Rexdale, Ontario, 1984.

20. *Standard Specification for Mortar for Unit Masonry (ASTM C270-89),* American Society for Testing and Materials, Philadelphia, 1989

21. Hamid, A. A., *Behavior Characteristics of Concrete Masonry,* Ph.D. Thesis, McMaster University, 1978.

22. Sahlin, S., *Structural Masonry,* Prentice Hall, Englewood Cliffs, NJ, 1971.

23. Roberts, J. J., *A Survey of Literature Relating to the Properties and Use of Concrete Blocks,* Technical Report 42.467, Cement and Concrete Association, London, 1972.

24. *Masonry Design and Construction for Buildings (CSA-S304-1977),* Canadian Standards Association, Ontario, 1977.

25. Slater, W. A. and I. Lyse, "Column Tests at Lehigh University", *Journal of American Concrete Institute,* Proceedings, Vol. 27, pp. 677-730, 1931.

26. Lyse, I. and C. L. Kreidler, "Column Tests at Lehigh University", *Journal of American Concrete Institute Proceedings,* Vol. 28, pp. 317-346, 1932.

27. Lyse, I., "Column Tests at Lehigh University", *Journal of American Concrete Institute Proceedings*, Vol. 29, pp. 433-442, 1933.

28. Richart, F. E. and G. C. Staehle, "Column Tests at the University of Illinois", *Journal of American Concrete Institute Proceedings*, Vol. 27, pp. 731-760, 1931.

29. Richart, F. E. and R. L. Brown, *An Investigation of Reinforced Concrete Columns*, Engineering Experiment Station Bulletin, No. 267, University of Illinois, 1934.

30. *Use of Masonry (BS5628),* British Standards Institution, 1985.

31. *Betonarme Yapıların Hesap ve Yapım Kuralları (TS-500),* Turkish Standards, February 2000.

32. *Beton Agregaları (TS-706),* Turkish Standards, December 1980.

33. *Standard Specification for Loadbearing Concrete Masonry Units (ASTM C90-01),* American Society for Testing and Materials, Philadelphia, February 2001.

34. *Standard Test Methods of Sampling and Testing Concrete Masonry Units (ASTM C140-98b),* American Society for Testing and Materials, Philadelphia, November 1998.

35. *Kagir Duvar Harçları (TS-2848),* Turkish Standards, October 1977.

36. *Harç Kumları (TS-2717),* Turkish Standards, April 1977.

37. Finite Elements Analysis Software Products (LUSAS 13.3), "Examples Manual", Issue 2, FEA Ltd., United Kingdom.

38. Chen, W. F., *Plasticity in Reinforced Concrete,* McGraw-Hill, 1982.

39. Launay, P. and H. Gachon, "Strain and Ultimate Strength of Concrete Under Triaxial Stress", *ACI Special Publication,* No. 34, 1972.

40. Richart F. E., A. Bradzaeg and R. L. Brown, *A Study of the Failure of Concrete under Combined Compressive Stresses,* Engineering Experiment Station Bulletin, No. 185, University of Illinois, 1928.

41. Kupfer, H., *Das Betons unter Mahrechigen Kurtzzeitbelagstung unter Besonderer Berücksichtigung der Zweiachsigen Beansprucheng,* Ausschuss Stahlbeton, Vol. 229, 1973.

42. Karakoç, C. and H. O. Köksal, "The Modelling of Concrete Fracture", *Studi e Ricerhe,* pp. 271-283, 1997.

43. Lubnier, J., J. Oliver, S. Ollers and E. Onatei, "A Plastic-Damage Model for Concrete", *International Journal of Solids and Structures,* Vol. 25, No. 5, pp. 299-326, 1989.

44. Köksal, H. O., C. Karakoç and H. Yıldırım, "Compression Strength of Hollow Block Masonry Prisms", *Studi e Ricerhe,* Vol. 24, pp. 271-283, 2003.